

# LABORATORY TESTING OF GROSS SOLIDS REMOVAL DEVICES

Prepared for:

California Department of  
Transportation  
1120 N Street  
Sacramento, CA 95826



CTSW-RT-05-73-18.1

By:

Bassam A. Younis, Professor  
Department of Civil and Environmental Engineering  
University of California, Davis  
Davis, CA 95616  
May 2005

## Executive Summary

This report details the outcome of tests carried out at the Hydraulics Laboratory of the University of California, Davis to assess the performance of three alternative Gross Solids Removal Devices (GSRDs) developed by Caltrans to remove litter and solids from storm water runoff. These devices were: the Linear-Radial GSRD, the parabolic screen (Type 1) GSRD and the straight screen (Type 2) GSRD.

A large-scale test facility was designed and built specifically for the purpose of testing full scale devices under conditions of flow rates and litter-loading percentages that correspond to those actually encountered in Caltrans drainage facilities. The litter used in the tests was manufactured in accordance with the results of previously commissioned studies by Caltrans on the characterization of highway litter.

The main conclusions to emerge from the present study are as follows. The litter-capture efficiency of the Linear-Radial device is very high, with insignificant volume of litter having dimensions greater than 0.25 inches square leaving the device. At high percentage litter loading, overflow occurs from this device flow rates that are below the design maximum. This overflow occurs through a hatch built into the device in order to prevent the runoff flow from backing up on to the highway. The hydraulic efficiency of this device is acceptable at mild slopes and is shown to improve with the use of 45° wing walls to streamline the flow at outlet from the vault. Observations indicate that removal of compacted litter from inside this device when deployed in the field is likely to pose an operational difficulty. The present results are incorporated in a design methodology based on HEC-22 procedure.

The parabolic screen (Type 1) GSRD also proved to be very efficient in its litter capture capabilities. The flow over the weirs remained attached to the screens over large portion of their lengths. This produced two beneficial effects; namely increased conveyance of clean water through the screens to the exit from the device, thereby reducing the overall volume of storage required, and, a mechanism for forcing litter to move along the screen and into the litter storage device. Litter accumulation inside the inlet troughs eventually caused blockage of 'weep holes' that are placed there to drain the inflow. Consequently, drainage times of two days or more were recorded, though this feature is not thought likely to seriously degrade this device's field performance.

The straight screen (Type 2) GSRD failed very badly for flow rates and litter loading percentages well below the design maximums. The device failure was by overflow of litter-laden water over the outer walls. This was due to the total blockage of the screens by litter, leading to drastic reduction in conveyance of clean water to the exit from this device. The blockage occurs due to lack of

adherence of flow to the screens and thus the performance of this device can be drastically improved by making design changes to force the inflow water to remain attached to the screens for greater distances along their lengths. This will create the self-cleaning mechanism that was clearly evident in the Type 1 parabolic screen tests.

## TABLE OF CONTENTS

Section 1: Introduction .....	1
1.1 Scope of study .....	1
1.2 Objectives of study .....	3
1.3 Personnel.....	4
1.4 Report Organization.....	5
Section 2: Description of test facility .....	6
Section 3: Composition of gross solids .....	24
Section 4: Results for Linear-Radial GSRD .....	29
4.1 Description of Linear-Radial device .....	29
4.2 Test procedure and data collection.....	32
4.3 Test results .....	36
4.3.1 7-Section GSRD (S<0.1%).....	36
4.3.2 7-Section GSRD (S=1.9%).....	48
4.3.3 Tests on 7, 6 and 5-Section GSRDs (S<0.1%) .....	51
4.3.4 Tests on 7, 6 and 5-Section GSRDs (S=1.9%) .....	54
4.3.5 Tests with 45 degree wing walls (S<0.1%).....	57
4.3.6 Tests with 45 degree wing walls (S=1.9%).....	63
4.3.7 Tests with 45 degree wing walls and S=2.75%, 3.25% and 4.4%...	69
4.4 Observations.....	75
4.5 Data correlations.....	79
4.6 Conclusions .....	85
Section 5: Results for parabolic screens (Type 1) GSRD .....	87
5.1 Description of Type 1 device.....	87
5.3 Test results .....	96
5.4 Data correlations.....	99
5.5 Observations.....	100
5.6 Closure .....	107
Section 6: Results for straight screens (Type 2) GSRD.....	108
6.1 Description of Type 2 device.....	108
6.2 Scope and procedure .....	110
6.3 Data collection and analysis .....	112
6.3.1 Head Water .....	112
6.3.2 Head loss .....	113
6.3.3 Data correlations .....	116
6.4 Observations.....	118
6.4.1 Clean water runs .....	118
6.4.2 Tests with gross solids .....	121
6.5 Conclusions .....	167
Section 7: Summary and recommendations .....	168
References .....	170
APPENDIX 1.....	171
Guidelines on Design of Storm Drains with Linear-Radial GSRD .....	171

1. Description of GSRD .....	171
2. Hydraulic Considerations .....	172
3. Example of design of storm drain outlet with Linear-Radial GSRD .....	174
Part I: Preliminary Design of Storm Drain Outlet with GSRD (English Units) .....	175
Part II: Energy grade Line Evaluation Computations-English Units .....	181
APPENDIX 2.....	187
CDs for Linear-Radial GSRD footage .....	187
APPENDIX 3.....	188
CDs for screens GSRDs footage .....	188

## LIST OF FIGURES

Fig. 2.1: Overview of layout of test facility for Linear-Radial GSRD. ....	8
Fig. 2.2: Layout of test facility for Types 1 and 2 GSRDs.....	9
Fig. 2.3a: Sump, pump and overflow return. ....	10
Fig. 2.3b: View of sump, pump, and pipes for return flow. ....	11
Fig. 2.4: Pump and supply to devices and overspill weir.....	12
Fig. 2.5: Square pipe supply to first receiving tank.....	13
Fig. 2.6: Gate valve to regulate flow rate through GSRDs.....	14
Fig. 2.7: Overspill weir and return to sump. ....	15
Fig. 2.8: Delivery to trash insertion tank.....	16
Fig. 2.9: Vault on flat trailer bed. ....	16
Fig. 2.10: Inside of vault showing Linear Radial device. ....	17
Fig. 2.11: Outfall from vault and downstream receiving tank. ....	18
Fig. 2.12: Downstream receiving tanks. ....	18
Fig. 2.13: 0.25" square wire mesh used for litter capture downstream of GSRD.....	19
Fig. 2.14: 3' diameter return pipe to sump. ....	19
Fig. 2.15: Water supply to Types 1 and 2 GSRDs. ....	20
Fig. 2.16: Vault containing Type 1 inclined screen.....	21
Fig. 2.17: Gross solids insertion box for Types 1 and 2 GSRDs. ....	22
Fig. 2.18: Return flow from Types 1 and 2 GSRDs.....	23
Fig 3.1: Gross solids including vegetation and sediment .....	26
Fig. 3.2: Dry gross solids collected from Caltrans outfalls.....	26
Fig. 3.3: Relative composition of litter from highway outfalls based on count, weight and volume (from Kayhanian et al., 2002) .....	27
Figure 3.4: Gross solids mix manufactured in the Hydraulics Laboratory. ....	28
Fig. 4.2: Linear-Radial GSRD in vault at UC Davis.....	31
Fig. 4.3: Cross section through Linear-Radial device showing locations of measurements stations.....	34
Fig. 4.4: Variation of water surface elevation with distance along vault. Results shown are for 7 section device for 50% dry loading and for slope <0.1%.....	36
Fig. 4.5: Variation of water surface elevation with distance along vault. Results shown are for 7 section device for 90% dry loading and for slope <0.1%.....	37
Fig. 4.6: Variation of water surface elevation with distance along vault. Results shown are for 7 section device for 90% wet loading and for slope <0.1% .....	37
Fig. 4.7: Variation of water surface elevation at inlet to the vault with flow rate. Results shown are for 7 section device and for slope <0.1%.....	38
Fig. 4.8: Manning's n vs flow rate for 7 section device with no gross solids loading and for S<0.1%.....	39
Fig. 4.9: Manning's n vs flow rate for 7 section device with 50% dry gross solids loading and for S<0.1%.....	40
Fig. 4.10: Manning's n vs flow rate for 7 section device with 90% dry gross solids loading and for S<0.1%.....	40
Fig. 4.11: Manning's n vs flow rate for 7 section device with 90% wet gross solids loading and for S<0.1%.....	41

Fig. 4.12: Average value of Manning's n vs flow rate for 7 section device for S<0.1%.....	41
Fig. 4.13: Variation of head water with flow rate for S<0.1%.....	42
Fig. 4.14: Plot of total head $H_1$ vs flow rate for S<0.1%.....	43
Fig. 4.15: Plot of total head $H_1$ vs Re for S<0.1%.....	43
Fig. 4.16: Plot of total head $H_1$ vs $V^2/2g$ for S<0.1%.....	44
Fig. 4.17: $\Delta h$ vs $V^2/2g$ for S<0.1%.....	44
Fig. 4.18: Variation of head water with flow rate for S=1.9%.....	48
Fig. 4.19: $H_1$ vs Q for S=1.9%.....	49
Fig. 4.20: $H_1$ vs Re for S=1.9%.....	49
Fig. 4.21: $H_1$ vs $V^2/2g$ for S=1.9%.....	50
Fig. 4.22: $\Delta h$ vs $V^2/2g$ for S=1.9%.....	50
Fig. 4.23: $y_1$ vs Q for S<0.1%.....	51
Fig. 4.24: $H_1$ vs Q for S<0.1%.....	52
Fig. 4.25: $H_1$ vs Re for S<0.1%.....	52
Fig. 4.26: $H_1$ vs $V^2/2g$ for S<0.1%.....	53
Fig. 4.27: $\Delta h$ vs $V^2/2g$ without the 45 degree wing walls for S<0.1%.....	53
Fig. 4.28: $y_1$ vs Q for S=1.9%.....	54
Fig. 4.29: $H_1$ vs Q for S=1.9%.....	55
Fig. 4.30: $H_1$ vs Re for S=1.9%.....	55
Fig. 4.31: $H_1$ vs $V^2/2g$ for S=1.9%.....	56
Fig. 4.32: $\Delta h$ vs $V^2/2g$ without the 45 degree wing walls for S=1.9%.....	56
Fig. 4.33: $y_1$ vs Q for S<0.1%.....	57
Fig. 4.35: $H_1$ vs Re for S<0.1%.....	58
Fig. 4.36: $H_1$ vs $V^2/2g$ for S<0.1%.....	59
Fig. 4.38: $\Delta h$ vs Q for S<0.1%.....	60
Fig. 4.39: $\Delta h$ vs Re for S<0.1%.....	60
Fig. 4.40: $y_1$ vs Q for S=1.9%.....	63
Fig. 4.41: $H_1$ vs Q for S=1.9%.....	64
Fig. 4.42: $H_1$ vs Re for S=1.9%.....	64
Fig. 4.43: $H_1$ vs $V^2/2g$ for S=1.9%.....	65
Fig. 4.44: $\Delta h$ vs $V^2/2g$ with the 45 degree wing walls for S=1.9%.....	65
Fig. 4.45: $\Delta h$ vs Q for S=1.9%.....	66
Fig. 4.46: $\Delta h$ vs Re for S=1.9%.....	66
Fig. 4.47: $y_1$ vs flow rate for all slopes.....	69
Fig. 4.48: $H_1$ vs Q for all slopes.....	70
Fig. 4.49: $H_1$ vs Re for all slopes.....	70
Fig. 4.50: $H_1$ vs $V^2/2g$ for all slopes.....	71
Fig. 4.51: $\Delta h$ vs Q for all slopes.....	71
Fig. 4.52: $\Delta h$ vs Re for all slopes.....	72
Fig. 4.53: $\Delta h$ vs $V^2/2g$ for all slopes.....	72
Fig. 4.54: $\Delta h/H_1$ vs Q for all slopes.....	73
Fig. 4.55: $\Delta h/H_1$ vs Re for all slopes.....	73
Fig. 4.56: $\Delta h/H_1$ vs $V^2/2g$ for all slopes.....	74
Fig. 4.57: Overflow for Q=29 cfs and 90% loading.....	76
Fig. 4.58: Close-up of overflow.....	76

Fig. 4.59: Patterns of accumulation of gross solids.....	77
Fig. 4.60: loss of conveyance through louvers due to accumulation of gross solids.....	78
Fig. 4.61: Correlation of $\Delta h/H_1$ with Re for $S<0.1\%$ and $S=1.9\%$ .....	81
Fig. 4.62: Correlation of $\Delta h/H_1$ with Q for $S<0.1\%$ and $S=1.9\%$ .....	82
Fig. 4.63: Correlation of $\Delta h/H_1$ with $V^2/2g$ for $S<0.1\%$ and $S=1.9\%$ .....	82
Fig. 5.1a: Layout of Type 1 parabolic screens tested.....	88
Fig. 5.1b: Dimensions for Type1L GSRD.....	89
Fig. 5.2: A close-up of the parabolic screen attached to a weir.....	90
Fig. 5.3: Detail of the screen where it meets the sloped litter storage area.....	91
Fig. 5.4: Weep holes used to drain the runoff which accumulates in the influent trough.....	92
Fig. 5.5: View of the influent trough and solids trap showing the parabolic wedgewire screens in place below the curved weirs.....	93
Fig. 5.6: Plot of water depth in influent trough (in inches) and in the litter storage area vs flow rate Q (in cfs). ....	96
Fig. 5.7: Plot of water depth in influent trough (in inches) vs time from pump stop (plotted as natural log of time (in minutes)). ....	97
Fig. 5.8: Gross solids retained in inflow trough after completion of test. ....	101
Fig. 5.9: Screens remain clear of trash after flow rate of 1.1 cfs and 10% loading. ....	102
Fig. 5.10: Flow remains attached to the screens at $Q=5.5$ cfs and 10% loading. ....	102
Fig. 5.11: Blockage of inflow trough 24 hours after completion of test. ....	102
Fig. 5.12: Inflow trough storage after completion of test with $Q=5.5$ cfs and 50% loading. ....	103
Fig. 5.13: Clear screen is in evidence after test with $Q=5.5$ cfs and 50% loading. ....	103
Fig. 5.14: Flow remaining attached to screen at $Q=11.1$ cfs. ....	104
Fig. 5.15: Strong streamline curvature above weir for $Q=11.1$ cfs. ....	104
Fig. 5.16: Conveyance through the screen at high flow rate. ....	104
Fig. 5.17: Gross solids conveyance over the screens at $Q=11.1$ cfs and 50% loading. ....	105
Fig. 5.18: Efficient conveyance of gross solids over the screens at $Q=11.1$ cfs and 50% loading. ....	105
Fig. 5.19: Gross solids trapped in recirculation zone ( $Q=11.1$ cfs, 50% loading). ....	106
Fig. 5.20: Clear screen with most of the gross solids settled in the litter storage tank. ....	106
Fig. 6.1b: Construction plan for Type 2 panel. ....	109
Fig. 6.2: Water depth vs discharge for inclined straight screen.....	112
Curves plotted are: 1: water depth at outlet of trash insertion tank ( $y_1$ ), 2: water depth inside the litter storage area ( $y$ ), and 3: water depth at outlet pipe from the device ( $y_2$ ). ....	112
Fig. 6.3: $H_1$ vs Q for Type 2 inclined screen.....	114
Fig. 6.4: $H_1$ vs $V^2/2g$ for Type 2 inclined screen.....	114

Fig. 6.5: $\Delta h$ vs $V^2/2g$ for Type 2 inclined screen. ....	115
Fig. 6.6: $\Delta h/ H_1$ vs $V^2/2g$ for Type 2 inclined screen. ....	115
Fig. 6.7: Inflow conditions for $Q=0.94$ cfs. ....	121
Fig. 6.8: View inside inflow pipe for $Q=0.94$ cfs. ....	122
Fig. 6.9: Deflected flow into gross-solids storage area.....	123
Fig. 6.10: Flow inside inflow pipe for $Q=1.85$ cfs.....	124
Fig. 6.11: Non-uniform distribution for $Q=1.85$ cfs. ....	125
Fig. 6.12: Water distribution over screen for $Q=1.85$ cfs. ....	126
Fig. 6.13: Outflow at $Q=1.85$ cfs. ....	127
Fig. 6.14: Conditions inside inflow pipe at $Q=2.7$ cfs. ....	128
Fig. 6.15: Conditions over screen at $Q=2.7$ cfs. ....	129
Fig. 6.16: Flow over screen at $Q=3.5$ cfs ....	130
Fig. 6.17: Increase in water surface level produced by splash plate. ....	131
Fig. 6.18: Flow over screens for $Q=4.35$ cfs. ....	132
Fig. 6.19: View of water accumulation towards end of inflow shelf for $Q=4.35$ cfs. .....	133
Fig. 6.20: Flow over screens for $Q=5.0$ .....	134
Fig. 6.21: Water surface elevation at splash shelf for $Q=5.0$ cfs. ....	135
Fig. 6.22: Inlet conditions for $Q=6.13$ cfs.....	136
Fig. 6.23: Flow over shelf showing significant loss of screen conveyance efficiency.....	137
Fig. 6.24: Conditions at outflow for $Q=6.13$ cfs. ....	138
Fig. 6.25: Inflow conditions for $Q=7.06$ cfs. ....	139
Fig. 6.26: Water level rise in gross solids storage tank for $Q=7.06$ cfs. ....	140
Fig. 6.27: Conditions at outlet tank for $Q=7.06$ cfs. ....	141
Fig. 6.28: Inflow conditions for $Q=8.24$ cfs. ....	142
Fig. 6.29: Inlet conditions for $Q=9.0$ cfs. ....	143
Fig. 6.30: Conditions in gross solids storage device for $Q=9.0$ cfs.....	144
Fig. 6.31: Conditions in exit tank and the spill over of flow from the inflow shelf. .....	145
Fig. 6.32: Water overflow from gross solids storage device for $Q=9.0$ cfs. ....	146
Fig. 6.33: Overflow over splash plate for $Q=9.0$ cfs. ....	147
Fig. 6.34: Litter transport with $Q=1.1$ cfs (10% loading). ....	149
Fig. 6.35: Gross solids not being cleared entirely at low flow rates ( $Q=1.1$ cfs, 10% loading). ....	150
Fig. 6.36: 50% loading at $Q=1.1$ cfs.....	151
Fig. 6.37: Build-up of gross solids over portions of the screens ( $Q=1.1$ cfs, 50% loading). ....	152
Fig. 6.38: Clogging of screens for $Q=1.1$ cfs and 50% loading. ....	153
Fig. 6.39: View of clear water in outflow tank ( $Q=1.1$ cfs, 50% loading). ....	154
Fig. 6.40: Inflow patterns for $Q=1.1$ cfs and 90% loading. ....	155
Fig. 6.41: Screen clogging with $Q=1.1$ cfs and 90% loading. ....	156
Fig. 6.42: A view of screen operation for $Q=1.1$ cfs and 90% loading.....	157
Fig. 6.43: Inflow patterns with $Q=5.5$ cfs and 10% loading. ....	158
Fig. 6.44: Gross solids being carried over the splash plate and deposited in outflow tank.....	159

Fig. 6.45: Overflow for Q=5.5 cfs and 50% loading.....	160
Fig. 6.46: Overflow for Q=5.5 cfs and 50% loading.....	161
Fig. 6.47: Overflow for Q=5.5 cfs and 50% loading.....	162
Fig. 6.48: Aftermath of Q=5.5 cfs and 50% loading. ....	163
Fig. 6.49: Aftermath of Q=5.5 cfs and 50% loading. ....	164
Fig. 6.50: Aftermath of Q=5.5 cfs and 50% loading. ....	165
Fig. 6.51: Aftermath of Q=5.5 cfs and 50% loading. ....	166

## LIST OF TABLES

Table 3-1: Composition of gross solids as found in highway runoff. ....	24
Table 3-2: Composition of gross solids manufactured in Hydraulics Laboratory. ....	25
Table 4.1: Range of flow and gross-solids loading tested. ....	32
Table 4.2: $h^*$ (in) vs. $x$ (ft) with 50% dry loading for various $Q$ (cfs). $S < 0.1\%$ . ....	45
Table 4.3: $h^*$ (in) vs. $x$ (ft) with 90% dry loading for various $Q$ (cfs). $S < 0.1\%$ . ....	45
Table 4.4 $h^*$ (in) vs. $x$ (ft) with 90% wet loading for various $Q$ (cfs). $S < 0.1\%$ ....	45
Table 4.5: $h^*(x=0)-h^*$ (in) vs. $x$ (ft) with 50% dry loading for various $Q$ (cfs). $S < 0.1\%$ . ....	45
Table 4.6: $h^*(x=0)-h^*$ (in) vs. $x$ (ft) with 90% dry loading for various $Q$ (cfs). $S < 0.1\%$ ....	46
Table 4.7 $h^*(x=0)-h^*$ (in) vs. $x$ (ft) with 90% wet loading for various $Q$ (cfs). $S < 0.1\%$ ....	46
Table 4.8 $n$ vs $Q$ with no trash. $S < 0.1\%$ . ....	46
Table 4.9 $n$ vs $Q$ with 50% dry loading. $S < 0.1\%$ ....	46
Table 4.10 $n$ vs $Q$ with 90% dry loading. $S < 0.1\%$ ....	47
Table 4.11 $n$ vs $Q$ with 50% wet loading. $S < 0.1\%$ ....	47
Table 4.12: 7 section without wing wall, $S < 0.1\%$ ....	61
Table 4.13: 7 section with wing wall, $S < 0.1\%$ ....	61
Table 4.14: 6 section without wing wall, $S < 0.1\%$ ....	61
Table 4.15: 6 section with wing wall, $S < 0.1\%$ ....	61
Table 4.16: 5 section without wing wall, $S < 0.1\%$ ....	62
Table 4.17: 5 section with wing wall, $S < 0.1\%$ ....	62
Table 4.18: 7 section without wing wall, $S = 1.9\%$ ....	66
Table 4.19: 7 section with wing wall, $S = 1.9\%$ ....	67
Table 4.20: 6 section without wing wall, $S = 1.9\%$ ....	67
Table 4.21: 6 section with wing wall, $S = 1.9\%$ ....	67
Table 4.22: 5 section without wing wall, $S = 1.9\%$ ....	68
Table 4.23: 5 section with wing wall, $S = 1.9\%$ ....	68
Table 4.24: $K$ and $A'$ values for the $S < 0.1\%$ tests. ....	79
Table 4.25: $K$ and $A'$ values for the $S = 1.9\%$ tests. ....	80
Table 4.26: $S < 0.1\%$ ....	83
Table 4.27: $S = 1.9\%$ ....	83
Table 4.28: $S = 2.75\%$ ....	83
Table 4.29: $S = 3.25\%$ ....	84
Table 4.30: $S = 4.4\%$ ....	84
Table 5.1: Schedule of tests on the Type 1 parabolic screens GSRD. ....	94
Table 5.2: Measured water depths obtained for various flow rates and gross solids loading. ....	97
Table 5.3: Measured water depth (in) at influent trough as a function of time (min). Column (A): results for test with 5.5 cfs and 50% loading of litter. Column (B): results for test with 11.1 cfs and 90% loading of litter. Time=1 min corresponds to time just before closing of pump. ....	98
Table 6.1: Tests performed on straight inclined screens (Type 2) ....	110

Table 6.2: Clean water tests energy loss calculations for Type 2 inclined screen.  
..... 116

# Section 1: Introduction

## 1.1 Scope of study

In a recent 303(d) list prepared by the California State Water Resources Control Board, at least 36 water bodies were identified where solid trash is considered to be a pollutant of concern (1). The first solid trash TMDL was adopted by the Los Angeles area Regional Water Quality Control Board for the Los Angeles River (2). Similar TMDLs are currently being developed for other watersheds in the State of California.

Concerned with litter accumulation at freeway sites, and in response to the Los Angeles litter TMDL, the California Department of Transportation (Caltrans) commissioned a number of studies to assess the characteristics and potential impact of litter generated from their freeways (3, 4, 5 and 6). The results of these studies provided a basis for Caltrans to develop potential treatment technologies and Best Management Practices to control pollutants in runoff from Caltrans roadways. As part of this effort, Caltrans evaluated the practical applications of several alternative litter capturing devices (6 and 7).

Two generic types of Gross Solids Removal Devices (GSRDs) are being considered for field deployment. One device, designated hereafter as Linear-Radial GSRD, consists of a length of circular stainless steel tube with 0.25 in louvers that is contained in a concrete vault. Litter-laden water enters from one end and litter-free water leaves through the louvers to be accumulated inside the vault before eventually being discharged through an outfall. Gross solids accumulated within this device are removed at specified intervals through access hatches and an end door. The other type of device consists of a large vault with screens of different designs and installation details. The design allows for litter-laden water to flow over the screens permitting clean water to be conveyed through the screens while detaining litter in a storage tank for later removal. Two types of screens are being considered: one which is parabolic in the direction of flow while the other is straight. The two types of screen differ in significant aspects of their operation and installation thereby requiring vaults of significantly different designs and sizes.

The successful deployment of these devices requires knowledge of a number of performance parameters that can only be obtained by actual tests under controlled conditions that resemble as closely as possible the conditions likely to be encountered in Caltrans drainage facilities. The primary parameter of interest relates to the efficiency of the device in the removal of solids under different conditions that influence their hydraulic performance. Those conditions include the flow rate of the storm runoff, the longitudinal slope of the Linear-Radial device and the actual volume of gross solids loading relative to the volume of the device.

In particular, and in order to meet the current requirements, the devices are required to capture gross solids having dimensions greater than 5 mm. Another parameter that is of practical interest relates to the head loss encountered by the water as it flows through the device. This parameter is especially critical for the case of the Linear-Radial GSRD where the head difference between inflow and outflow is relatively small. A device which introduces a large head loss could cause under some configurations the inflow to back-up onto the highway. Moreover, a large head loss would lead to a greater water depth for a given flow rate thus requiring vaults of greater volume than would otherwise be necessary to discharge the clean flow.

In order to assess the hydraulic and solids-capturing performance of these alternative devices, a program of testing was conducted at the Hydraulics Laboratory of the University of California, Davis. The testing was performed on full-scale devices (Linear-Radial and both parabolic and straight screens) that were obtained from their respective manufacturers. The test facility which was used to conduct these tests (consisting essentially of water delivery and circulation systems, trash introduction system and flow and depth measurement instrumentation) was custom built to facilitate the testing over the full-scale versions of devices under controlled conditions.

The expected outcome of this study consisted of the following items:

1. Quantitative data relating to the performance of the three different GSRDs tested under different flow rate and gross solids loading conditions,
2. Observations related to the performance of these devices under operational conditions,
3. Incorporation of the test results for the Linear-Radial GSRD into a design procedure based on HEC-22 guidelines.

This report documents the extent to which each of these outcomes has been attained.

## 1.2 Objectives of study

The principal objectives of this study were as follows:

1. Construct a test facility to facilitate the testing of full-scale models of the Linear-Radial GSRD and of two different types of screen GSRDs: the parabolic (Type 1) and the straight (Type 2) screens. The program of testing is to be carried out for conditions of flow rate and gross-solids loading conditions that are representative of those encountered in Caltrans drainage facilities. The gross solids are to be 'manufactured' in accordance with results of Caltrans-commissioned studies on the composition of highway litter.
2. Conduct tests to obtain data to quantify the hydraulic performance and the gross-solids capturing efficiency of the proposed GSRDs. The tests are also to yield insight into operational aspects relevant to the field deployment of these devices.
3. Incorporate the results of tests on the Linear-Radial GSRD into a design methodology based on HEC-22 procedures.

## 1.3 Personnel

The Principal Investigator was Dr B. A. Younis, Professor of Civil & Environmental Engineering at the University of California, Davis.

Dr M. Kayhanian, Associate Research Engineer, provided technical advice on various aspects of the work, particularly on the composition of gross solids associated with highway runoff.

The Project Development Engineer was Mr W. Hartman, PE.

Dr J. De Vries and Dr I. Tod acted as technical consultants in matters related to analysis of the test results.

The principal contributor to this project in tasks related to data collection and presentation was Mr Ali Ercan, PhD candidate in the Department of Civil & Environmental Engineering. Other contributors were Mr Owen Ransom, a recent graduate of the Department of Land, Air and Water and Mr T. S. Yang, a graduate student in the Department of Civil and Environmental Engineering.

Numerous undergraduate students assisted on ad-hoc basis in various aspects of the testing program.

Construction of the test facility was accomplished by Mark Hannum and Victor Ray, development technicians.

## 1.4 Report Organization

This report is organized in seven sections.

Section 1 presents the scope of the study, its objectives and lists the personnel involved.

Section 2 provides a description of the test facility constructed at the Hydraulics Laboratory to perform the tests described herein.

Section 3 describes the composition of the gross solids manufactured in the Laboratory and used in all the tests

Section 4 reports the test results for the Linear-Radial GSRD.

Section 5 reports the test results for the inclined parabolic screen (Type 1) GSRD.

Section 6 details the results for the inclined straight screen (Type 2) GSRD.

Section 7 presents summary of findings and recommendations.

The report also contains three appendices.

Appendix 1 provides guidelines for the design of a Linear-Radial GSRD based on the HEC-22 Urban Drainage Design Manual. An Excel computation sheet is provided with the electronic version of this report.

Appendix 2 consists of 2 CDs containing digital video footage of tests carried out on the Linear-Radial GSRD. These CDs are labeled: "Linear-Radial 0-55 min" and "Linear-Radial 55+".

Appendix 3 consists of two CDs of footage of tests conducted on the parabolic and the straight inclined screens (Phases II and III). These CDs are labeled: "Phase II parabolic screen" and "Phase II parabolic screen and straight screen".

**Copyright of all images provided in this report remains with the University of California, Davis.**

## Section 2: Description of test facility

The test facility was specially constructed for the purpose of carrying out the GSRD tests.

A schematic of the test facility for the Linear-Radial GSRD is shown in Figure 2.1.

A schematic of the test facility for the Phase 2 and 3 GSRDs is shown in Figure 2.2.

Clean water was extracted from a sump measuring 15'x10'x12' (Figs. 2.3a and 2.3b) using an axial pump manufactured by the Cascade Pump Co. and running at constant speed of 880 RPM (Fig. 2.4). The maximum delivery flow rate was 35 cfs. The discharge was piped through a 30" square duct into a receiving tank measuring 5'x4'x6' (Fig. 2.5). Inflow to this tank was controlled by means of a gate valve (Fig. 2.6). The water volume in excess of that required for a particular test passed through an overspill weir (Fig. 2.7) and from there via a 30" diameter pipe returned to the sump. Water in the receiving tank was then piped through a 24" diameter pipe to a tank measuring 5'x4'x6' (Fig. 2.8). Solids were introduced into this tank and transported by the flowing water to the GSRD being tested.

For the purpose of testing the Linear-Radial device, a vault 40' long, 5' wide and 5' deep was constructed from ¼" plywood sections and installed on a flat trailer bed (Fig. 2.9). This arrangement allowed the vault to be sloped at different slopes in the longitudinal direction. The surfaces of this vault were sealed with water proof paint containing amounts of fine sand added to simulate the texture of the concrete-lined vaults used in the field. The Linear-Radial device was attached to the inlet of this vault (Fig. 2.10). The outlet from the vault was connected to a sloped 24" diameter pipe which discharged into a receiving tank measuring 5'x4'x6' (Fig. 2.11). This, in turn connected to a 24" diameter pipe leading to a downstream receiving tank of dimensions 5'x4'x6' (Fig. 2.12). A collection bag made of wire mesh having openings of 0.25 in square was attached inside this tank to capture solid not captured in the tested devices (Fig. 2.13). A rectangular weir was installed in this tank in order to ensure that the upstream pipe was always running full. This was necessary to ensure proper operation of the ultrasound flow meter (supplied by Dynasonics Inc.). Downstream of this last tank, the water was returned via a 3' diameter pipe to the sump for recirculation (Fig. 2.14).

For the purposes of testing the Type 1 and 2 screens, water supply into their vaults was obtained via a 24" pipe fed from the first storage tank downstream of the pump where the gate valve was located (Figs. 2.2 and 2.15). The vaults in which these screens were mounted were not placed on the trailer but, rather, they were placed directly on the ground. This was due to their excessive size and

weight (Fig. 2.16) and, also, because testing for the effect of vault slope was not required.

An inflow tank was installed upstream of the vaults in order to introduce the solids (Fig. 2.17).

The outflow was connected to the same receiving tank used for the Linear-Radial device (Fig. 2.18) and returned to the same sump for recirculation.

Water loss by leakage from various components of the test facility was replaced by fresh water from the mains supply feeding directly into the sump.

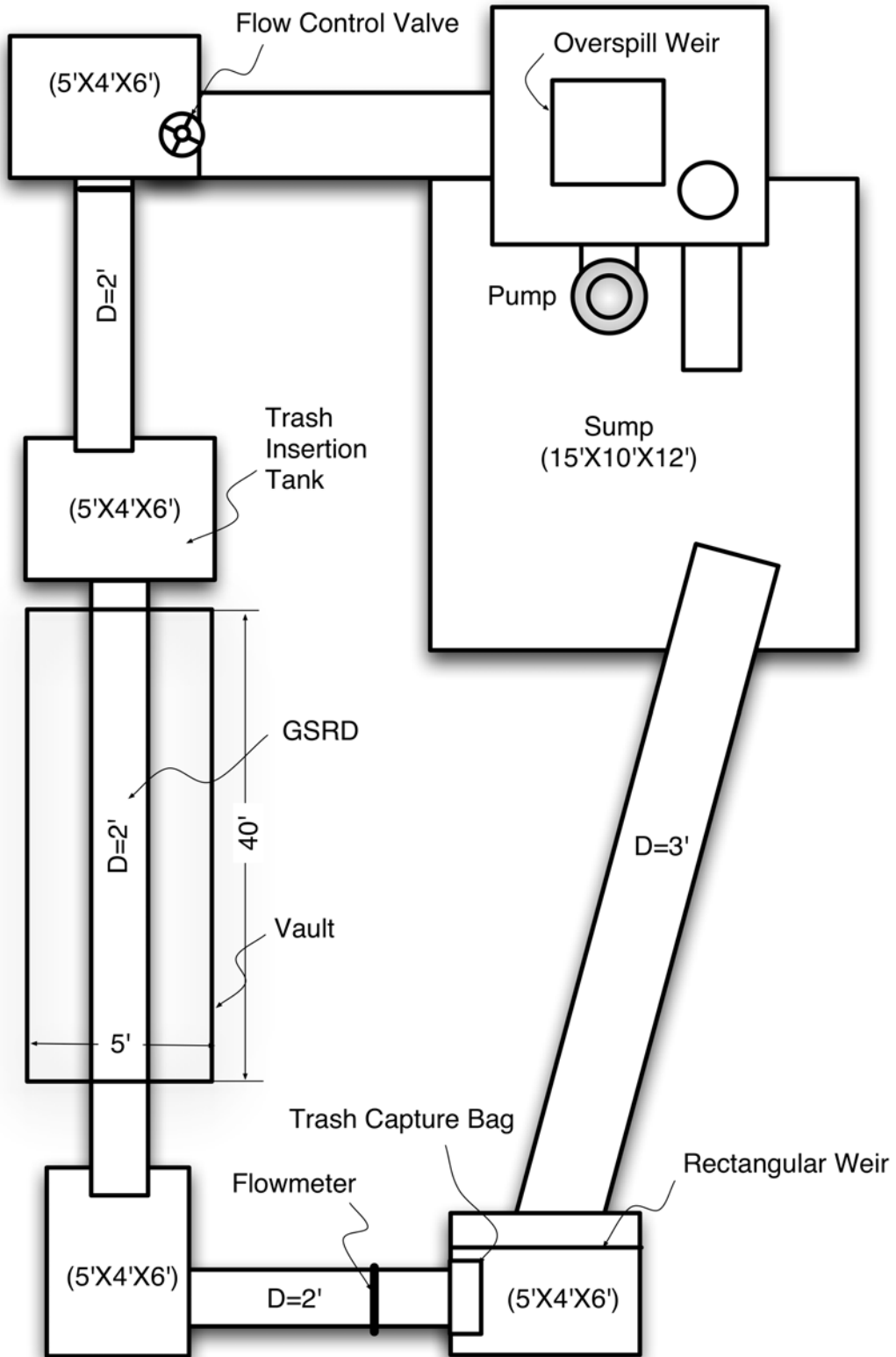


Fig. 2.1: Overview of layout of test facility for Linear-Radial GSRD.

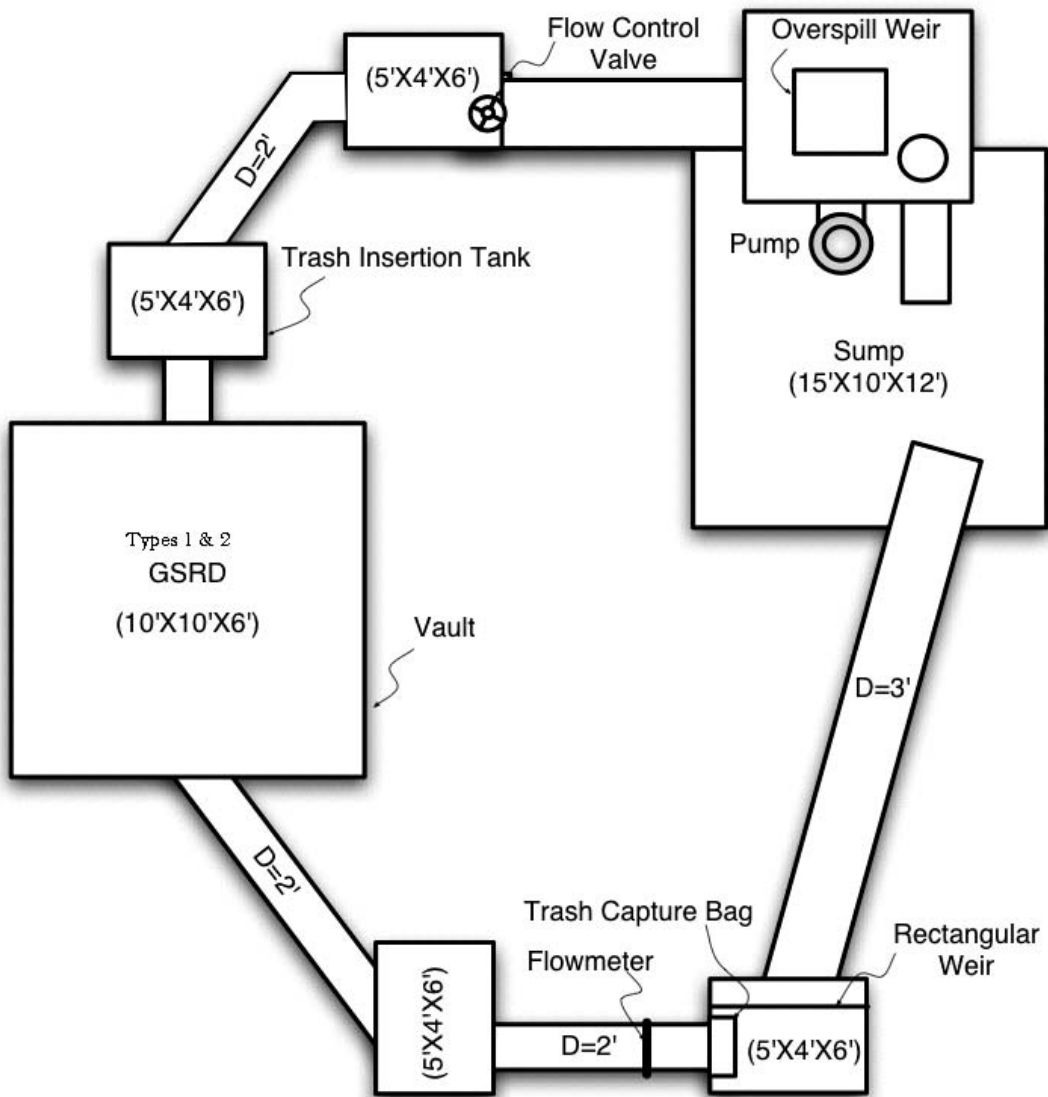


Fig. 2.2: Layout of test facility for Types 1 and 2 GSRDs.



Fig. 2.3a: Sump, pump and overflow return.



Fig. 2.3b: View of sump, pump, and pipes for return flow.



Fig. 2.4: Pump and supply to devices and overspill weir



Fig. 2.5: Square pipe supply to first receiving tank.

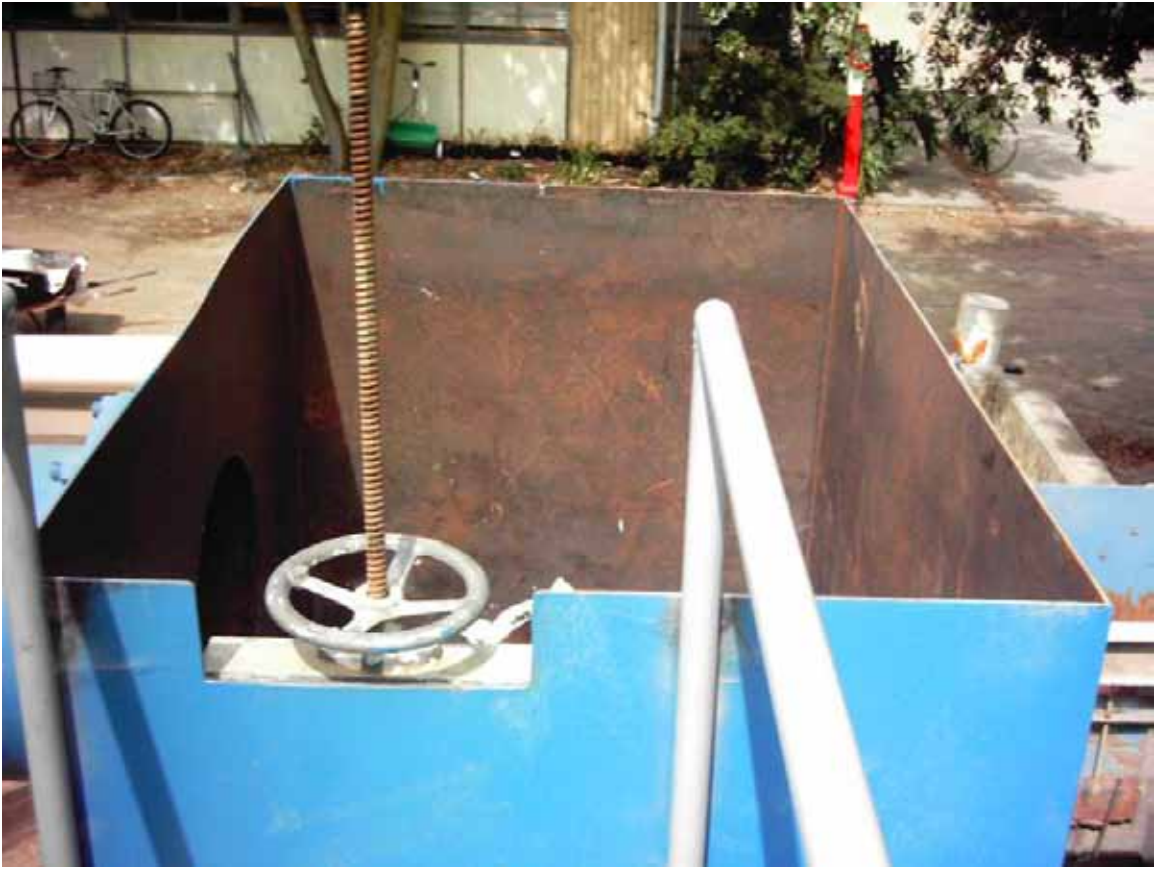


Fig. 2.6: Gate valve to regulate flow rate through GSRDs.



Fig. 2.7: Overspill weir and return to sump.



Fig. 2.8: Delivery to trash insertion tank



Fig. 2.9: Vault on flat trailer bed.



Fig. 2.10: Inside of vault showing Linear Radial device.



Fig. 2.11: Outfall from vault and downstream receiving tank.



Fig. 2.12: Downstream receiving tanks.



Fig. 2.13: 0.25" square wire mesh used for litter capture downstream of GSRD.



Fig. 2.14: 3' diameter return pipe to sump.



Fig. 2.15: Water supply to Types 1 and 2 GSRDs.



Fig. 2.16: Vault containing Type 1 inclined screen.



Fig. 2.17: Gross solids insertion box for Types 1 and 2 GSRDs.



Fig. 2.18: Return flow from Types 1 and 2 GSRDs.

### Section 3: Composition of gross solids

All gross solids used in the tests were ‘manufactured’ in the Hydraulics Laboratory. A standard mix was prepared according to the previous gross solids characterization studies carried out in the Department of Civil and Environmental Engineering on behalf of Caltrans. Fortunately, most of Caltrans’s commissioned field gross solids characterization studies were performed in the Los Angeles area which is also where the proposed GSRDs are likely to be deployed. The gross solids collected usually included vegetation and sediments and are captured from Caltrans storm discharge outfalls using the nylon mesh bags.

Figures 3.1 and 3.2 show a typical gross solids load collected from Caltrans highway outfalls. The manufactured mix contained vegetation in the form of tree leaves. The mix also contained sediments which circulated throughout the test facility.

The standard mix was used for all tests carried out on all three GSRDs performance evaluation.

The target composition of gross solids by percentage volume and weight is given in Table 3.1 and in Figure 3.3.

Category	% by Air Dried Weight	% by Volume
Cardboard/chipboard	11	11
Cigarette butts	14	13
Cloth	7	5
Metal (foil and molded)	8	5
Paper	15	22
Plastic-film	6	14
Plastic-moldable	22	11
Styrofoam	4	12
Wood	10	6
Glass	1	<1
Other	2	1

Table 3-1: Composition of gross solids as found in highway runoff.

This composition shown in Table 3-1 was replicated for the tests by using commercially available materials.

Specifically, cigarette butts were simulated by new cigarette filters (50,000 were purchased). Plastic film was simulated using sheets of 1 foot square clear plastic having the same constitution as plastic grocery bags. Paper was mainly in the form of newsprint and other office paper obtained from the UC Davis recycling plant. Wood was in the form of popsicle sticks.

No glass was used in the present tests. The composition of the laboratory gross solids is given in Table 3-2.

<b>Category</b>	<b>Material in mix</b>	<b>% by Volume</b>
Cardboard/chipboard	Shredded cardboard	11
Cigarette butts	Filter stock	13
Cloth	Cloth strips	5
Metal (foil and molded)	Shredded aluminum foil	5
Paper	Shredded newspaper	23
Plastic-film	Shredded plastic film	14
Plastic-moldable	Chopped plastic	11
Styrofoam	Shredded Styrofoam popcorn and cups	12
Wood	Popsicle sticks	6

Table 3-2: Composition of gross solids manufactured in Hydraulics Laboratory.

The gross solids mix was prepared in large batches and mixed thoroughly. It was stored in containers till required for the tests. Used solids were recycled after each test. By the end of the testing period, the solids were 'weathered' and resembled very closely in texture and size the actual solids found in highway runoffs.



Fig 3.1: Gross solids including vegetation and sediment



Fig. 3.2: Dry gross solids collected from Caltrans outfalls.

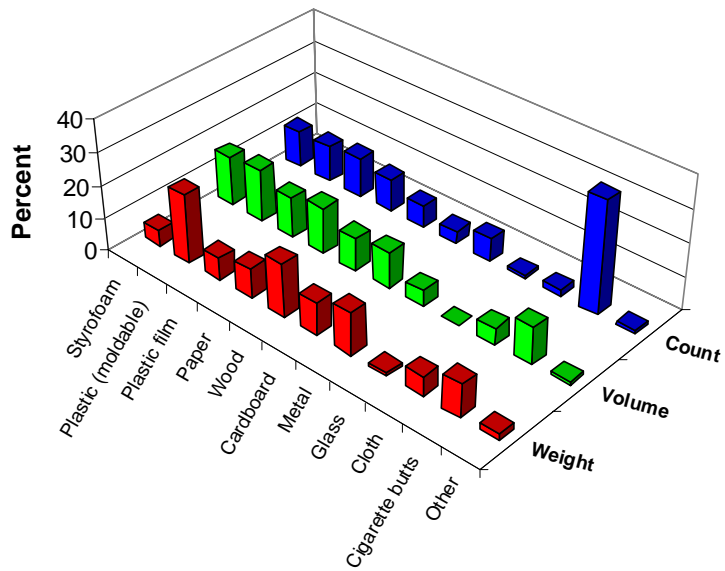


Fig. 3.3: Relative composition of litter from highway outfalls based on count, weight and volume (from Kayhanian et al., 2002)

A view of the gross solids mix manufactured in the Hydraulics Laboratory is shown in Fig. 3.4. Repeated use and re-use rendered the texture very similar to that collected from highway runoffs.



Figure 3.4: Gross solids mix manufactured in the Hydraulics Laboratory.

## **Section 4: Results for Linear-Radial GSRD**

### **4.1 Description of Linear-Radial device**

The Linear-Radial device tested was manufactured and delivered by Roscoe-Moss (4360 Worth Street, Los Angeles, CA 90063, Tel: (323)263-4111, Fax: (323) 263-4497).

This device is basically a water-well screen, except that 60 degrees around the circumference is non-louvered (invert when placed). The louvers were 5 mm across and 6 cm long.

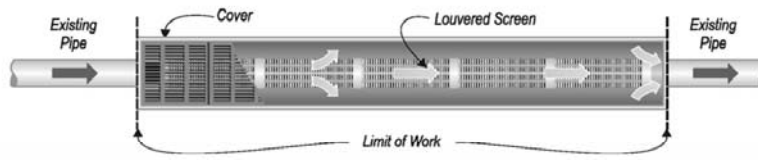
Below are the manufacturer's specifications of the device delivered for testing:

1. 7 sections of Linear-Radial device. This is referred to by the manufacturer as "Storm Flo Screen". Each section is 5 ft long making a maximum total length of 35 ft. Each section is 24 inches in diameter and has 0.25 in openings. The bottom of each section was unlouvered (blank).
2. 1 section of steel pipe with overflow, 3 ft long, 24 inches in diameter.
3. 7 steel perforated top hatches, each 3 ft long, with hinges, latches and handles to facilitate gross solids removal.
4. 1 steel louvered end door, 24 inches in diameter, with latch and hinge
5. 32 Steel bottom supports
6. 16 Steel lifting eyelets
7. 7 sets Steel coupling collars with bolts, nuts and washers
8. 1 - 36" x 36" x 1/2" steel anchor plate with 24" diameter opening and bolt holes (anchor plate to be furnished welded to the 3' blank pipe section, see item 2)

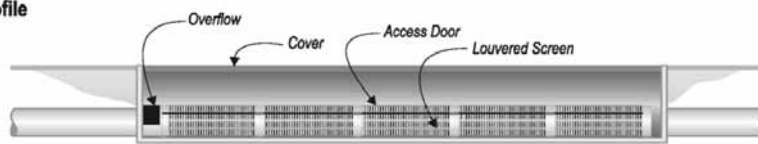
All material used was Type 304 stainless steel.

The Linear-Radial device was installed inside a vault made of 0.75 in treated and finished plywood sheets (Fig 4.2). The total length of the vault was 40 ft, the width of the vault was 5 ft and the height was 4 feet.

**Plan View**



**Profile**



**Section**



**Isometric**

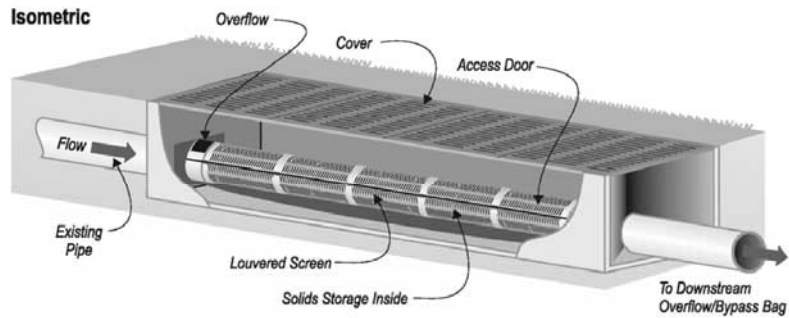


Fig. 4.1: Schematic of the Linear-Radial GSRD.



Fig. 4.2: Linear-Radial GSRD in vault at UC Davis.

## 4.2 Test procedure and data collection

The tests were designed to obtain quantitative measurements as well as qualitative information (by visualization) related to the gross-solids capture efficiency and the hydraulic performance of the Linear-Radial device under a wide range of flow and debris loading conditions.

The Task Order called for tests to be conducted for two values of the longitudinal slopes:  $S < 0.1\%$  and  $S = 1.9\%$ . On completion of those tests, it was thought useful to carry out further tests to determine the head losses for greater values of the slope. Therefore, tests were carried out for  $S = 2.75\%$ ,  $3.25\%$  and  $4.4\%$ ; the latter being the greatest value of slope attainable in the test set-up.

In the course of carrying out the tests, it was observed that the hydraulic efficiency of the outlet from the vault could be improved by the addition of wing walls inclined at 45 degrees from the head wall. Further tests were therefore carried out with such wing walls in place.

Table 4.1 lists the range of flow rates and gross solids loadings tested:

<b>Flow (% of Capacity/cfs)</b>	<b>Percent of gross solids loading</b>
10%/2.7 cfs	0
10%/2.7 cfs	10
10%/2.7 cfs	50
10%/2.7 cfs	90
50%/13.5 cfs	10
50%/13.5 cfs	50
50%/13.5 cfs	90
110%/30 cfs	50
110%/30 cfs	50
110%/30 cfs	90
110%/30 cfs	0

Table 4.1: Range of flow and gross-solids loading tested.

The 'Gross-solids' column in Table 4.1 refers to the volume of added debris used for each test. The terminology used here is as follows: 100% of design loading corresponds to one half the total volume of a 7-sectioned Linear-Radial device. This latter volume amounts to approximately 100 cubic feet. Thus a '10% gross-solids volume' loading corresponds to a dry mix of gross solids having a volume of 5 cubic feet.

The test procedure was as follows:

1. The specified volume of dry gross solids mix was introduced into the receiving tank immediately upstream of the Linear-Radial GSRD.
2. The specified flow rate was applied. The vast majority of the tests reported below were conducted for steady state flow rate conditions only. Selected tests were repeated with the flow rate applied in the form of a one hour triangular hydrograph and these showed similar behavior to the steady-state cases performed at the same peak flow rate.
3. Measurements were collected at 15-minute intervals and included the following parameters:
  - The flow rate as indicated by the Dynasonis ultrasound flow meter.
  - The hydrostatic head at exit of 24" inflow pipe
  - The hydrostatic head at 8 locations along the length of the vault
  - The hydrostatic head at inlet of 24" outflow pipe

For each of the tests involving gross solids, a removable bag was installed downstream of the Linear-Radial GSRD. This bag was emptied at the end of each test and its contents examined in order to determine the nature and quantity of gross solids not captured by the device.

At conclusion of each test, the gross solids captured in the device were removed, dried and reused in later tests.

For selected tests, measurements of the mean velocity in the vault in planes normal to the direction of flow were obtained at selected locations along the direction of flow using a calibrated propeller meter.

All tests were documented using a digital video camcorder. A CD of all footage taken is included as Appendix 2.

In order to account for small variations in the vault bed elevation, all measurements of the water surface elevation are referenced to a common datum. This datum is defined as a line parallel to the surface of still water contained in the vault to a depth equal to the invert of the exit pipe. The elevation is referred to in the text as  $h^*$ .

Figure 4.3 presents a longitudinal cross section indicating the locations where depth measurements were made.

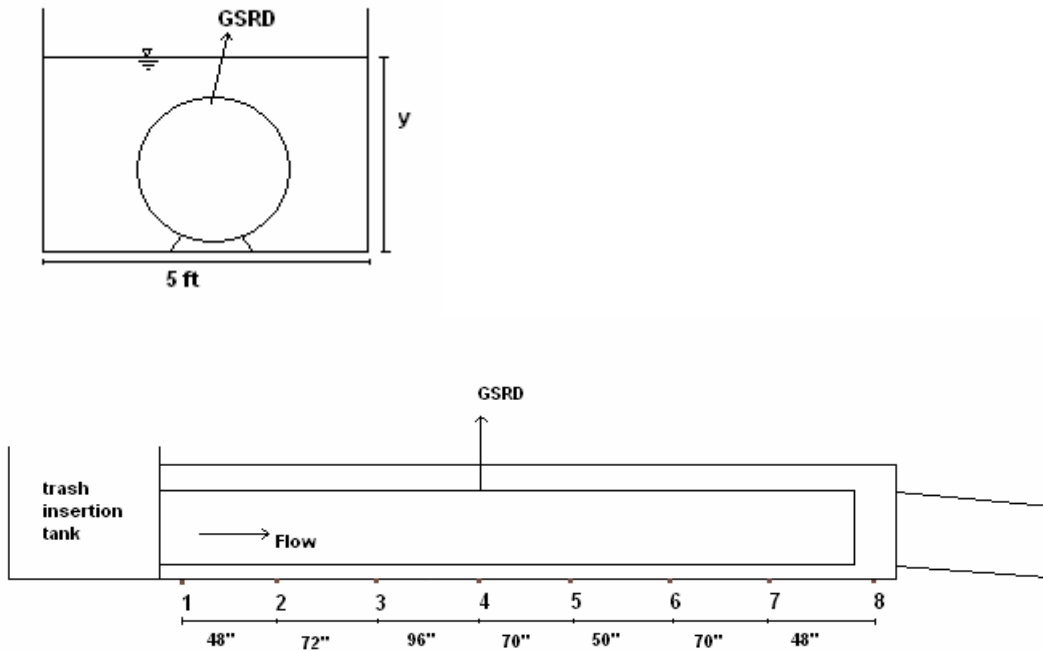


Fig. 4.3: Cross section through Linear-Radial device showing locations of measurements stations.

The head water ( $y_1$ ) at the inlet tank upstream of the Linear-Radial GSRD refers to the water depth in the inlet tank relative to the base of the tank. The invert of the inlet pipe is at distance of approximately 1" from the base of the tank. Measurements of the variation of the  $y_1$  with flow rate serve as the starting point in backwater curve calculations.

The total energy head at the inlet tank is found from

$$H_1 = y_1 + \frac{V_1^2}{2g} + z_1 \quad \dots 1$$

where  $y_1$  is the head water depth,  $\frac{V_1^2}{2g}$  is the velocity head, and  $z_1$  is the elevation of the tank bed.

The average velocity in at inlet was calculated from:

$$V_1 = \frac{Q}{A_1}$$

where  $A_1$  is flow area.

Head loss is defined in the usual way, i.e. the difference between the EGL at inlet and exit from the vault:

$$y_1 + \frac{V_1^2}{2g} + z_1 = y_2 + \frac{V_2^2}{2g} + z_2 + \Delta h \quad \dots 2$$

When results are plotted vs. Reynolds number, this parameter is defined as:

$$Re = \frac{VD}{\nu} \quad \dots 3$$

where  $D$  is the diameter of circular pipe and  $V$  is a representative velocity obtained from  $V=Q/A$  where  $A$  is the cross-sectional area of a circular pipe of diameter 24".

The tests enabled an estimate for Manning's  $n$  appropriate to the combination of vault and Linear-Radial device to be obtained. This was done using the equation for conveyance in open-channel flows:

$$Q = \frac{C_m}{n} AR^{2/3} S^{1/2} \quad \dots 4$$

The measurements of water surface elevation and the constant width of the vault were used to evaluate the flow cross-sectional area and the hydraulic radius.

The slope was calculated in two ways:

1. From measurement of the bed surface elevation and,
2. From measurements of water surface elevation. The slope of the water surface would equal the slope of the channel bed if uniform flow conditions are assumed to apply.

## 4.3 Test results

[All tests were recorded on a digital video camera. A CD of the recording is included in Appendix 1]

### 4.3.1 7-Section GSRD ( $S < 0.1\%$ )

The volume of the gross solids introduced into the Linear-Radial GSRD decreased in the course of the tests. This was due to both the wetting of material such as paper and cardboard and the compaction of the whole mix by the force of flow in the device. In order to quantify the blockage effect associated with the gross solids, tests were conducted wherein gross solids mix was continuously introduced over an extended period of time till it filled approximately one half of the total volume of the device. The loading for these runs is identified in Table 4.4 as 'wet'.

The water surface elevation inside the vault is expected to depend on the flow rate, distance along the vault from its inlet and on the volume of the gross solids loading.

This can be seen from figures 4.4 - 4.6 which show the variation of water-surface elevation with distance along the vault. This distance is measured from the vault inlet and is quoted in feet. The results shown in these figures are for gross solid volume loading values of 50% dry, 90% dry and 90% wet.

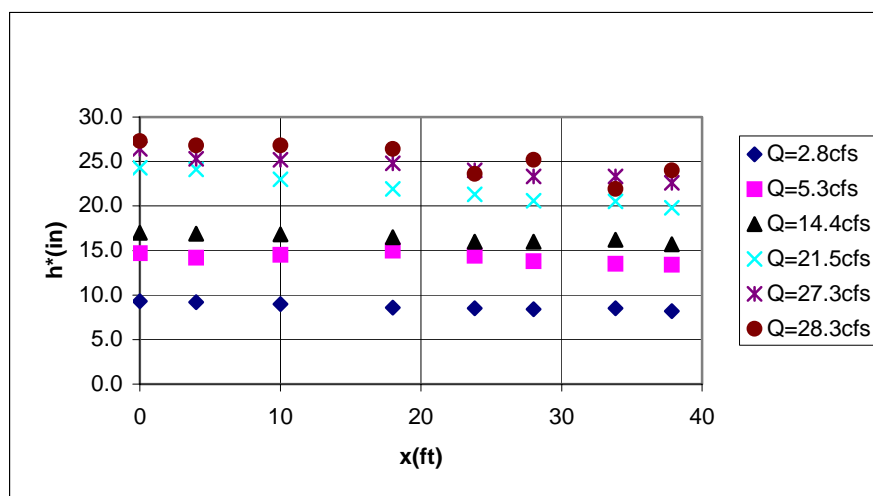


Fig. 4.4: Variation of water surface elevation with distance along vault. Results shown are for 7 section device for 50% dry loading and for slope  $< 0.1\%$

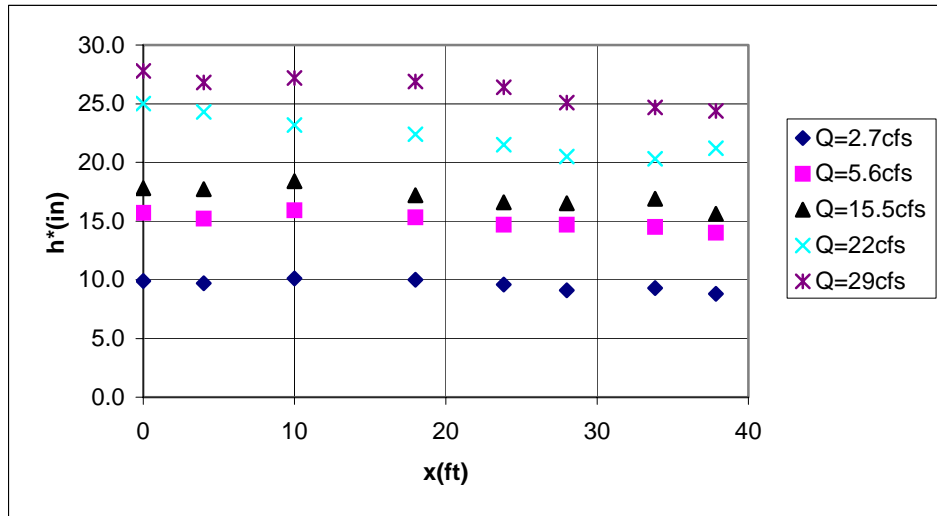


Fig. 4.5: Variation of water surface elevation with distance along vault. Results shown are for 7 section device for 90% dry loading and for slope <0.1%

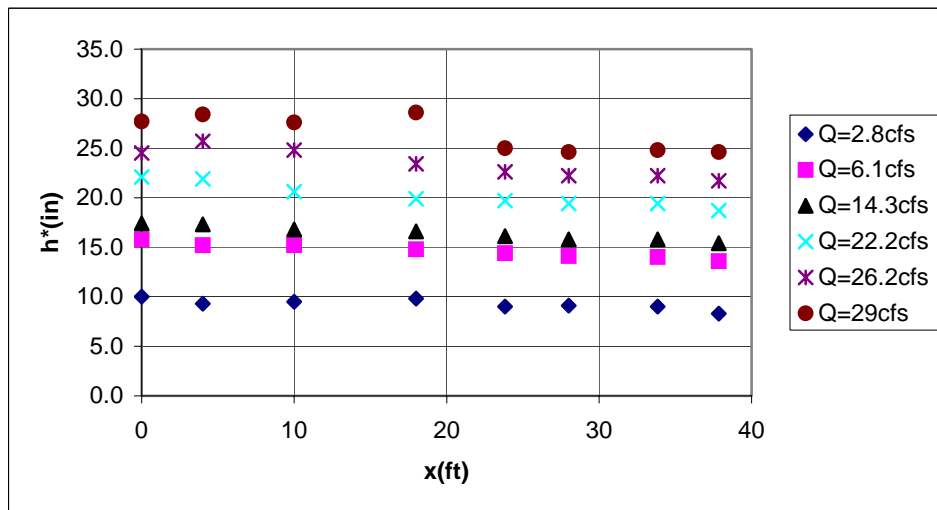


Fig. 4.6: Variation of water surface elevation with distance along vault. Results shown are for 7 section device for 90% wet loading and for slope <0.1%

The maximum of surface elevation obtained in the tests for  $S < 0.1\%$  was 28 inches. This value was recorded at inlet to the vault, for a flow rate of 29 cfs and for 90% dry litter loading.

The variation of the water surface elevation with flow rate is shown in Figure 4.6. Plotted there are the measurements obtained for all volumes of gross solids loading tested.

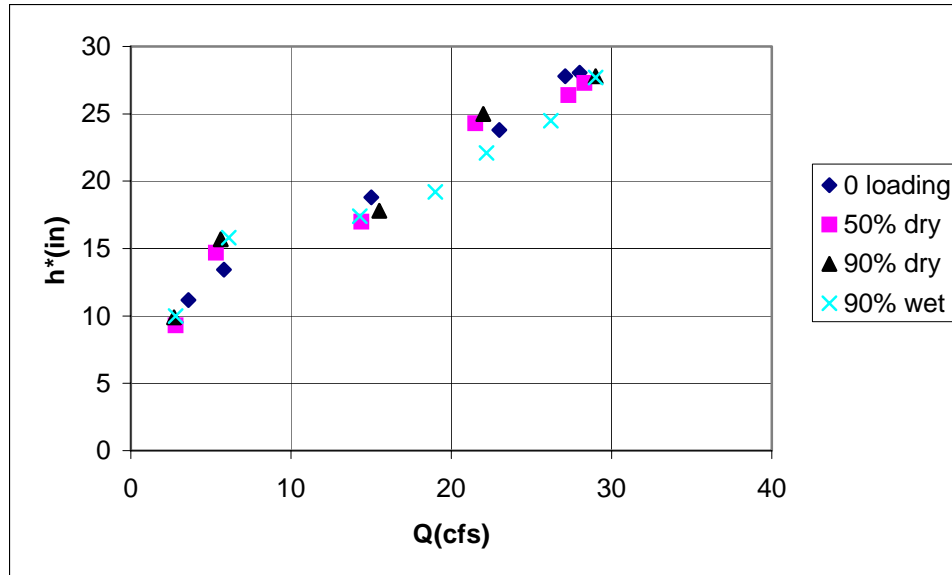


Fig. 4.7: Variation of water surface elevation at inlet to the vault with flow rate. Results shown are for 7 section device and for slope <0.1%

At inlet to the vault, the water surface elevation (in inches) is reasonably well correlated with flow rate (in cfs) by the relationship:

$$h^* = 7.0Q^{0.38} \quad \dots 5$$

Translating this into a relation of the volume of water contained within the vault to the inflow flow rate there results

$$Volume = 35.0Q^{0.38} \quad \dots 6$$

This result can be used to provide guidance on the sizing of the vault for a particular watershed.

The slope of the vault (assumed to be the same as the slope of the Linear-radial device) was calculated in two ways:

3. From measurement of the bed surface elevation and,
4. From measurements of water surface elevation. The slope of the water surface would exactly equal the channel slope if uniform flow conditions applied, but the two slopes are only approximately equal so here.

Due to flow disturbance close to the inlet to the vault, the value of  $n$  is not expected to be constant throughout the length but rather to initially vary with distance along the device till an asymptotic level is reached. This behavior is seen in Fig. 4.8 where the values of  $n$  deduced from depth measurements from various stations are plotted. In that figure, the notation  $n_{13}$  means that the value of  $n$  was deduced from measurements obtained at stations 1 and 3.

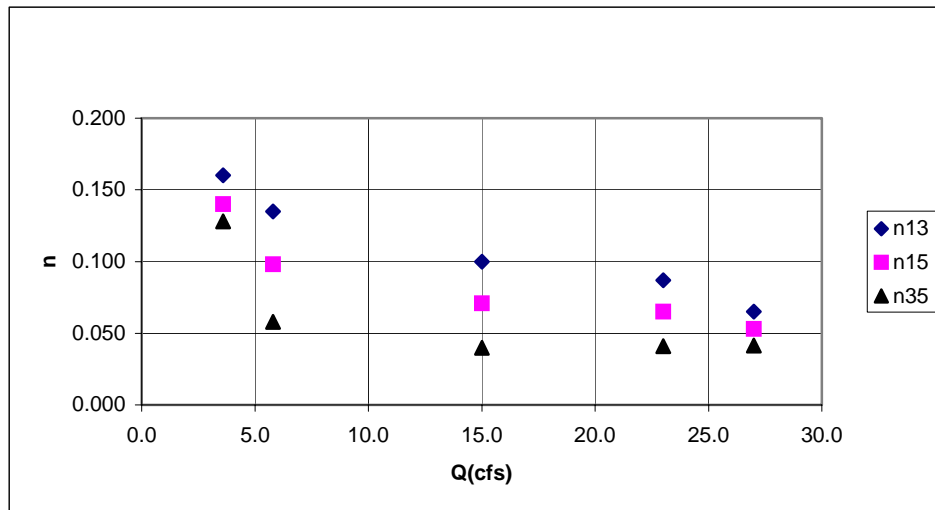


Fig. 4.8: Manning's  $n$  vs flow rate for 7 section device with no gross solids loading and for  $S < 0.1\%$ .

The value of  $n$  is also expected to depend on the flow rate  $Q$  since that determines the water level in the vault and the degree to which the Linear-Radial device is inundated by the flow. This dependence is shown in Figure 4.8.

It should be remembered that Manning's  $n$  is essentially a one-dimensional flow concept, applicable in unidirectional flows where the losses are principally due to friction at the wall. This is far from being the case here. The free-surface flow was observed to move in the opposite direction to the main flow in the vault. This induces significant additional shear losses which are not commonly accounted for in Manning's equation. This, in part, explains the high values of  $n$  obtained in the measurements.

The dependence of  $n$  on the litter loading is shown in Figures 4.9-4.11.

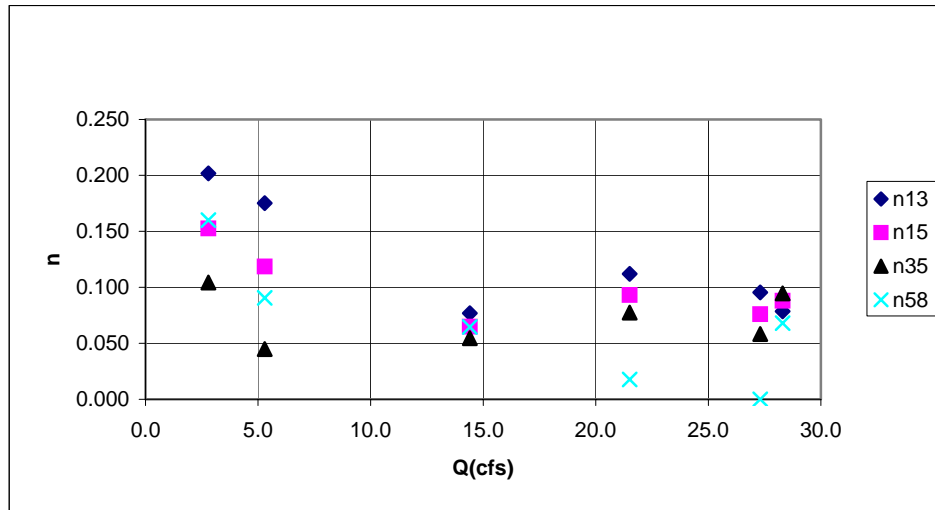


Fig. 4.9: Manning's  $n$  vs flow rate for 7 section device with 50% dry gross solids loading and for  $S < 0.1\%$ .

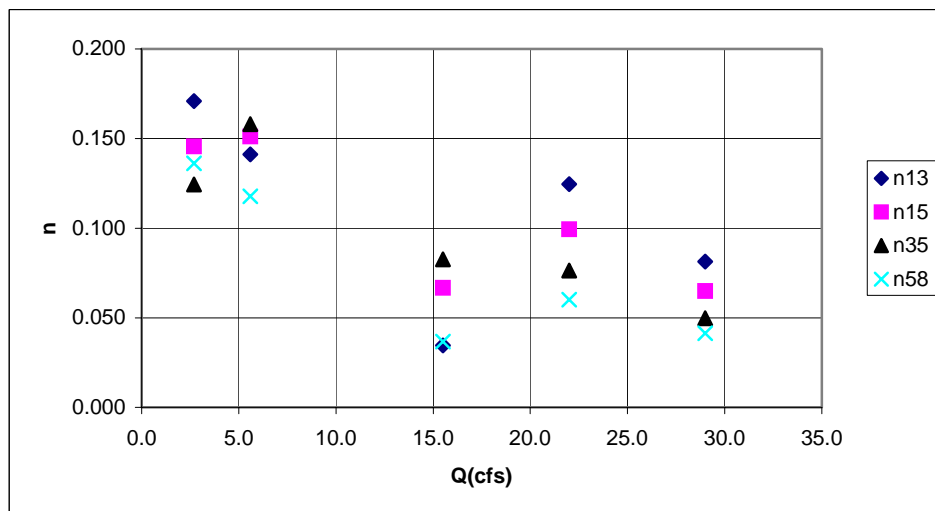


Fig. 4.10: Manning's  $n$  vs flow rate for 7 section device with 90% dry gross solids loading and for  $S < 0.1\%$ .

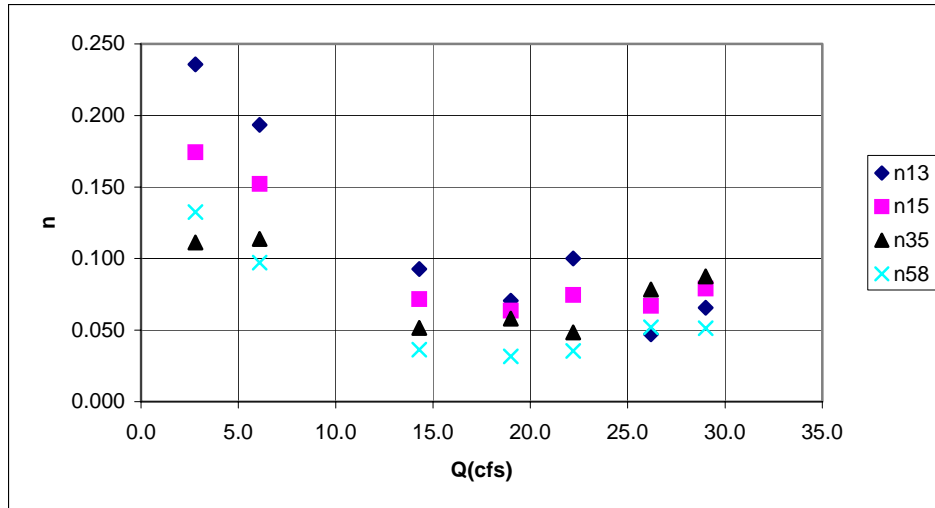


Fig. 4.11: Manning's n vs flow rate for 7 section device with 90% wet gross solids loading and for  $S < 0.1\%$ .

Figure 4.12 shows the dependence of the averaged value of n on the flow rate, Q. The results plotted there are for all % loading and show a clear trend of reduction in n with increase in Q. No clear dependence on the % litter loading can be discerned.

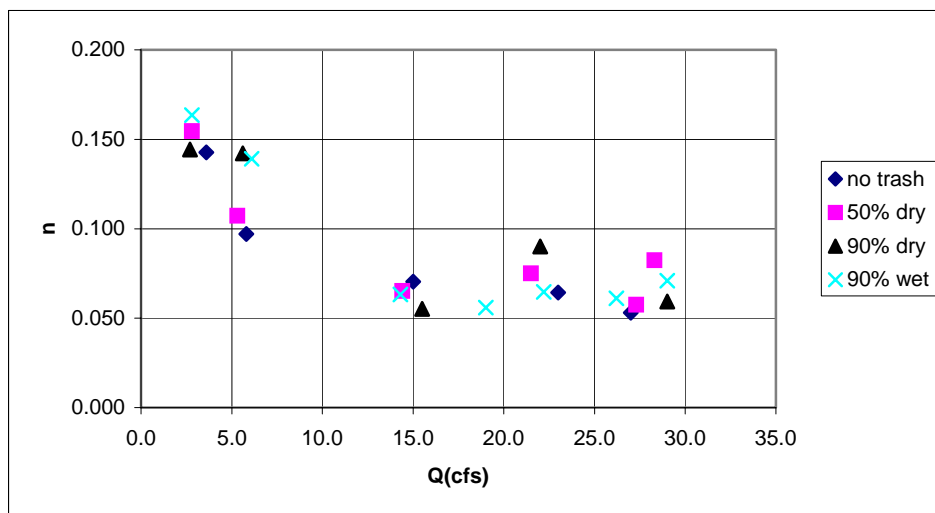


Fig. 4.12: Average value of Manning's n vs flow rate for 7 section device for  $S < 0.1\%$ .

Figure 4.13 shows the variation of head water at the inlet tank ( $y_1$ ) with flow rate.

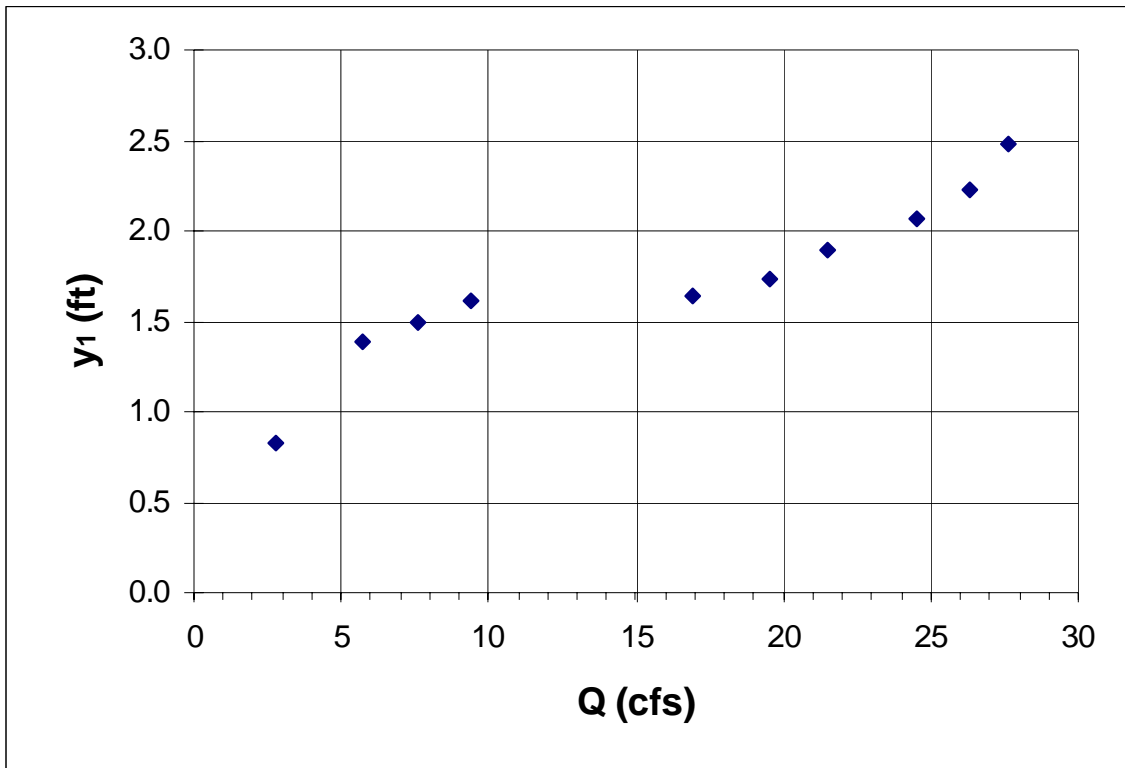


Fig. 4.13: Variation of head water with flow rate for  $S < 0.1\%$ .

The total head at inlet to the Linear-Radial GSRD is presented in Figs 4.14-4.16.

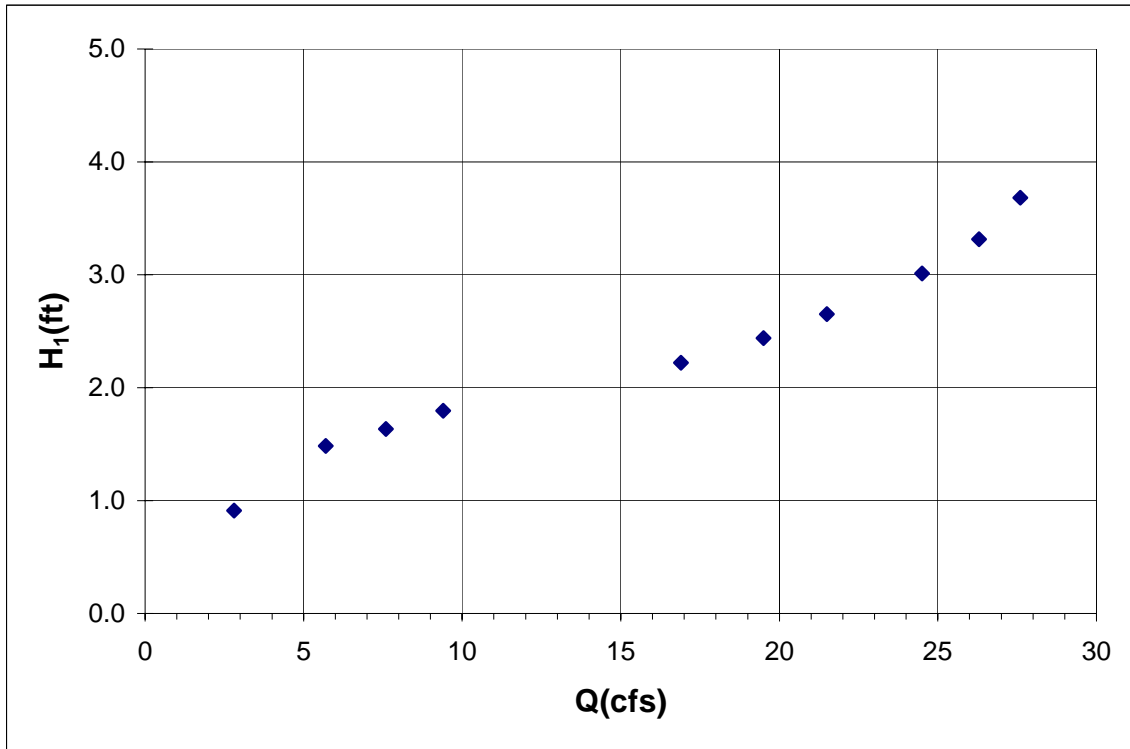


Fig. 4.14: Plot of total head  $H_1$  vs flow rate for  $S < 0.1\%$

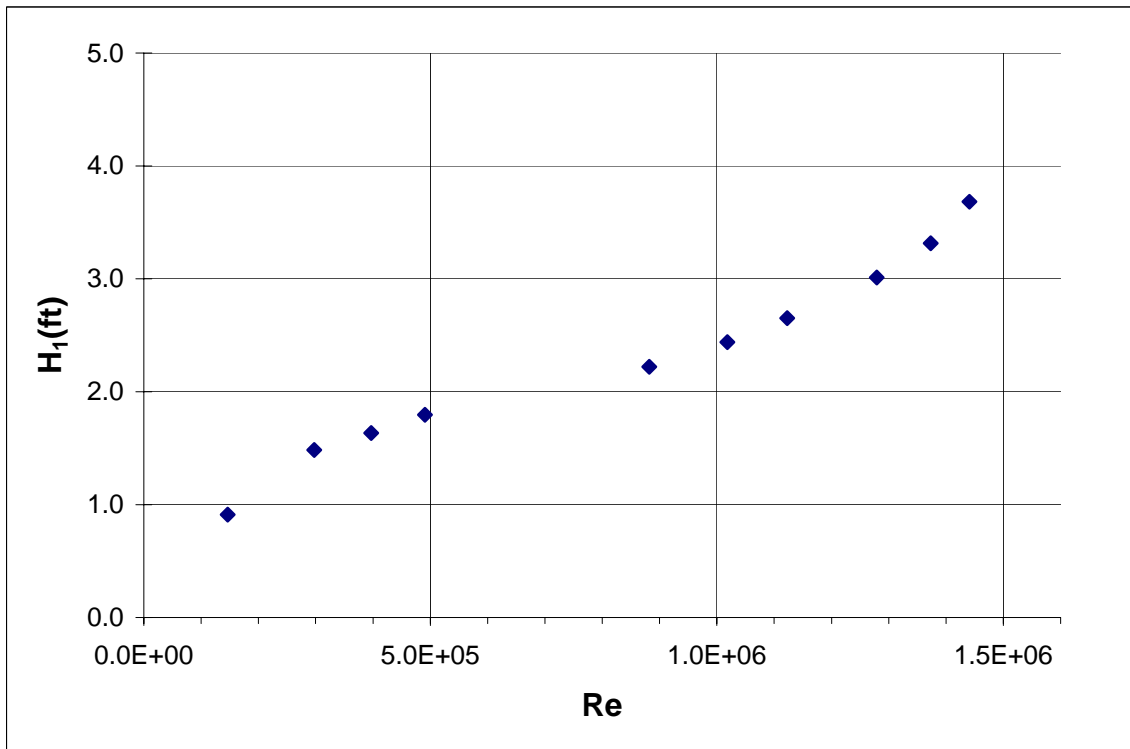


Fig. 4.15: Plot of total head  $H_1$  vs  $Re$  for  $S < 0.1\%$ .

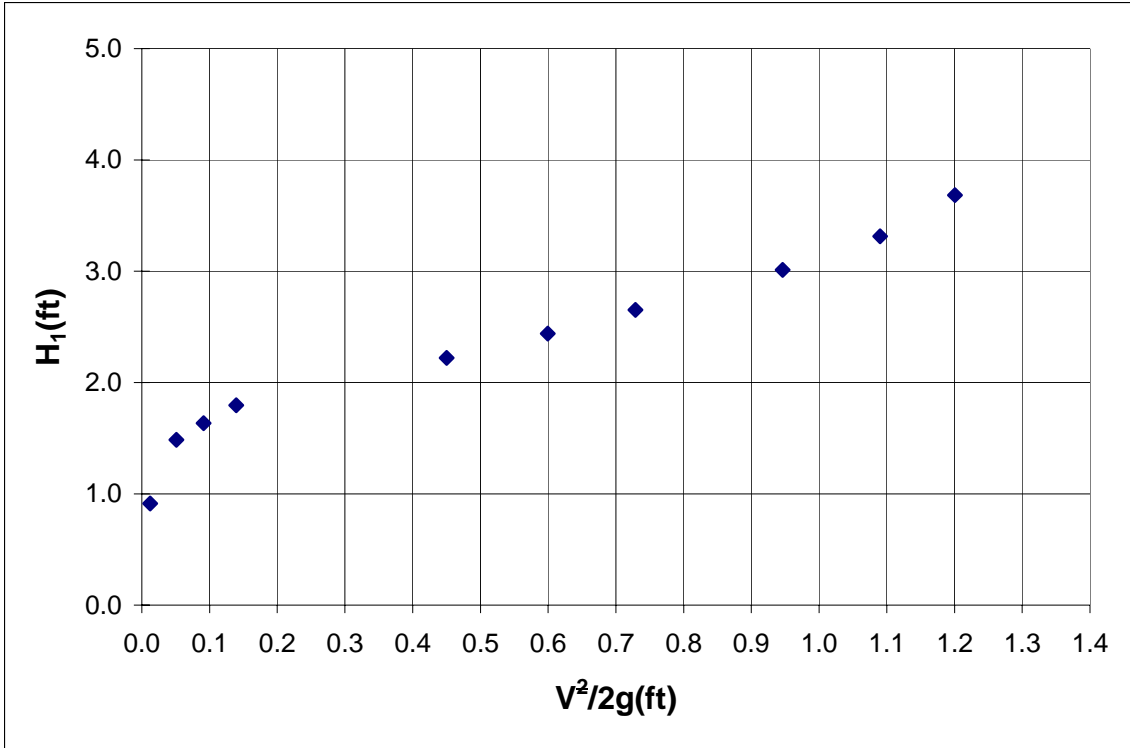


Fig. 4.16: Plot of total head  $H_1$  vs  $V^2/2g$  for  $S < 0.1\%$ .

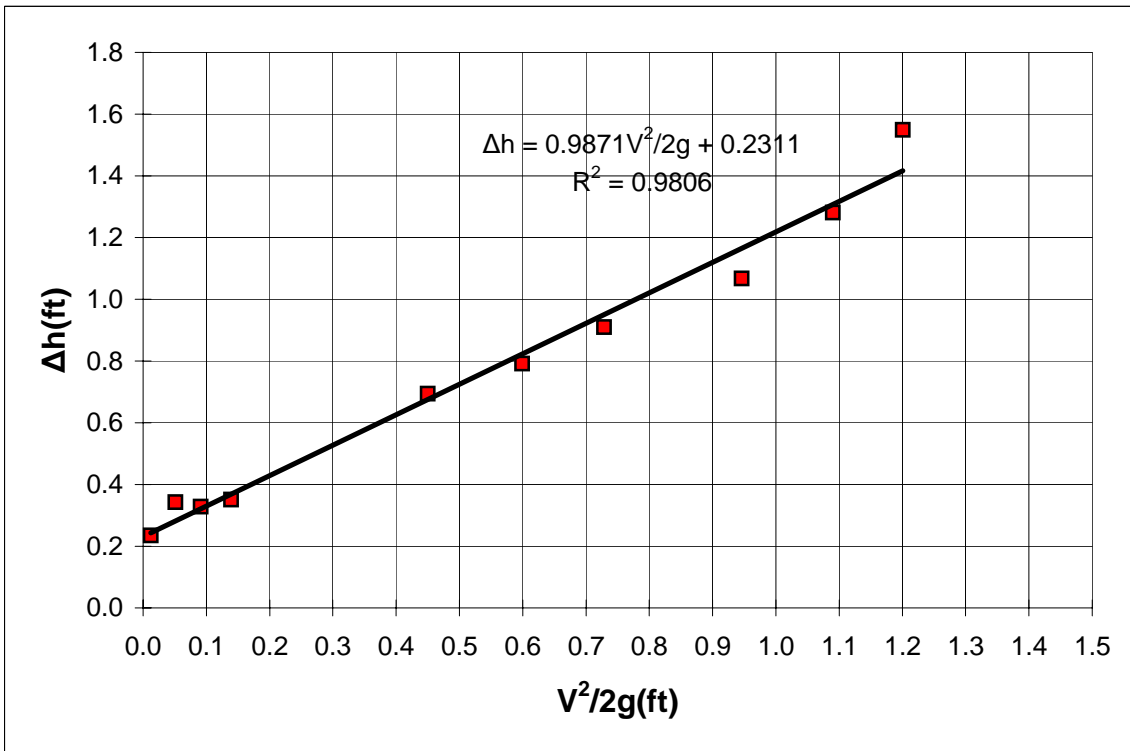


Fig. 4.17:  $\Delta h$  vs  $V^2/2g$  for  $S < 0.1\%$

	Q=2.8cfs	Q=5.3cfs	Q=14.4cfs	Q=21.5cfs	Q=27.3cfs	Q=28.3cfs
x=0 ft	9.3	14.7	17.0	24.3	26.4	27.3
x=4 ft	9.2	14.2	16.9	24.1	25.3	26.8
x=10 ft	9.0	14.5	16.8	23.0	25.2	26.8
x=18 ft	8.6	15.0	16.5	21.9	24.8	26.4
x=23.83 ft	8.5	14.4	16.0	21.3	24.0	23.6
x=28 ft	8.4	13.8	16.0	20.6	23.3	25.2
x=33.83 ft	8.5	13.5	16.2	20.5	23.3	21.9
x=37.83 ft	8.2	13.4	15.7	19.8	22.6	24.0

Table 4.2:  $h^*$  (in) vs.  $x$  (ft) with 50% dry loading for various  $Q$ (cfs).  $S < 0.1\%$ .

	Q=2.7cfs	Q=5.6cfs	Q=15.5cfs	Q=22cfs	Q=29cfs
x=0 ft	9.9	15.7	17.8	25.0	27.8
x=4 ft	9.7	15.2	17.7	24.3	26.8
x=10 ft	10.1	15.9	18.4	23.2	27.2
x=18 ft	10.0	15.3	17.2	22.4	26.9
x=23.83 ft	9.6	14.7	16.6	21.5	26.4
x=28 ft	9.1	14.7	16.5	20.5	25.1
x=33.83 ft	9.3	14.5	16.9	20.3	24.7
x=37.83 ft	8.8	14.0	15.6	21.2	24.4

Table 4.3:  $h^*$  (in) vs.  $x$  (ft) with 90% dry loading for various  $Q$ (cfs).  $S < 0.1\%$

	Q=2.8 cfs	Q=6.1 cfs	Q=14.3 cfs	Q=22.2 cfs	Q=26.2 cfs	Q=29 cfs
x=0 ft	10.0	15.8	17.4	22.1	24.5	27.7
x=4 ft	9.3	15.2	17.3	21.9	25.7	28.4
x=10 ft	9.5	15.2	16.8	20.6	24.8	27.6
x=18 ft	9.8	14.8	16.6	19.9	23.4	28.6
x=23.83 ft	9.0	14.4	16.1	19.7	22.6	25.0
x=28 ft	9.1	14.1	15.8	19.4	22.2	24.6
x=33.83 ft	9.0	14.0	15.8	19.4	22.2	24.8
x=37.83 ft	8.3	13.6	15.4	18.7	21.7	24.6

Table 4.4  $h^*$  (in) vs.  $x$ (ft) with 90% wet loading for various  $Q$ (cfs).  $S < 0.1\%$

	Q=2.8cfs	Q=5.3cfs	Q=14.4cfs	Q=21.5cfs	Q=27.3cfs	Q=28.3cfs
x=0 ft	0	0	0	0	0	0
x=4 ft	0.1	0.5	0.1	0.2	1.1	0.5
x=10 ft	0.3	0.2	0.2	1.3	1.2	0.5
x=18 ft	0.7	-0.3	0.5	2.4	1.6	0.9
x=23.83 ft	0.8	0.3	1.0	3.0	2.4	3.7
x=28 ft	0.9	0.9	1.0	3.7	3.1	2.1
x=33.83 ft	0.8	1.2	0.8	3.8	3.1	5.4
x=37.83 ft	1.1	1.3	1.3	4.5	3.8	3.3

Table 4.5:  $h^*(x=0)-h^*$  (in) vs.  $x$  (ft) with 50% dry loading for various  $Q$ (cfs).  $S < 0.1\%$ .

	Q=2.7cfs	Q=5.6cfs	Q=15.5cfs	Q=22cfs	Q=29cfs
x=0 ft	0	0	0	0	0
x=4 ft	0.2	0.5	0.1	0.7	1.0
x=10 ft	-0.2	-0.2	-0.6	1.8	0.6
x=18 ft	-0.1	0.4	0.6	2.6	0.9
x=23.83 ft	0.3	1.0	1.2	3.5	1.4
x=28 ft	0.8	1.0	1.3	4.5	2.7
x=33.83 ft	0.6	1.2	0.9	4.7	3.1
x=37.83 ft	1.1	1.7	2.2	3.8	3.4

Table 4.6:  $h^*(x=0)-h^*$  (in) vs. x (ft) with 90% dry loading for various Q(cfs).  $S<0.1\%$

	Q=2.8 cfs	Q=6.1 cfs	Q=14.3 cfs	Q=22.2 cfs	Q=26.2 cfs	Q=29 cfs
x=0 ft	0	0	0	0	0	0
x=4 ft	0.7	0.6	0.1	0.2	-1.2	-0.7
x=10 ft	0.5	0.6	0.6	1.5	-0.3	0.1
x=18 ft	0.2	1.0	0.8	2.2	1.1	-0.9
x=23.83 ft	1.0	1.4	1.3	2.4	1.9	2.7
x=28 ft	0.9	1.7	1.6	2.7	2.3	3.1
x=33.83 ft	1.0	1.8	1.6	2.7	2.3	2.9
x=37.83 ft	1.7	2.2	2.0	3.4	2.8	3.1

Table 4.7  $h^*(x=0)-h^*$  (in) vs. x(ft) with 90% wet loading for various Q(cfs).  $S<0.1\%$

Q(cfs)	n13	n15	n35	average
3.6	0.160	0.140	0.128	0.143
5.8	0.135	0.098	0.058	0.097
15.0	0.100	0.071	0.040	0.070
23.0	0.087	0.065	0.041	0.064
27.0	0.065	0.053	0.042	0.053

Table 4.8 n vs Q with no trash.  $S<0.1\%$

Q(cfs)	n13	n15	n35	n58	average
2.8	0.202	0.153	0.104	0.160	0.155
5.3	0.175	0.118	0.045	0.091	0.107
14.4	0.077	0.065	0.055	0.064	0.065
21.5	0.112	0.093	0.077	0.018	0.075
27.3	0.096	0.076	0.058	0.000	0.057
28.3	0.079	0.088	0.095	0.068	0.082

Table 4.9 n vs Q with 50% dry loading.  $S<0.1\%$

<b>Q(cfs)</b>	<b>n13</b>	<b>n15</b>	<b>n35</b>	<b>n58</b>	<b>average</b>
2.7	0.171	0.146	0.124	0.136	0.144
5.6	0.141	0.151	0.158	0.118	0.142
15.5	0.035	0.067	0.083	0.037	0.055
22.0	0.124	0.099	0.076	0.060	0.090
29.0	0.081	0.065	0.050	0.041	0.059

Table 4.10 n vs Q with 90% dry loading. S<0.1%

<b>Q(cfs)</b>	<b>n13</b>	<b>n15</b>	<b>n35</b>	<b>n58</b>	<b>average</b>
2.8	0.236	0.174	0.111	0.133	0.163
6.1	0.193	0.152	0.114	0.097	0.139
14.3	0.093	0.072	0.052	0.036	0.063
19.0	0.071	0.064	0.058	0.032	0.056
22.2	0.100	0.075	0.048	0.036	0.065
26.2	0.047	0.067	0.078	0.052	0.061
29.0	0.066	0.079	0.088	0.051	0.071

Table 4.11 n vs Q with 50% wet loading. S<0.1%

### 4.3.2 7-Section GSRD (S=1.9%)

All tests were conducted with the maximum expected litter loading of 90% on the basis that that represents the worse case scenario.

The litter used in these tests was that from the previous series. The continuous wetting and drying that the gross-solids mix has been subjected to has had the effect of rendering it very representative of actual highway litter. In particular, the larger pieces of paper and cups were broken up into much smaller components. The wood, cloth and plastic components remained unchanged.

Further quantities of litter were introduced at the start of the tests to compensate for the reduction in litter volume arising from compaction by flow.

The variation of the head water at inlet tank with the flow rate is shown in Fig. 4.18.

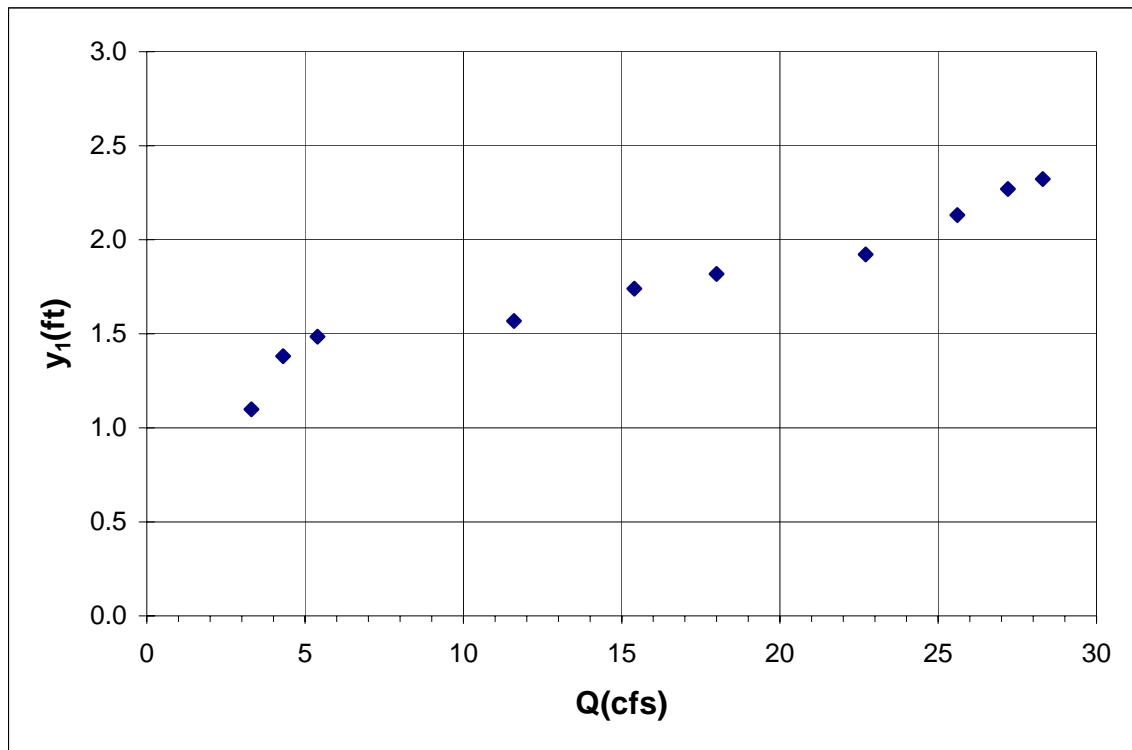


Fig. 4.18: Variation of head water with flow rate for S=1.9%.

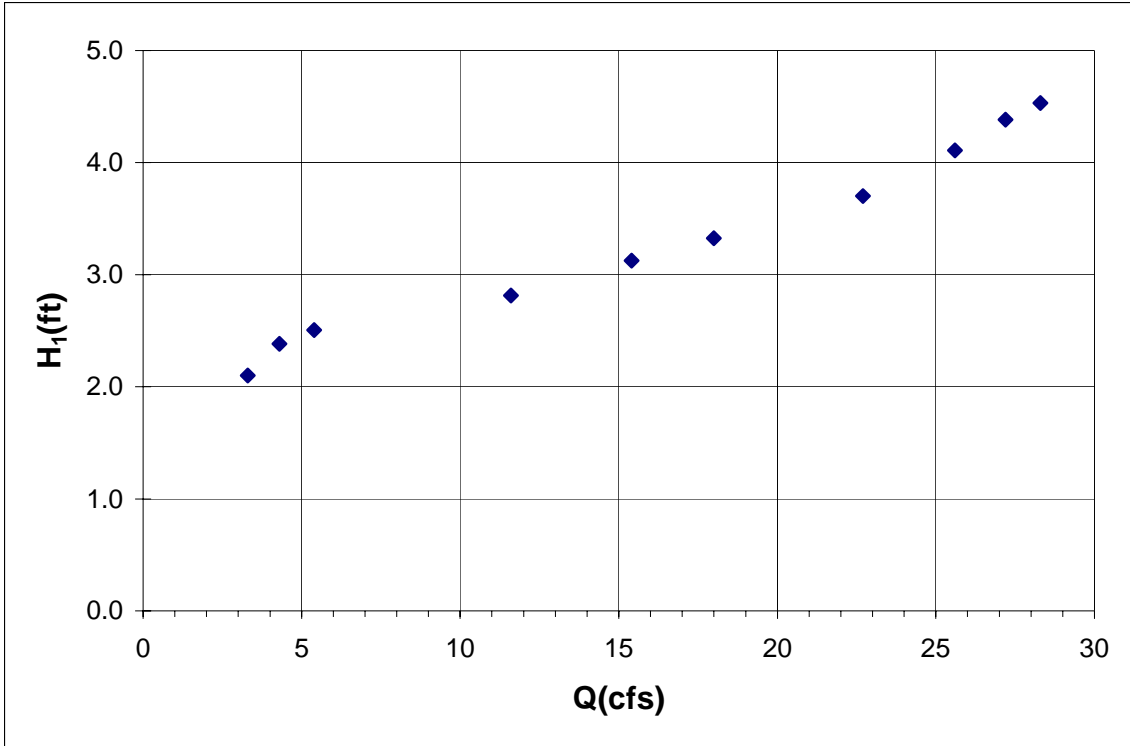


Fig. 4.19:  $H_1$  vs  $Q$  for  $S=1.9\%$

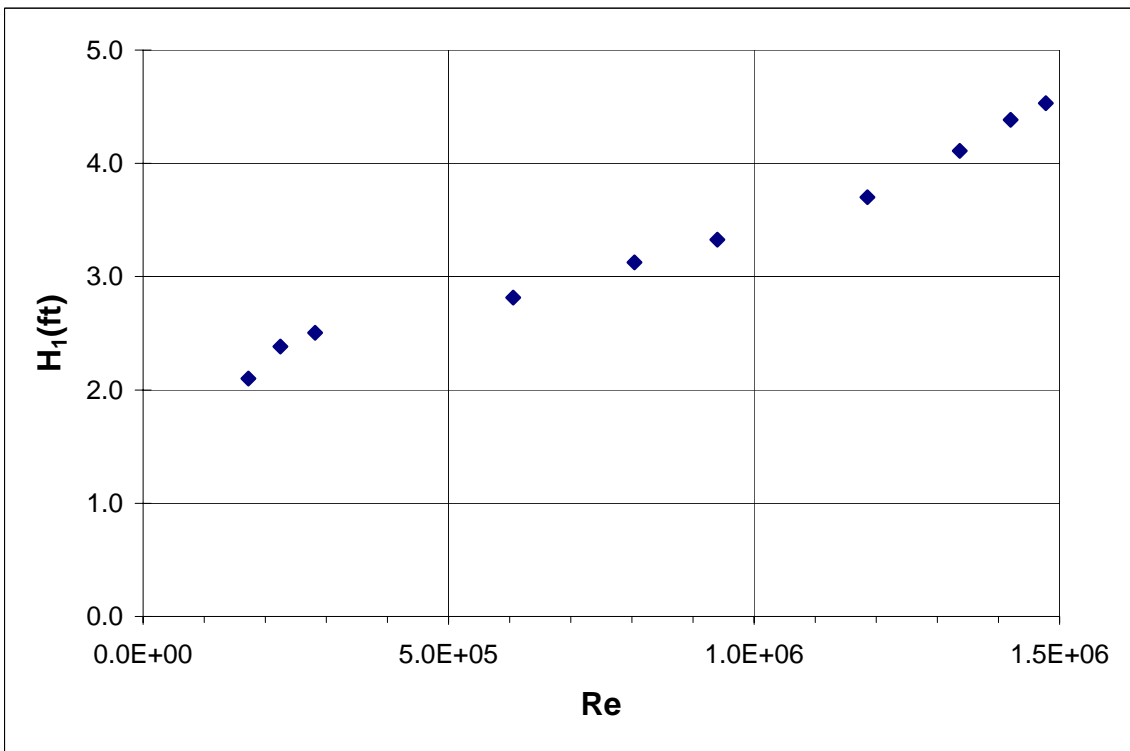


Fig. 4.20:  $H_1$  vs  $Re$  for  $S=1.9\%$

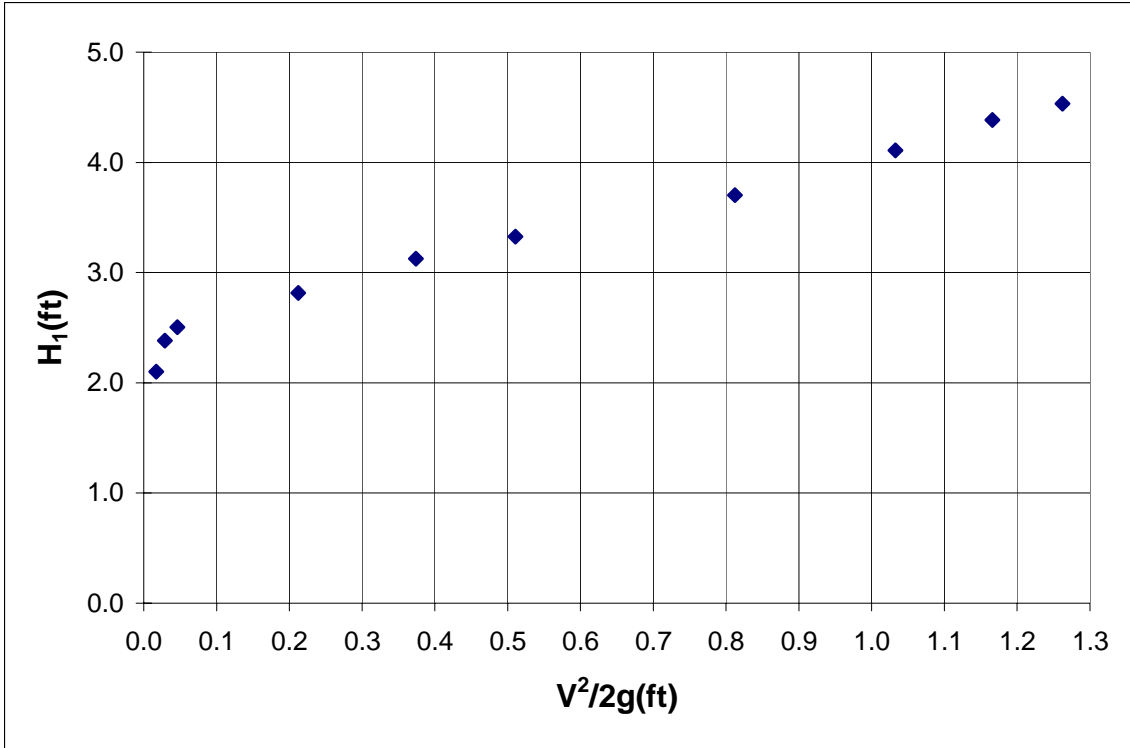


Fig. 4.21:  $H_1$  vs  $V^2/2g$  for  $S=1.9\%$

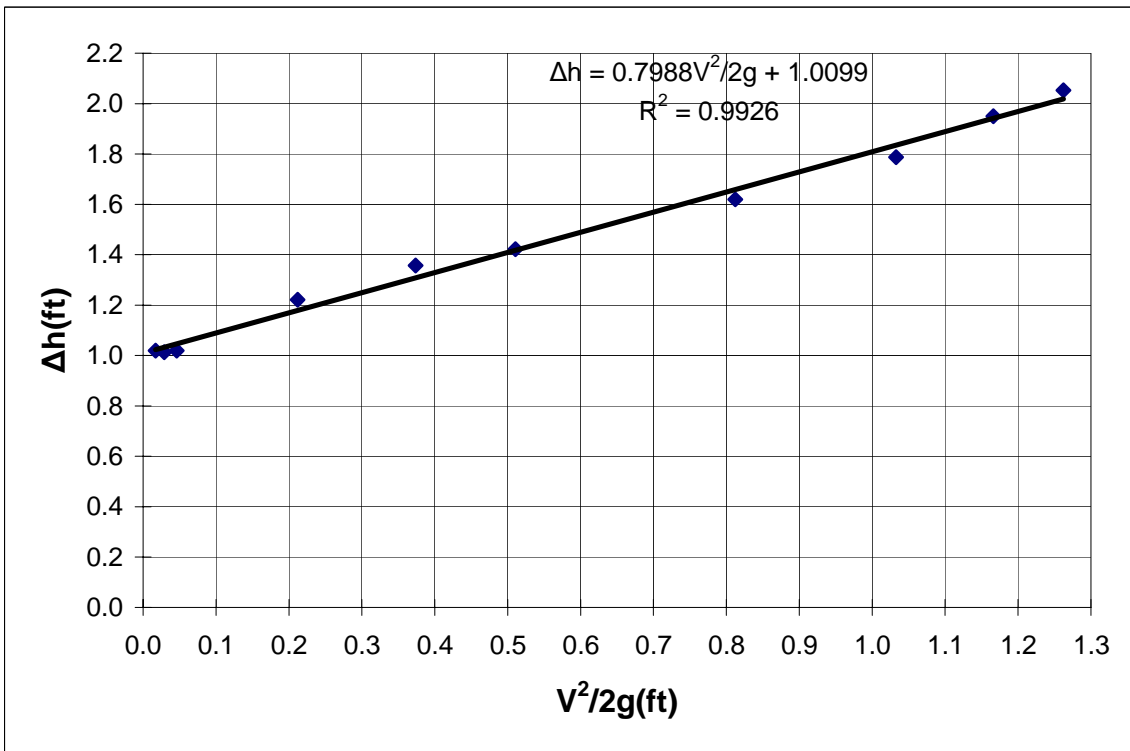


Fig. 4.22:  $\Delta h$  vs  $V^2/2g$  for  $S=1.9\%$

### 4.3.3 Tests on 7, 6 and 5-Section GSRDs ( $S < 0.1\%$ )

Tests were conducted to determine the efficiency and hydraulic performance of the Linear-radial GSRD when 6 and 5 sections are used.

Figure 4.23 for clean flow shows that the device with 5 sections experiences marginally greater head loss than with 6 or 7 sections.

The label "Without" indicates that the tests were carried out without the use of 45 degree wing walls at exit from the vault.

This result is to be expected as the fewer number of surface opening available for the flow to exit through implies greater velocities through these backward-facing opening and hence the increased losses.

Overall, however, the differences between the 5, 6 and 7 section devices are not too pronounced. This is because the head losses also increase with the number of sections used.

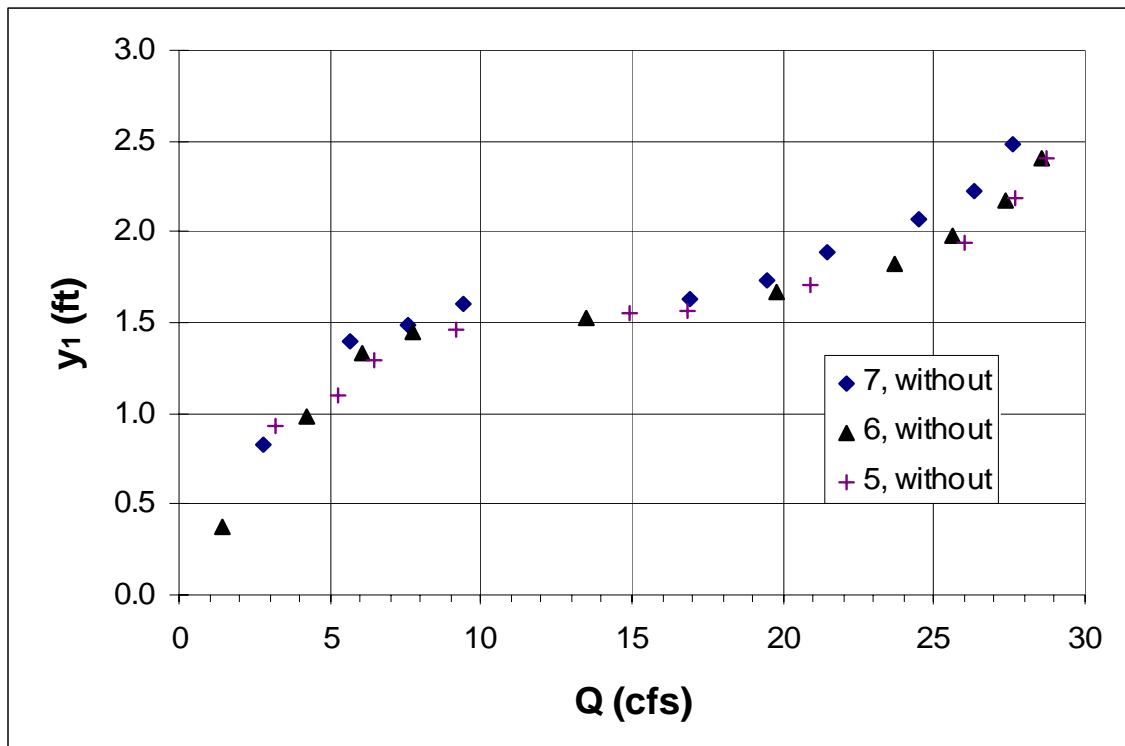


Fig. 4.23:  $y_1$  vs  $Q$  for  $S < 0.1\%$

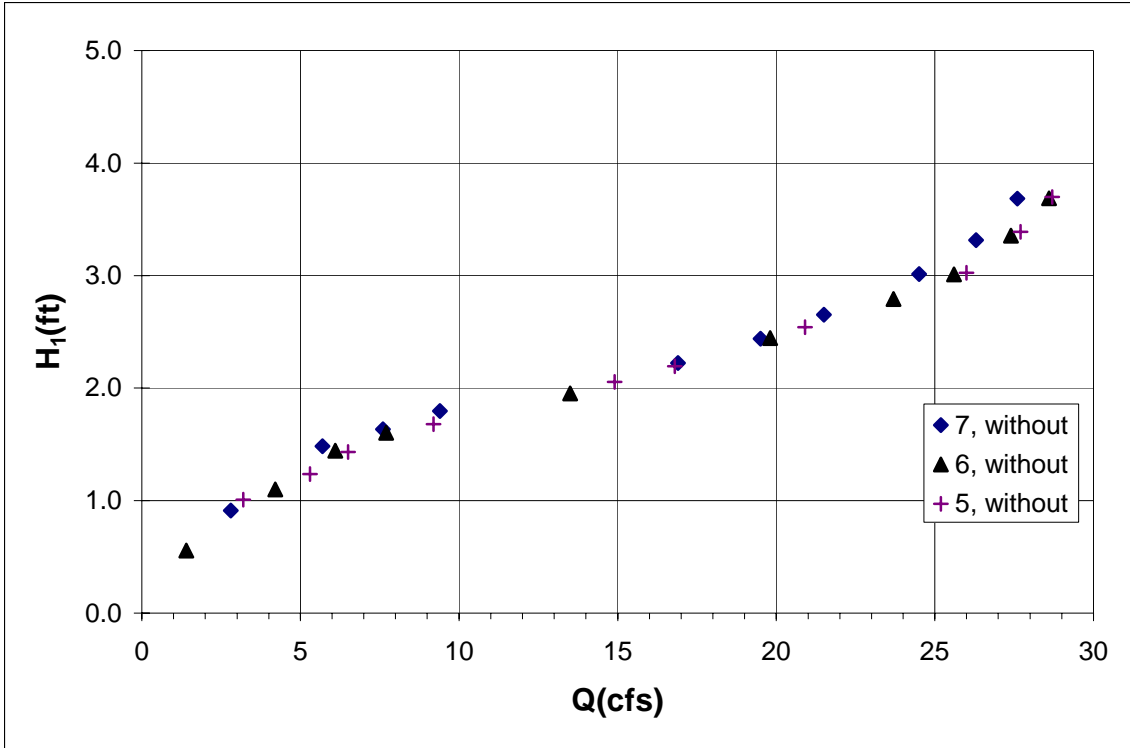


Fig. 4.24:  $H_1$  vs  $Q$  for  $S < 0.1\%$

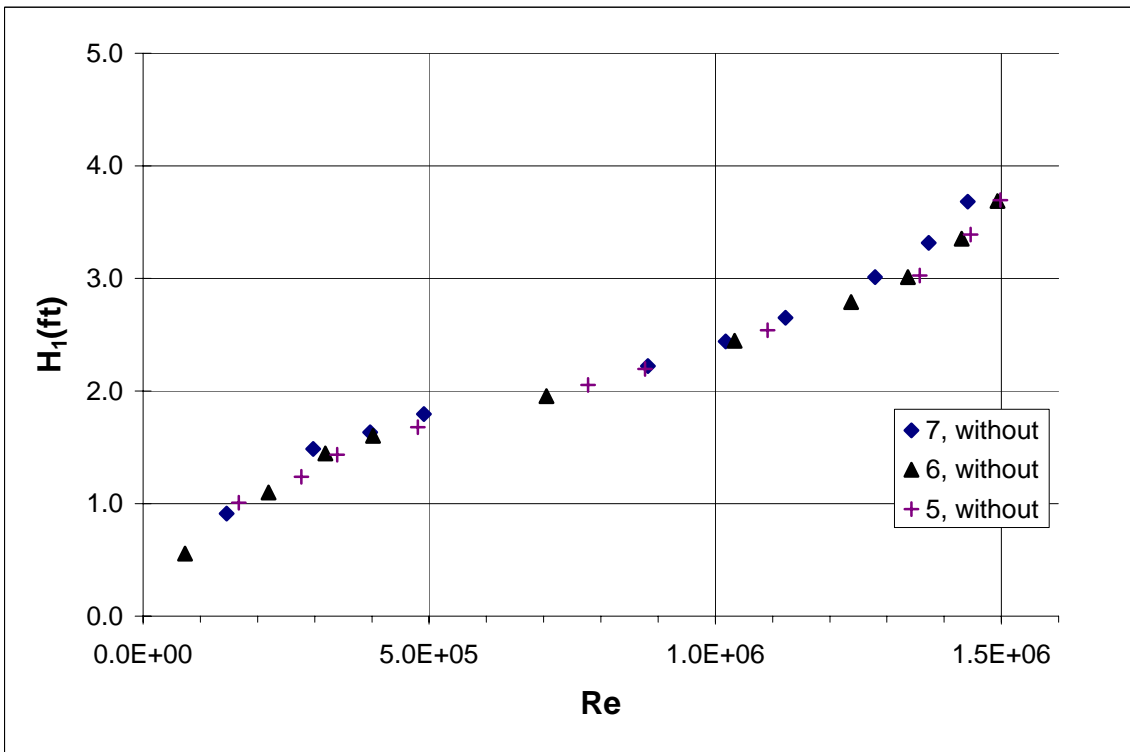


Fig. 4.25:  $H_1$  vs  $Re$  for  $S < 0.1\%$

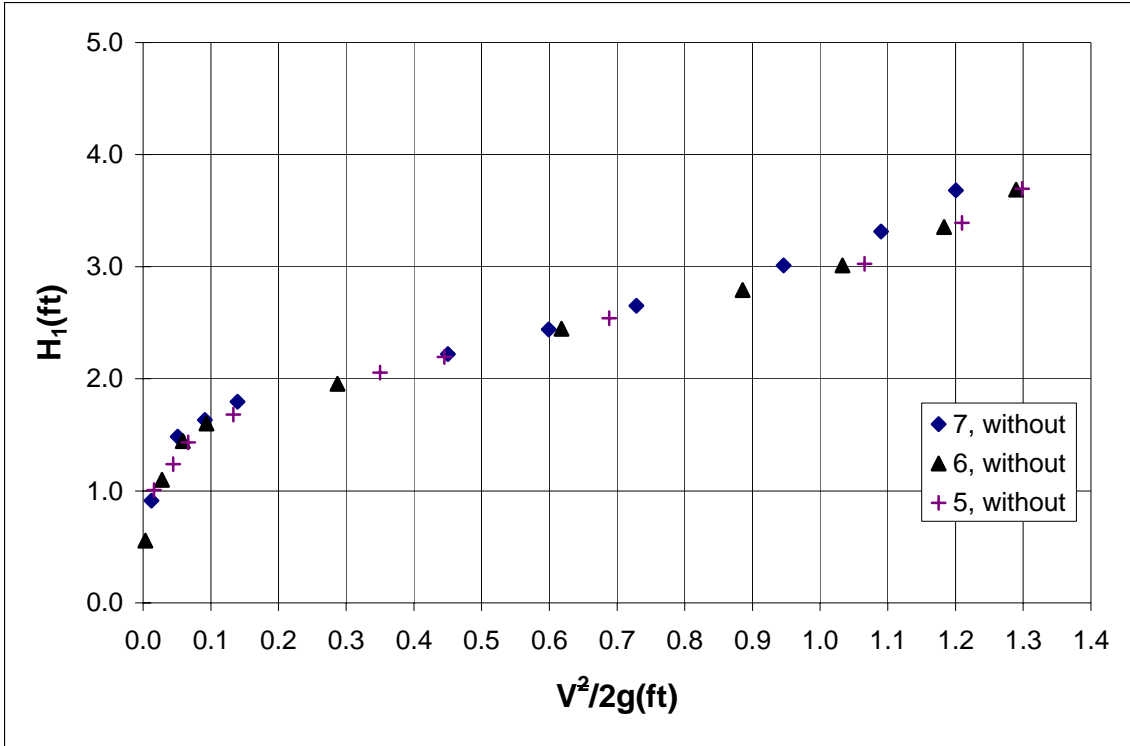


Fig. 4.26:  $H_1$  vs  $V^2/2g$  for  $S < 0.1\%$

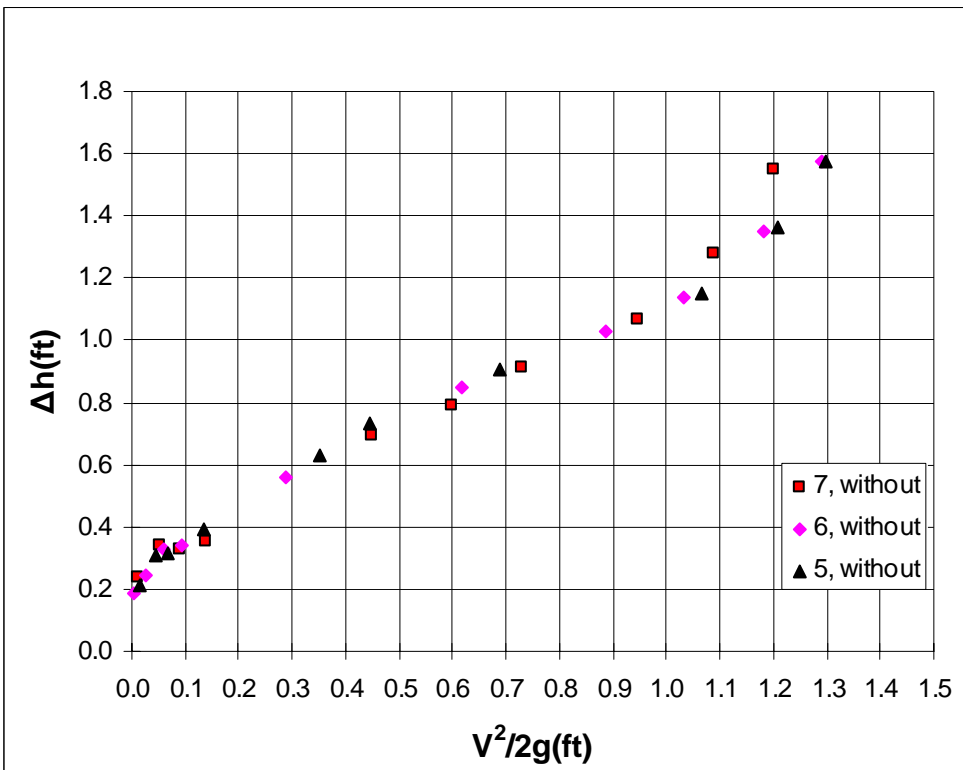


Fig. 4.27:  $\Delta h$  vs  $V^2/2g$  without the 45 degree wing walls for  $S < 0.1\%$

### 4.3.4 Tests on 7, 6 and 5-Section GSRDs (S=1.9%)

The results for 7, 6 and 5 sections for the greater slope of 1.9% are presented next.

Figures 4.28 - 4.30 shows that the losses for the 5 section GSRD are somewhat higher for this slope.

The total head at inlet to the device is plotted against the dynamic head in Fig. 4.31. The variation of the head loss across the vault with the dynamic head is shown in Figure 4.32. It is clear from this figure that the head loss variation can be fitted fairly reasonably by a straight line.

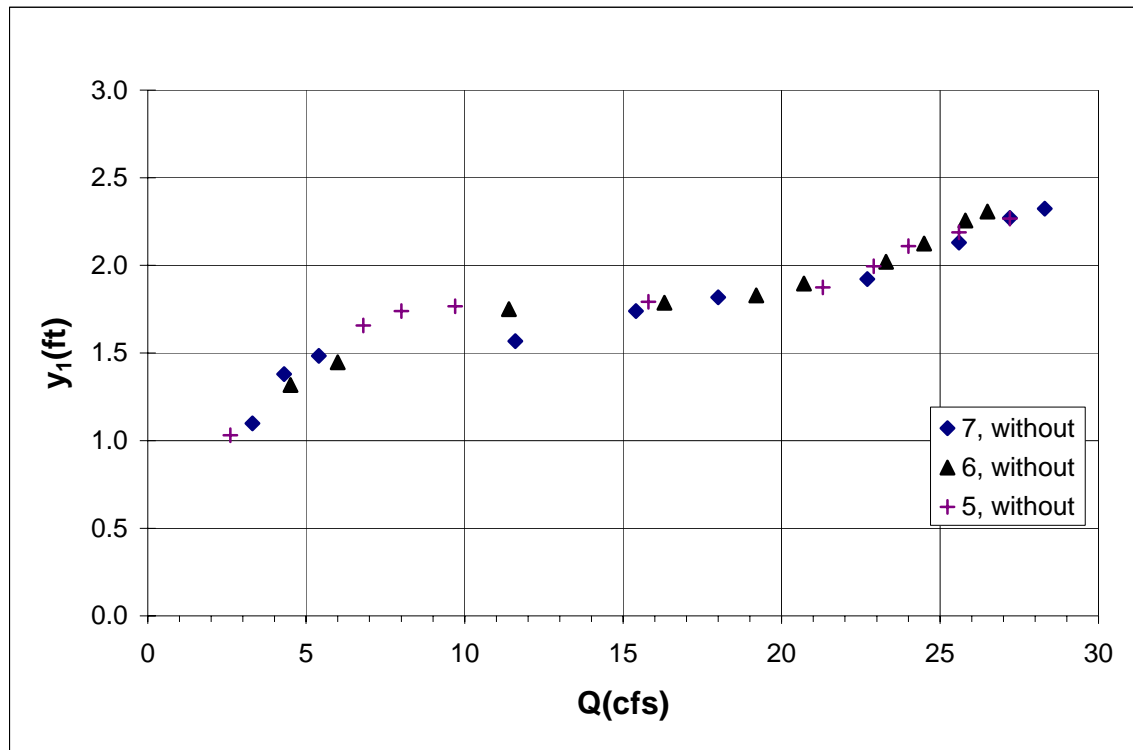


Fig. 4.28:  $y_1$  vs  $Q$  for  $S=1.9\%$

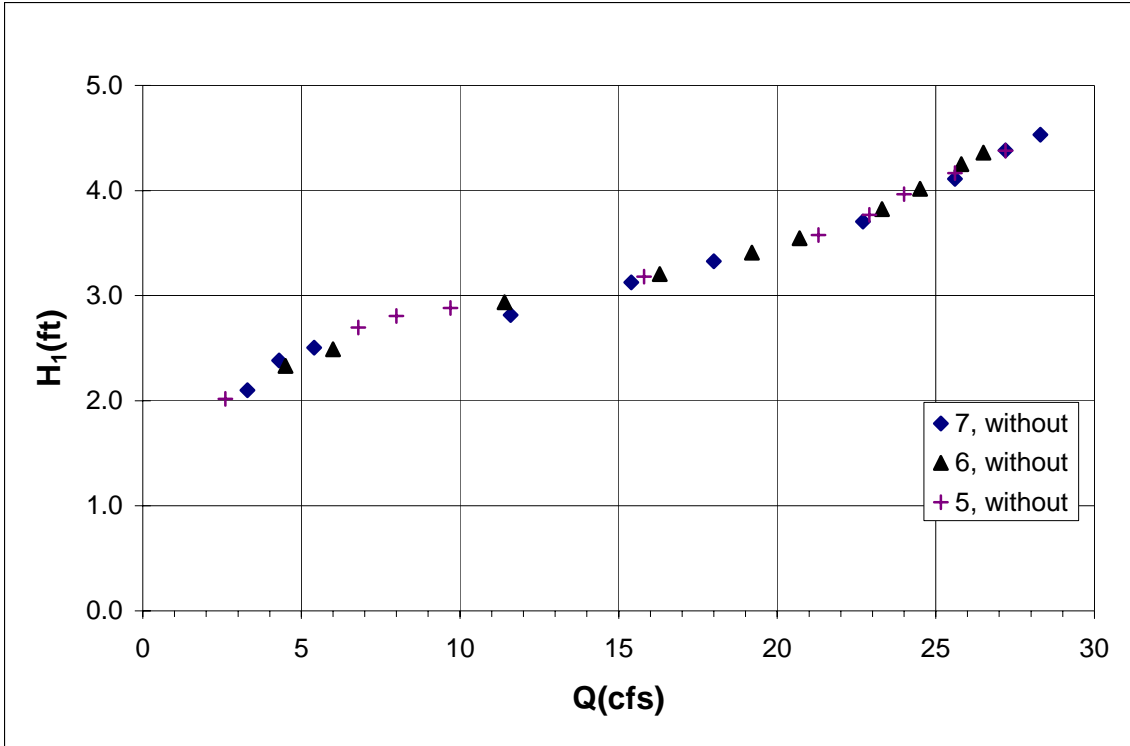


Fig. 4.29:  $H_1$  vs  $Q$  for  $S=1.9\%$

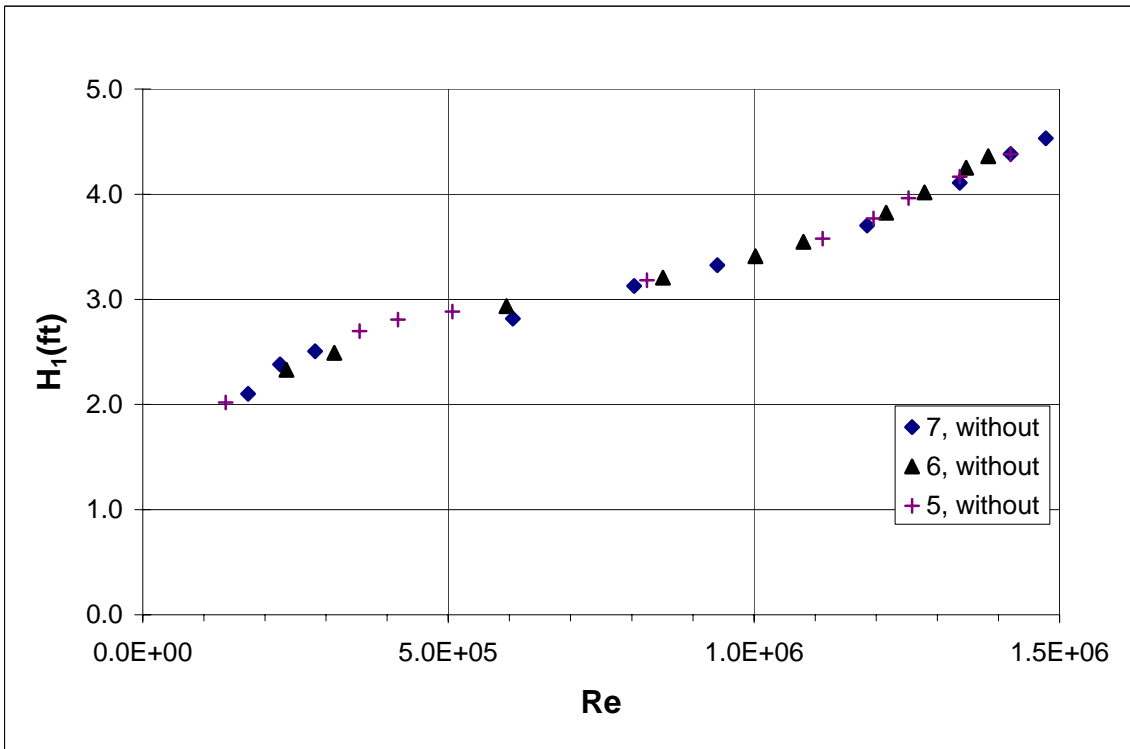


Fig. 4.30:  $H_1$  vs  $Re$  for  $S=1.9\%$

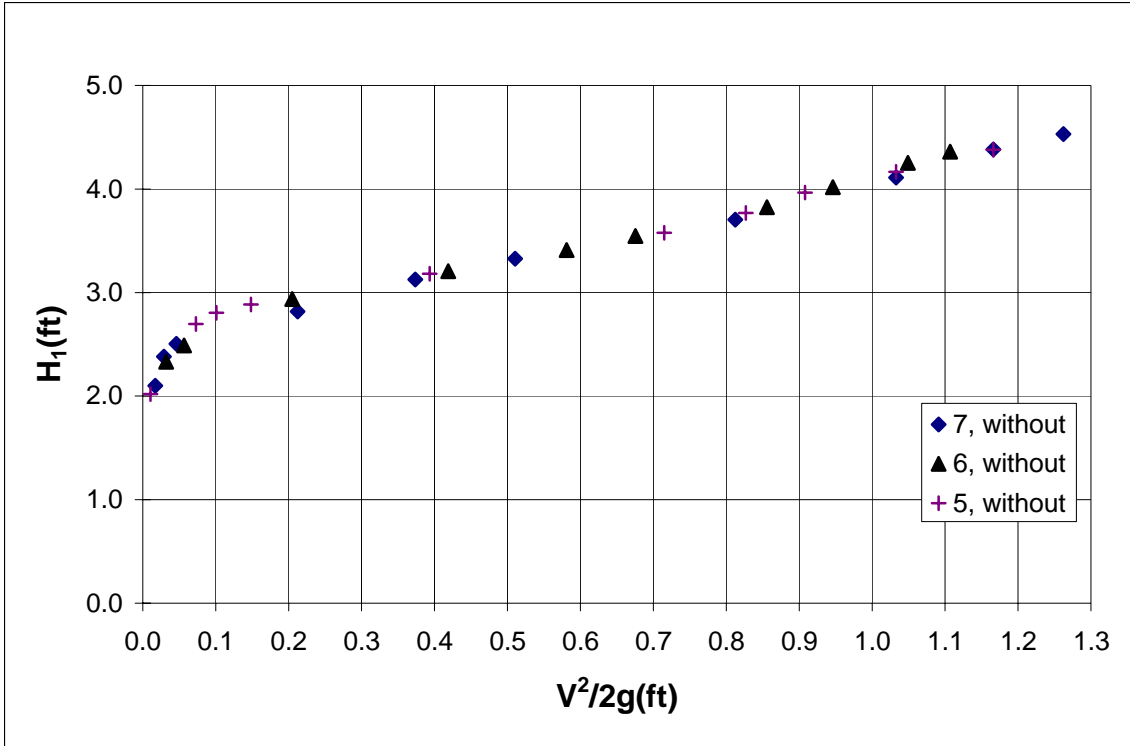


Fig. 4.31:  $H_1$  vs  $V^2/2g$  for  $S=1.9\%$

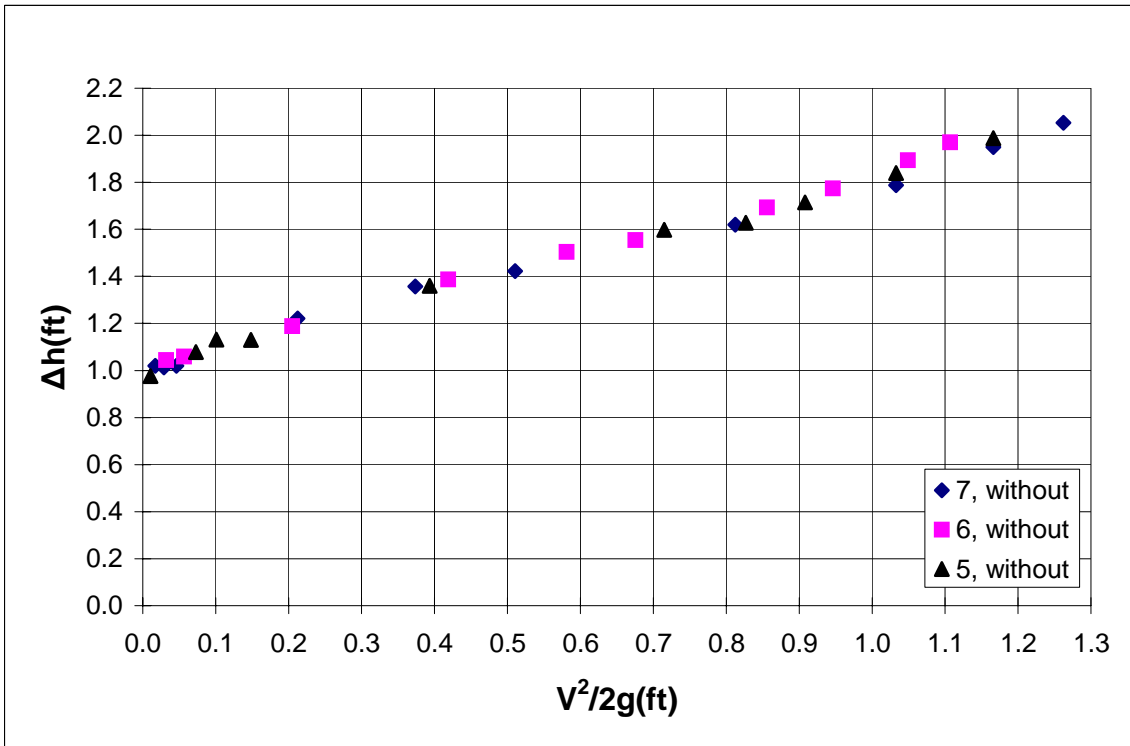


Fig. 4.32:  $\Delta h$  vs  $V^2/2g$  without the 45 degree wing walls for  $S=1.9\%$

### 4.3.5 Tests with 45 degree wing walls (S<0.1%)

The results for 7, 6 and 5 sections for the greater slope less than 0.1% are presented next.

The designations “with” and “without” refer to the wing walls at outlet.

Figures 4.33 - 4.36 present the measurements of water depth and total head in the litter insertion tank versus the flow rate, the Reynolds number and the dynamic head.

The variation of the head loss across the vault with the dynamic head is shown in Figure 4.37. It is clear from this figure that the head loss variation can be fitted fairly reasonably by a straight line.

Plots of the head loss vs. the flow rate and Reynolds number are presented in Fig. 4.38 and 4.39, respectively.

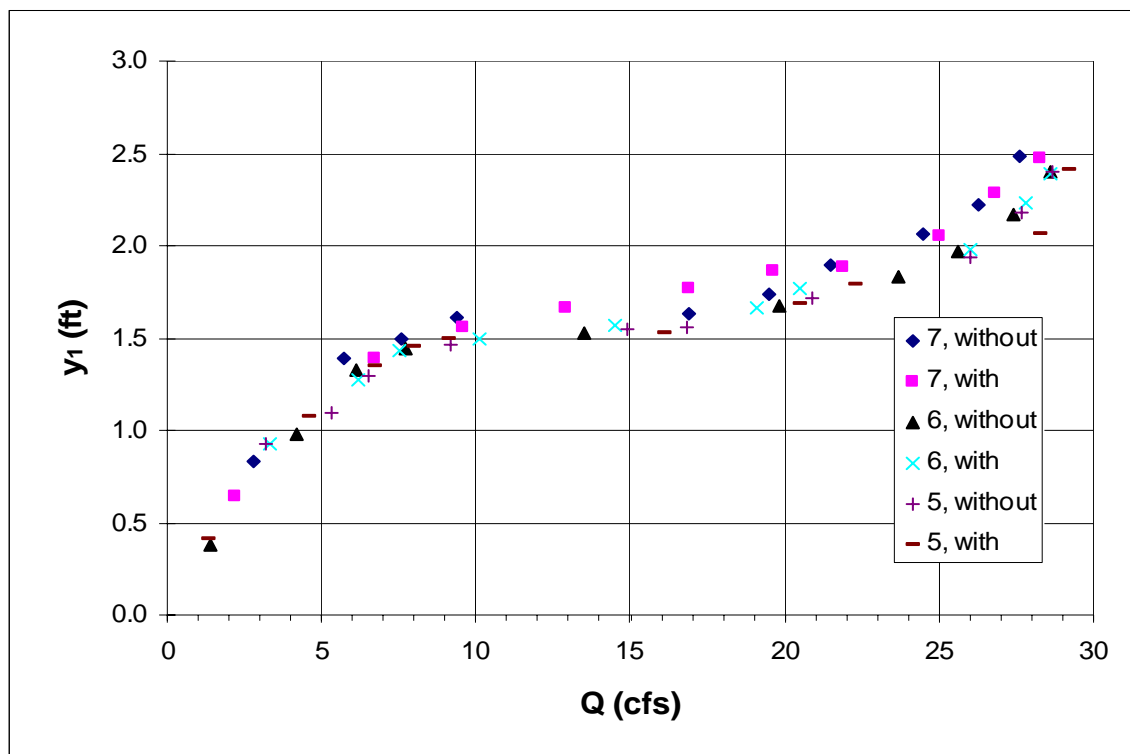


Fig. 4.33:  $y_1$  vs  $Q$  for  $S < 0.1\%$

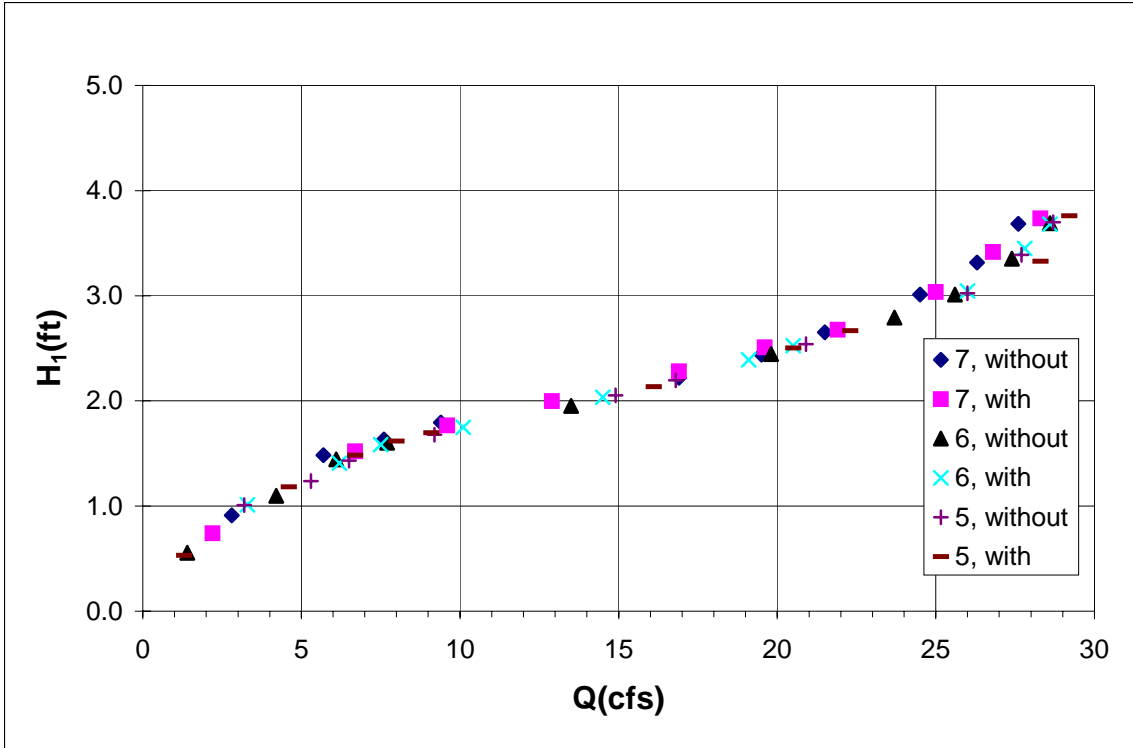


Fig. 4.34:  $H_1$  vs  $Q$  for  $S < 0.1\%$

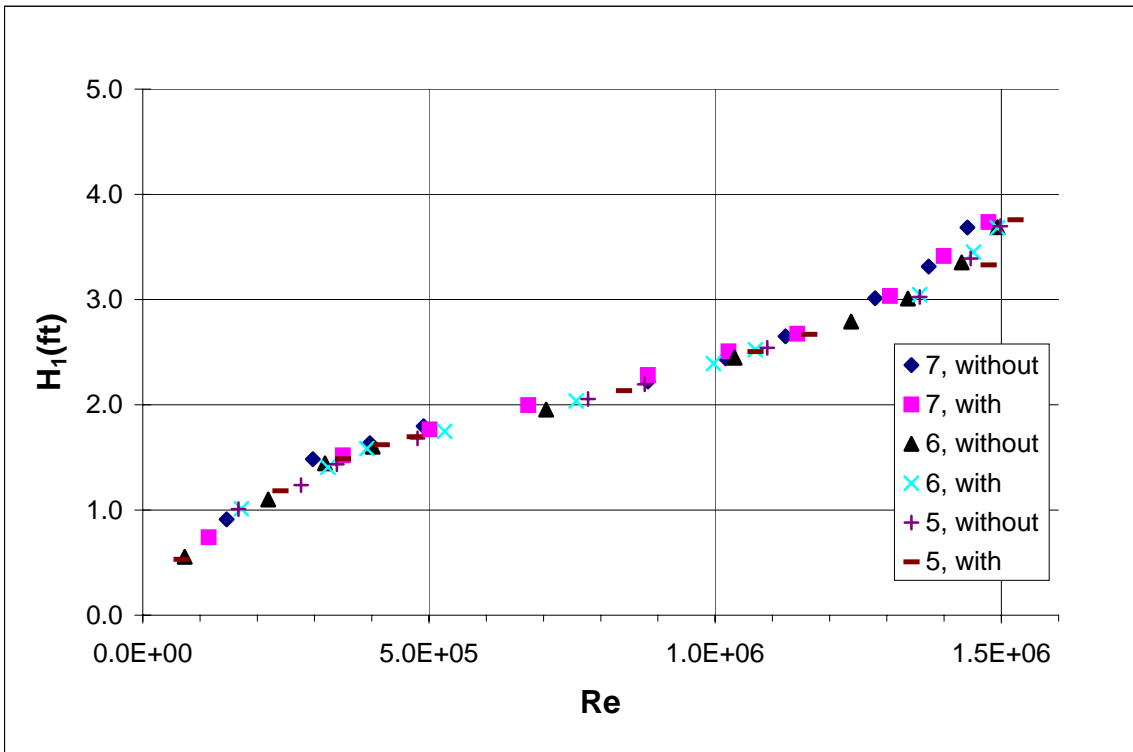


Fig. 4.35:  $H_1$  vs  $Re$  for  $S < 0.1\%$

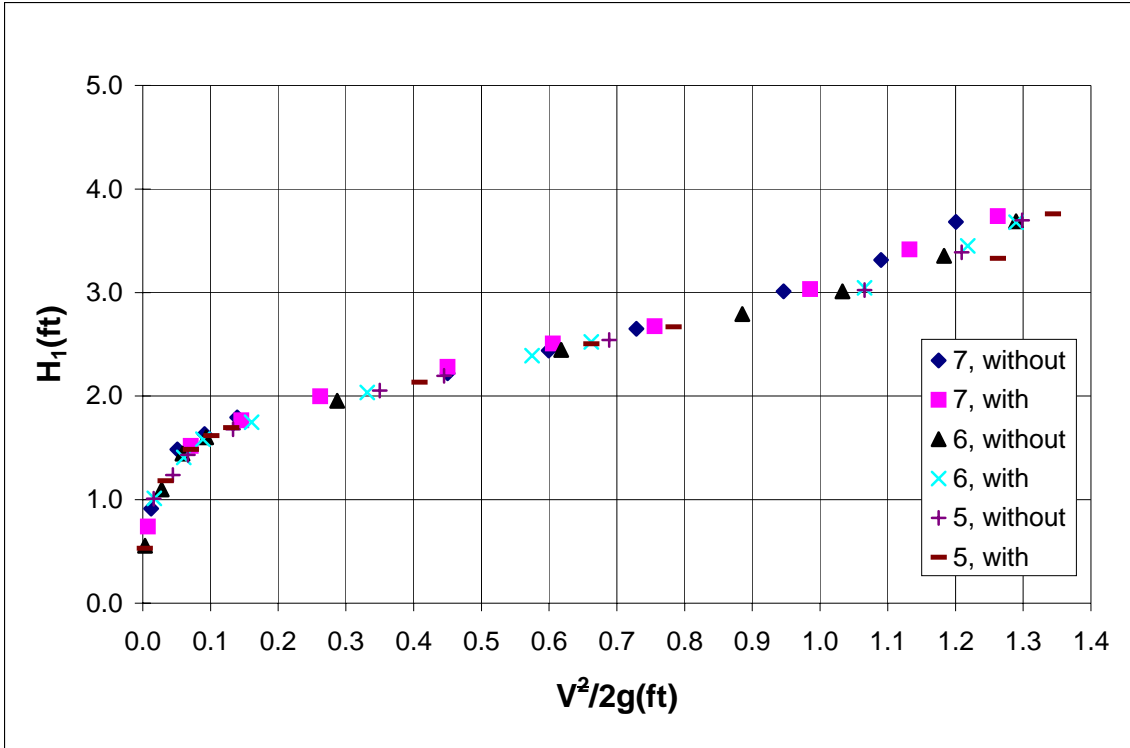


Fig. 4.36:  $H_1$  vs  $V^2/2g$  for  $S < 0.1\%$

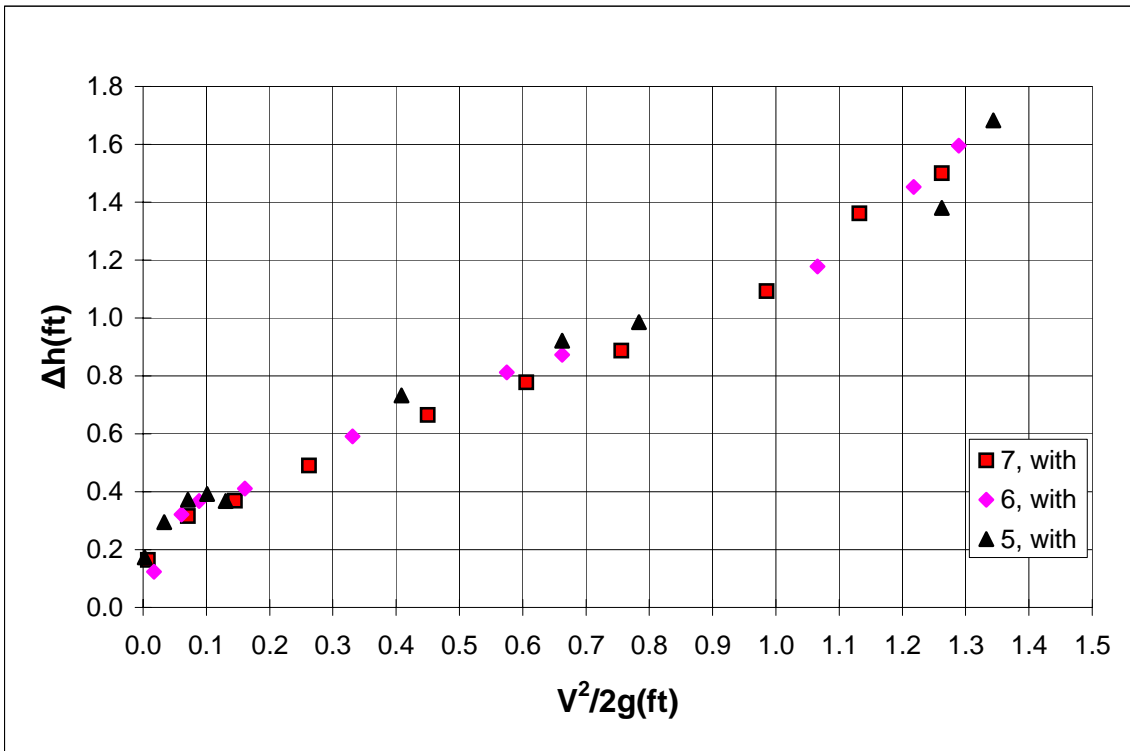


Fig. 4.37:  $\Delta h$  vs  $V^2/2g$  with the 45 degree wing walls for  $S < 0.1\%$

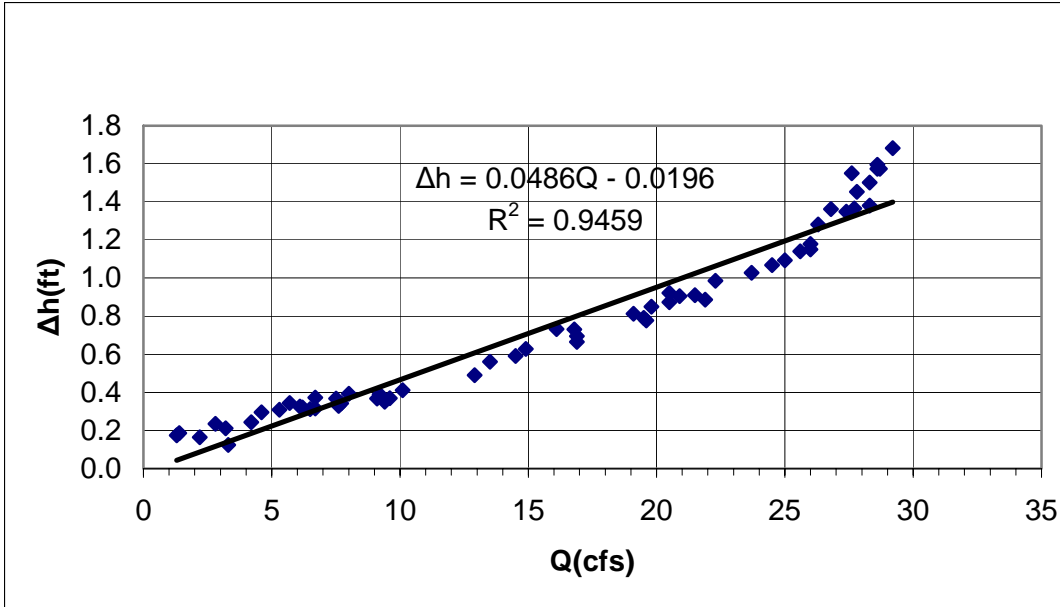


Fig. 4.38:  $\Delta h$  vs  $Q$  for  $S < 0.1\%$

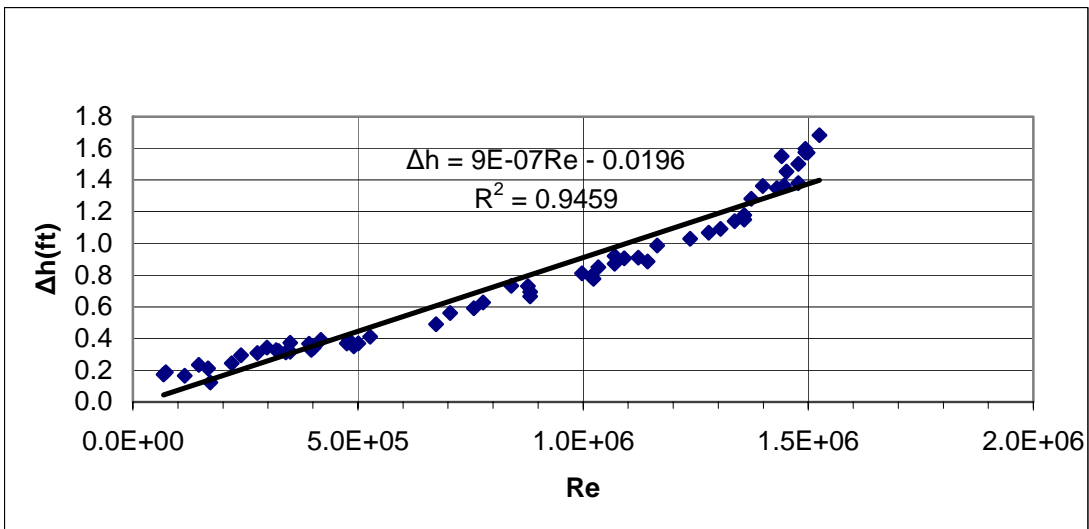


Fig. 4.39:  $\Delta h$  vs  $Re$  for  $S < 0.1\%$

Q (cfs)	Re	$V^2/2g$ (ft)	$\Delta h$ (ft)	$\Delta h/H_1$	H1 (ft)	$y_1$ (ft)
27.6	1440952	1.201	1.550	0.421	3.683	2.48
26.3	1373081	1.090	1.280	0.386	3.314	2.23
24.5	1279106	0.946	1.067	0.354	3.012	2.07
21.5	1122481	0.729	0.910	0.343	2.651	1.89
19.5	1018064	0.599	0.791	0.324	2.440	1.73
16.9	882322	0.450	0.695	0.313	2.222	1.63
9.4	490759	0.139	0.352	0.196	1.796	1.61
7.6	396784	0.091	0.329	0.201	1.634	1.49

5.7	297588	0.051	0.343	0.231	1.484	1.39
2.8	146184	0.012	0.235	0.258	0.913	0.83

Table 4.12: 7 section without wing wall,  $S < 0.1\%$

Q (cfs)	Re	$V^2/2g$ (ft)	$\Delta h$ (ft)	$\Delta h/H_1$	H1 (ft)	$y_1$ (ft)
28.3	1477498	1.262	1.501	0.402	3.736	2.48
26.8	1399186	1.132	1.361	0.399	3.414	2.28
25.0	1305210	0.985	1.092	0.360	3.034	2.05
21.9	1143364	0.756	0.887	0.331	2.675	1.88
19.6	1023285	0.606	0.777	0.310	2.508	1.87
16.9	882322	0.450	0.665	0.291	2.281	1.77
12.9	673489	0.262	0.490	0.245	1.997	1.67
9.6	501201	0.145	0.369	0.209	1.766	1.56
6.7	349796	0.071	0.317	0.208	1.520	1.39
2.2	114859	0.008	0.165	0.223	0.741	0.64

Table 4.13: 7 section with wing wall,  $S < 0.1\%$

Q (cfs)	Re	$V^2/2g$ (ft)	$\Delta h$ (ft)	$\Delta h/H_1$	H1 (ft)	$y_1$ (ft)
28.6	1493161	1.289	1.574	0.427	3.688	2.4
27.4	1430511	1.183	1.349	0.402	3.353	2.17
25.6	1336535	1.033	1.140	0.379	3.010	1.97
23.7	1237339	0.885	1.028	0.368	2.791	1.83
19.8	1033727	0.618	0.850	0.348	2.446	1.67
13.5	704814	0.287	0.560	0.287	1.954	1.53
7.7	402005	0.093	0.343	0.214	1.602	1.45
6.1	318471	0.059	0.326	0.226	1.445	1.33
4.2	219275	0.028	0.244	0.222	1.099	0.98
1.4	73092	0.003	0.187	0.336	0.557	0.38

Table 4.14: 6 section without wing wall,  $S < 0.1\%$

Q (cfs)	Re	$V^2/2g$ (ft)	$\Delta h$ (ft)	$\Delta h/H_1$	H1 (ft)	$y_1$ (ft)
28.6	1493161	1.289	1.596	0.434	3.680	2.39
27.8	1451394	1.218	1.453	0.421	3.450	2.23
26.0	1357419	1.065	1.178	0.387	3.044	1.98
20.5	1070273	0.662	0.872	0.346	2.524	1.77
19.1	997181	0.575	0.812	0.340	2.391	1.67
14.5	757022	0.331	0.591	0.291	2.035	1.57
10.1	527305	0.161	0.411	0.235	1.748	1.5
7.5	391563	0.089	0.368	0.232	1.584	1.43
6.2	323692	0.061	0.321	0.228	1.409	1.28
3.3	172288	0.017	0.124	0.122	1.014	0.93

Table 4.15: 6 section with wing wall,  $S < 0.1\%$

Q (cfs)	Re	$V^2/2g$ (ft)	$\Delta h$ (ft)	$\Delta h/H_1$	H1 (ft)	$y_1$ (ft)
28.7	1498382	1.298	1.573	0.425	3.697	2.4
27.7	1446173	1.209	1.364	0.403	3.389	2.18
26.0	1357419	1.065	1.151	0.381	3.024	1.94
20.9	1091156	0.688	0.905	0.356	2.540	1.71
16.8	877101	0.445	0.731	0.333	2.195	1.56
14.9	777905	0.350	0.628	0.306	2.054	1.55
9.2	480317	0.133	0.390	0.232	1.680	1.46
6.5	339355	0.067	0.312	0.218	1.433	1.29
5.3	276705	0.044	0.309	0.250	1.238	1.1
3.2	167067	0.016	0.211	0.209	1.009	0.93

Table 4.16: 5 section without wing wall,  $S < 0.1\%$

Q (cfs)	Re	$V^2/2g$ (ft)	$\Delta h$ (ft)	$\Delta h/H_1$	H1 (ft)	$y_1$ (ft)
29.2	1524486	1.344	1.683	0.448	3.758	2.42
28.3	1477498	1.262	1.380	0.415	3.328	2.07
22.3	1164248	0.784	0.986	0.370	2.667	1.79
20.5	1070273	0.662	0.921	0.368	2.503	1.68
16.1	840555	0.409	0.732	0.343	2.135	1.53
9.1	475097	0.131	0.368	0.217	1.697	1.49
8.0	417667	0.101	0.392	0.242	1.619	1.45
6.7	349796	0.071	0.372	0.251	1.485	1.35
4.6	240159	0.033	0.296	0.250	1.184	1.07
1.3	67871	0.003	0.174	0.326	0.532	0.41

Table 4.17: 5 section with wing wall,  $S < 0.1\%$

### 4.3.6 Tests with 45 degree wing walls (S=1.9%)

The results for 7, 6 and 5 sections for the greater slope of 1.9% with 45 degree wing walls are presented next.

The designations “with” and “without” refer to the wing walls at outlet.

Figures 4.40 - 4.43 present the measurements of water depth and total head in the litter insertion tank versus the flow rate, the Reynolds number and the dynamic head.

The variation of the head loss across the vault with the dynamic head is shown in Figure 4.44. It is clear from this figure that the head loss variation can be fitted fairly reasonably by a straight line.

Plots of the head loss vs. the flow rate and Reynolds number are presented in Fig. 4.45 and 4.46, respectively.

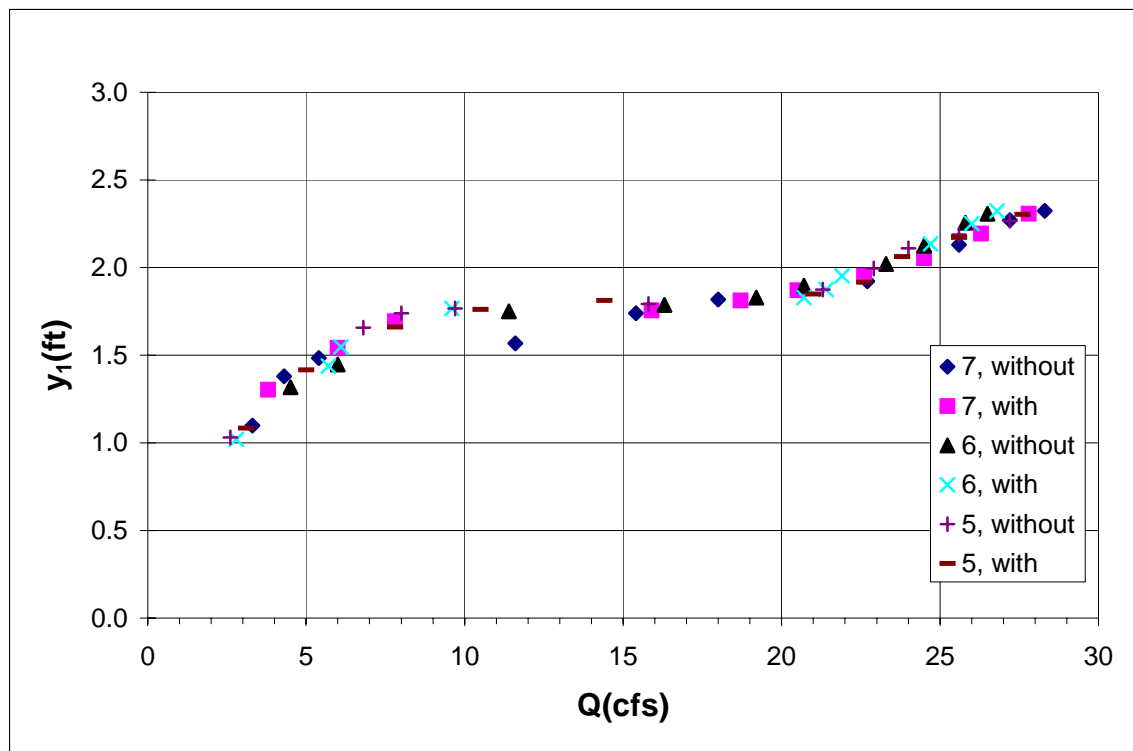


Fig. 4.40:  $y_1$  vs Q for S=1.9%

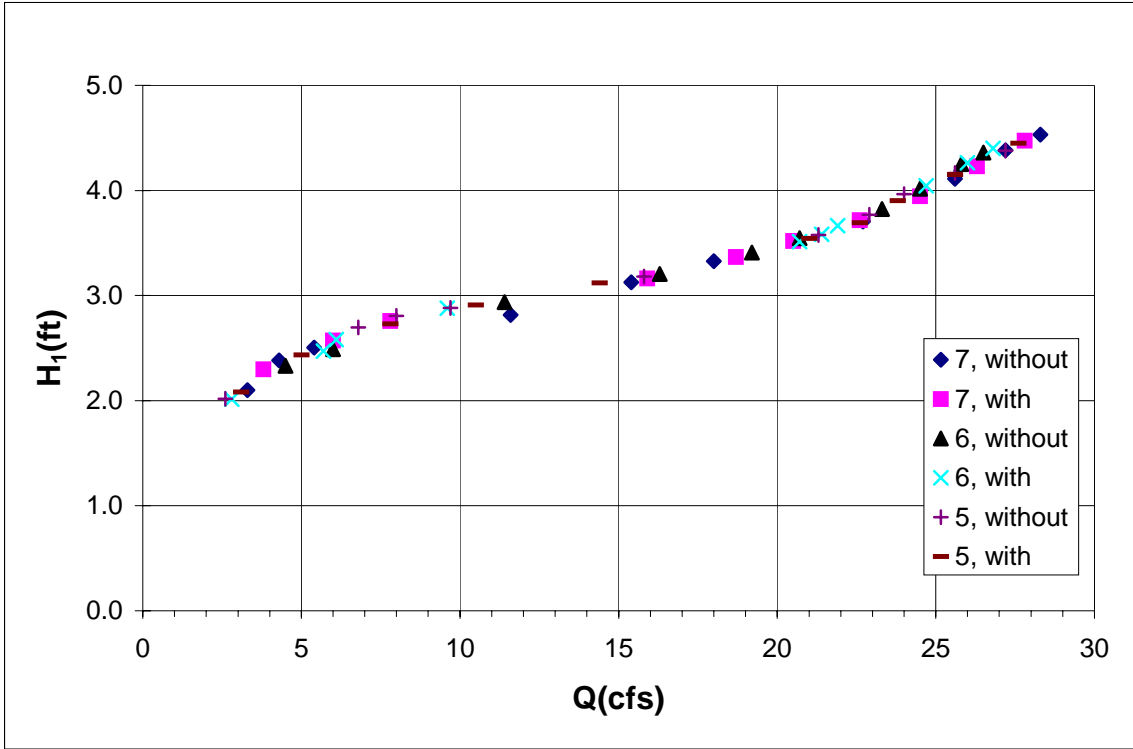


Fig. 4.41:  $H_1$  vs  $Q$  for  $S=1.9\%$

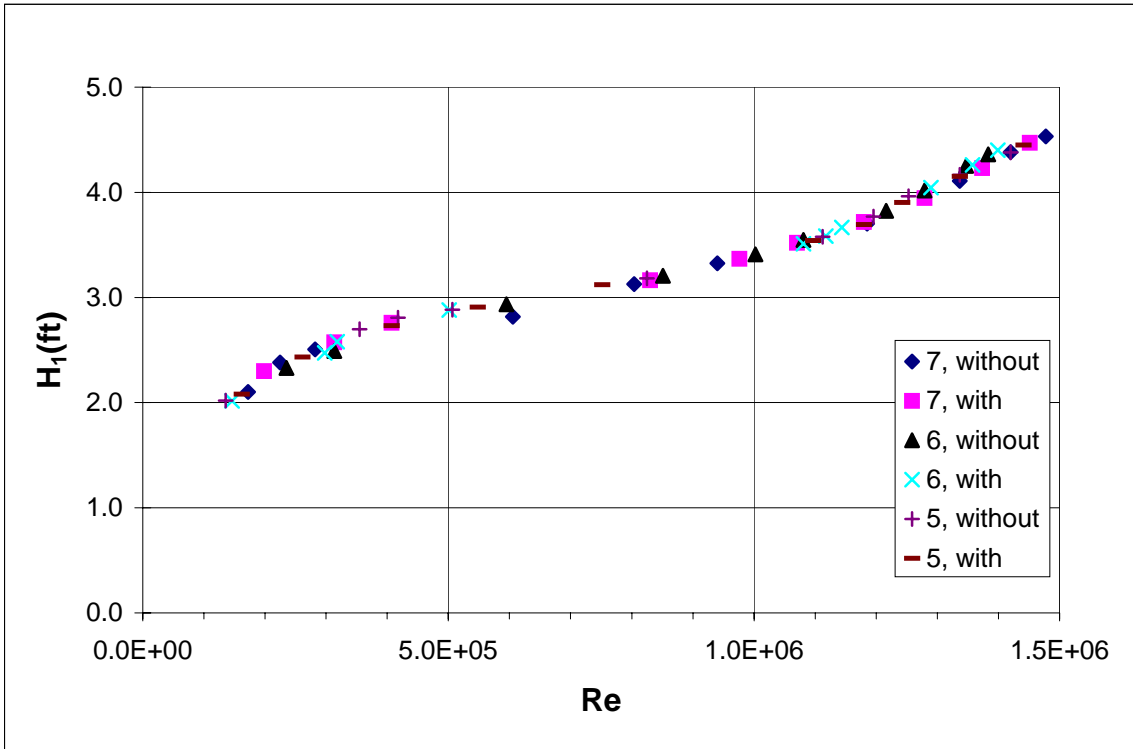


Fig. 4.42:  $H_1$  vs  $Re$  for  $S=1.9\%$

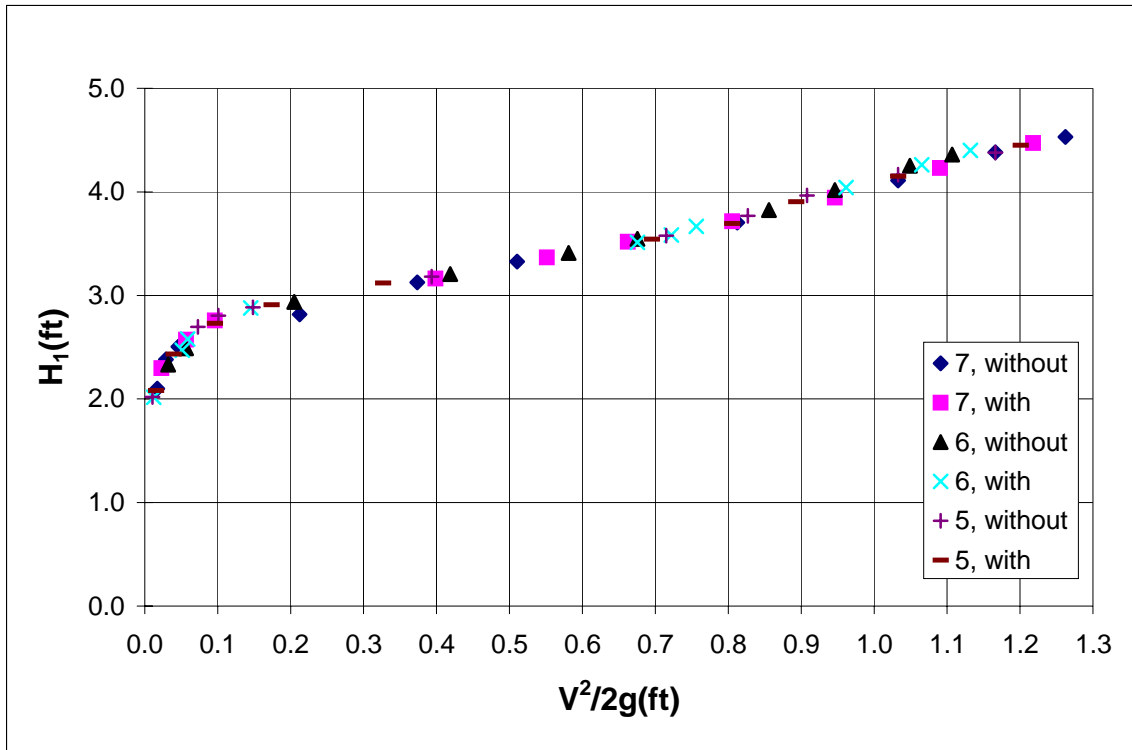


Fig. 4.43:  $H_1$  vs  $V^2/2g$  for  $S=1.9\%$

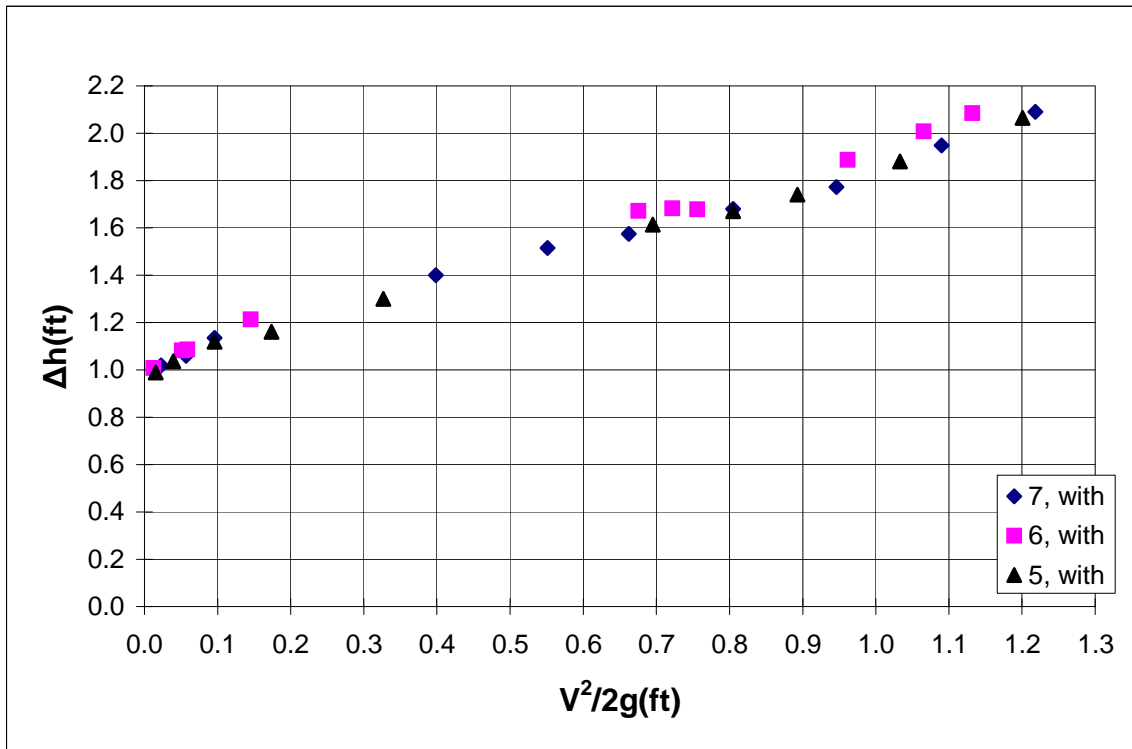


Fig. 4.44:  $\Delta h$  vs  $V^2/2g$  with the 45 degree wing walls for  $S=1.9\%$

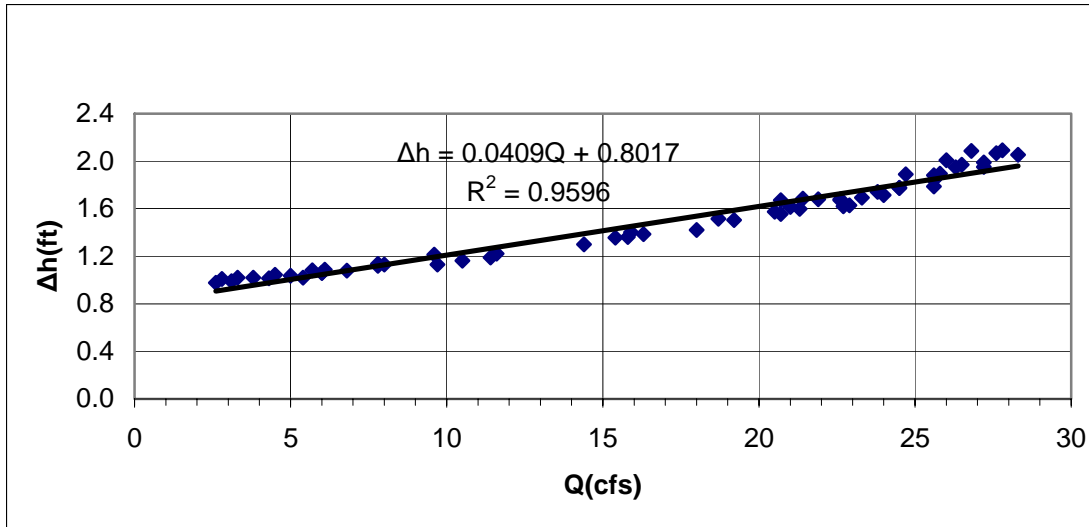


Fig. 4.45:  $\Delta h$  vs  $Q$  for  $S=1.9\%$

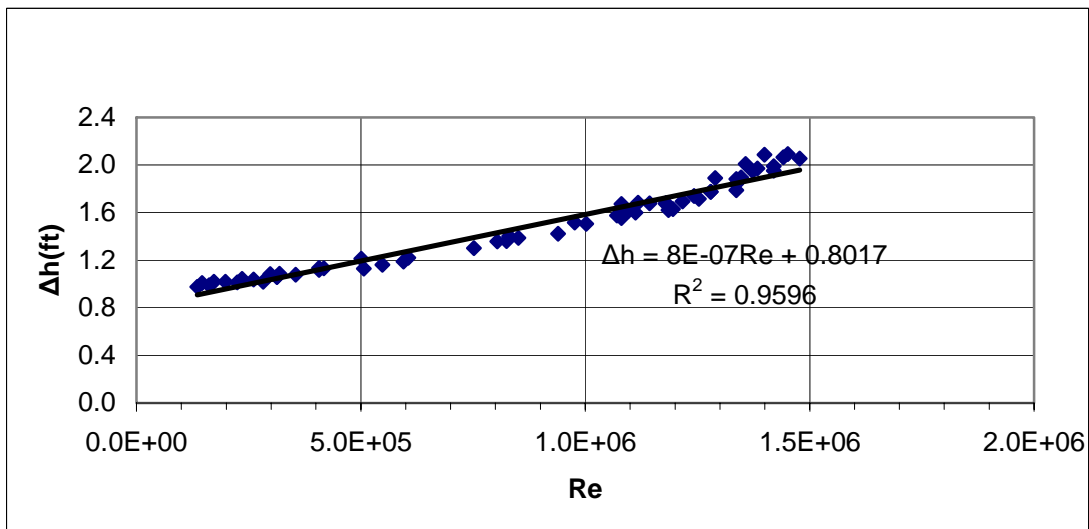


Fig. 4.46:  $\Delta h$  vs  $Re$  for  $S=1.9\%$

$Q$ (cfs)	$Re$	$V^2/2g$ (ft)	$\Delta h$ (ft)	$\Delta h/H_1$	$H_1$ (ft)	$y_1$ (ft)
28.3	1477498	1.262	2.053	0.453	4.532	2.323
27.2	1420069	1.166	1.950	0.445	4.384	2.271
25.6	1336535	1.033	1.788	0.435	4.110	2.130
22.7	1185131	0.812	1.620	0.437	3.703	1.922
18.0	939751	0.511	1.422	0.428	3.325	1.818
15.4	804010	0.374	1.357	0.434	3.125	1.740
11.6	605618	0.212	1.221	0.434	2.815	1.568
5.4	281925	0.046	1.020	0.407	2.505	1.484
4.3	224496	0.029	1.014	0.426	2.382	1.380
3.3	172288	0.017	1.019	0.485	2.101	1.099

Table 4.18: 7 section without wing wall,  $S=1.9\%$

Q (cfs)	Re	$V^2/2g$ (ft)	$\Delta h$ (ft)	$\Delta h/H_1$	H1 (ft)	$y_1$ (ft)
27.8	1451394	1.218	2.091	0.468	4.472	2.307
26.3	1373081	1.090	1.949	0.461	4.230	2.193
24.5	1279106	0.946	1.773	0.449	3.945	2.052
22.6	1179910	0.805	1.680	0.452	3.715	1.953
20.5	1070273	0.662	1.575	0.448	3.518	1.870
18.7	976297	0.551	1.515	0.450	3.367	1.813
15.9	830114	0.398	1.401	0.443	3.163	1.755
7.8	407226	0.096	1.135	0.412	2.758	1.693
6.0	313250	0.057	1.059	0.412	2.572	1.542
3.8	198392	0.023	1.019	0.443	2.298	1.302

Table 4.19: 7 section with wing wall, S=1.9%

Q (cfs)	Re	$V^2/2g$ (ft)	$\Delta h$ (ft)	$\Delta h/H_1$	H1 (ft)	$y_1$ (ft)
26.5	1383523	1.107	1.970	0.452	4.361	2.307
25.8	1346977	1.049	1.894	0.446	4.251	2.255
24.5	1279106	0.946	1.775	0.442	4.018	2.125
23.3	1216456	0.856	1.693	0.443	3.824	2.021
20.7	1080714	0.675	1.555	0.438	3.546	1.896
19.2	1002402	0.581	1.504	0.441	3.408	1.828
16.3	850997	0.419	1.386	0.433	3.205	1.786
11.4	595176	0.205	1.189	0.405	2.936	1.750
6.0	313250	0.057	1.059	0.425	2.490	1.448
4.5	234938	0.032	1.044	0.448	2.331	1.318

Table 4.20: 6 section without wing wall, S=1.9%

Q (cfs)	Re	$V^2/2g$ (ft)	$\Delta h$ (ft)	$\Delta h/H_1$	H1 (ft)	$y_1$ (ft)
26.8	1399186	1.132	2.085	0.474	4.402	2.323
26.0	1357419	1.065	2.008	0.471	4.262	2.250
24.7	1289548	0.962	1.888	0.467	4.044	2.135
21.9	1143364	0.756	1.678	0.458	3.665	1.953
21.4	1117260	0.722	1.683	0.470	3.583	1.875
20.7	1080714	0.675	1.672	0.476	3.511	1.828
9.6	501201	0.145	1.213	0.421	2.880	1.766
6.1	318471	0.059	1.087	0.421	2.580	1.547
5.7	297588	0.051	1.083	0.438	2.472	1.438
2.8	146184	0.012	1.008	0.500	2.016	1.021

Table 4.21: 6 section with wing wall, S=1.9%

Q (cfs)	Re	$V^2/2g$ (ft)	$\Delta h$ (ft)	$\Delta h/H_1$	H1 (ft)	$y_1$ (ft)
27.2	1420069	1.166	1.988	0.454	4.378	2.266
25.6	1336535	1.033	1.840	0.442	4.167	2.188
24.0	1253002	0.908	1.715	0.433	3.964	2.109
22.9	1195573	0.827	1.628	0.432	3.769	1.995
21.3	1112039	0.715	1.598	0.447	3.576	1.875
15.8	824893	0.393	1.360	0.428	3.180	1.792
9.7	506422	0.148	1.130	0.392	2.883	1.766
8.0	417667	0.101	1.131	0.403	2.806	1.740
6.8	355017	0.073	1.078	0.400	2.697	1.656
2.6	135742	0.011	0.976	0.483	2.019	1.031

Table 4.22: 5 section without wing wall, S=1.9%

Q (cfs)	Re	$V^2/2g$ (ft)	$\Delta h$ (ft)	$\Delta h/H_1$	H1 (ft)	$y_1$ (ft)
27.6	1440952	1.201	2.065	0.464	4.449	2.302
25.6	1336535	1.033	1.881	0.453	4.152	2.172
23.8	1242560	0.893	1.740	0.446	3.902	2.063
22.6	1179910	0.805	1.671	0.453	3.692	1.917
21.0	1096377	0.695	1.613	0.455	3.542	1.849
14.4	751801	0.327	1.300	0.417	3.120	1.813
10.5	548188	0.174	1.161	0.399	2.908	1.760
7.8	407226	0.096	1.118	0.410	2.731	1.661
5.0	261042	0.039	1.037	0.426	2.433	1.417
3.1	161846	0.015	0.990	0.476	2.081	1.083

Table 4.23: 5 section with wing wall, S=1.9%

### 4.3.7 Tests with 45 degree wing walls and S=2.75%, 3.25% and 4.4%

Additional tests on the Linear Radial GSRD were carried out to investigate the influence of longitudinal slope on the device performance.

The additional slopes tested were: 2.75%, 3.25% and 4.4%.

All tests were conducted with the maximum expected litter loading of 90% on the basis that that represents the worse case scenario.

Moreover, all tests are performed with 5 sections GSRD and with wing walls at vault outlet.

The litter used in these tests was that from the previous series. Further quantities of litter were introduced at the start of the tests to compensate for the reduction in litter volume arising from compaction by flow.

The Head Water at inlet tank ( $y_1$ ) refers to the water depth in the inlet tank relative to the base of the tank. The inlet pipe invert is at distance of approximately 1 in from the base. The measurements of the variation of the head water in the inlet tank ( $y_1$ ) with flow rate are shown in Figure 4.47 for all slopes. The plots there confirm that the water-surface elevation in the inlet tank is independent of slope.

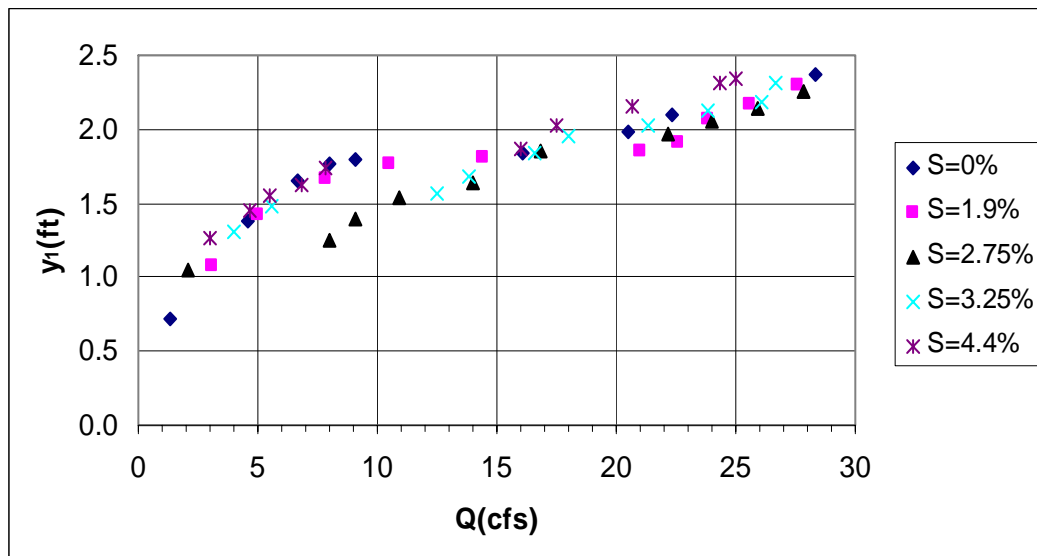


Fig. 4.47: Head water  $y_1$  vs flow rate for all slopes.

Measurements of the total head  $H_1$  are plotted against the flow rate, the Reynolds number and the velocity head in Figures 4.48-4.50, respectively.

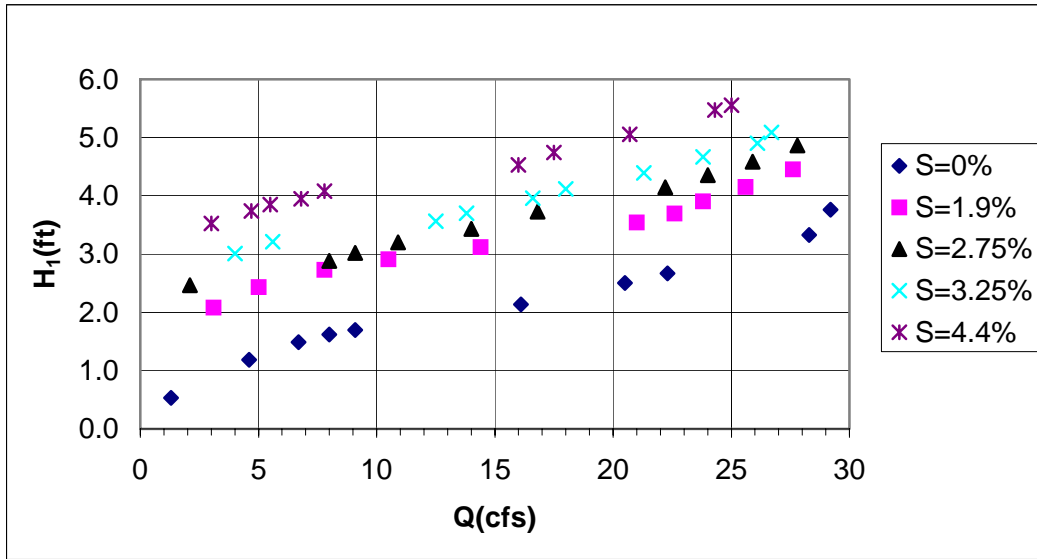


Fig. 4.48:  $H_1$  vs  $Q$  for all slopes

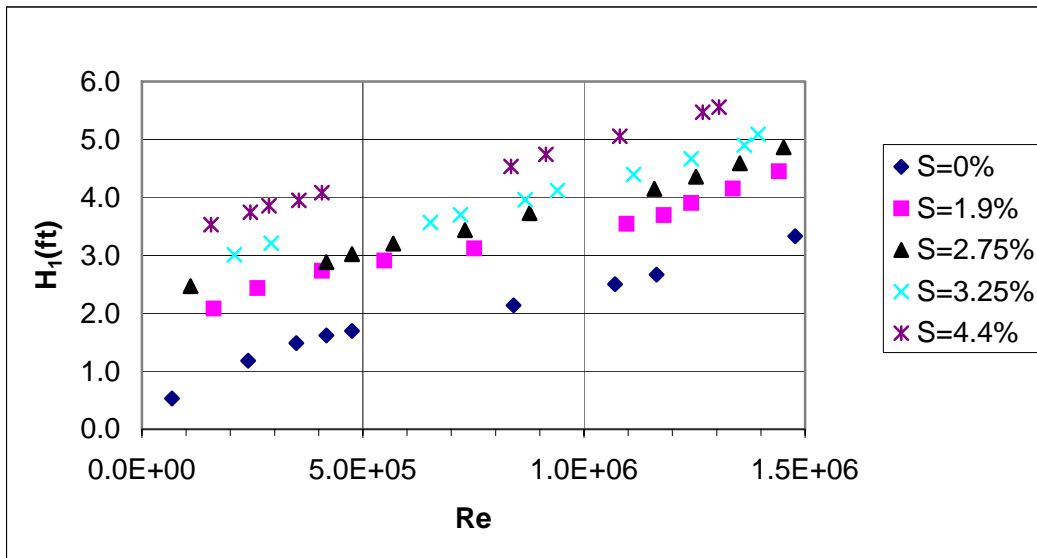


Fig. 4.49:  $H_1$  vs  $Re$  for all slopes

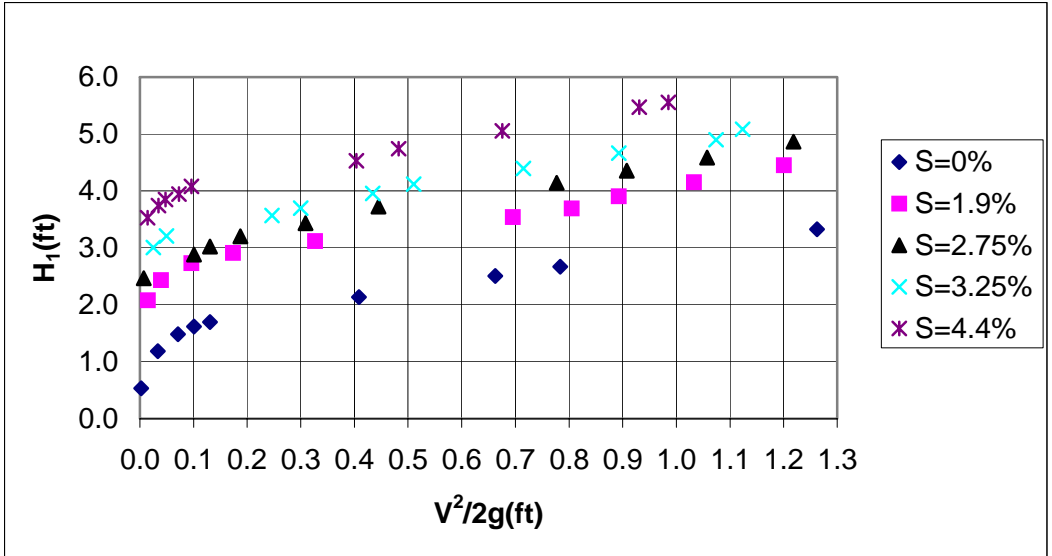


Fig. 4.50:  $H_1$  vs  $V^2/2g$  for all slopes

The computed head loss values are shown in Figures 4.51-4.53. All plots show that the head loss increases with the slope.

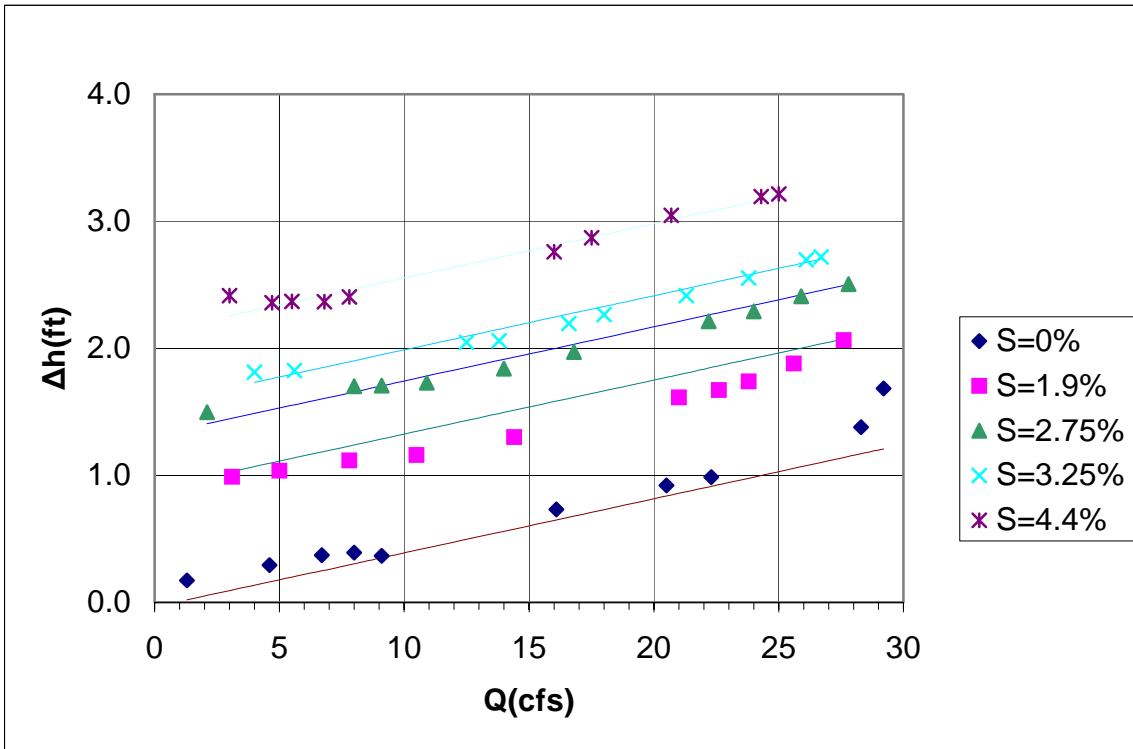


Fig. 4.51:  $\Delta h$  vs  $Q$  for all slopes.

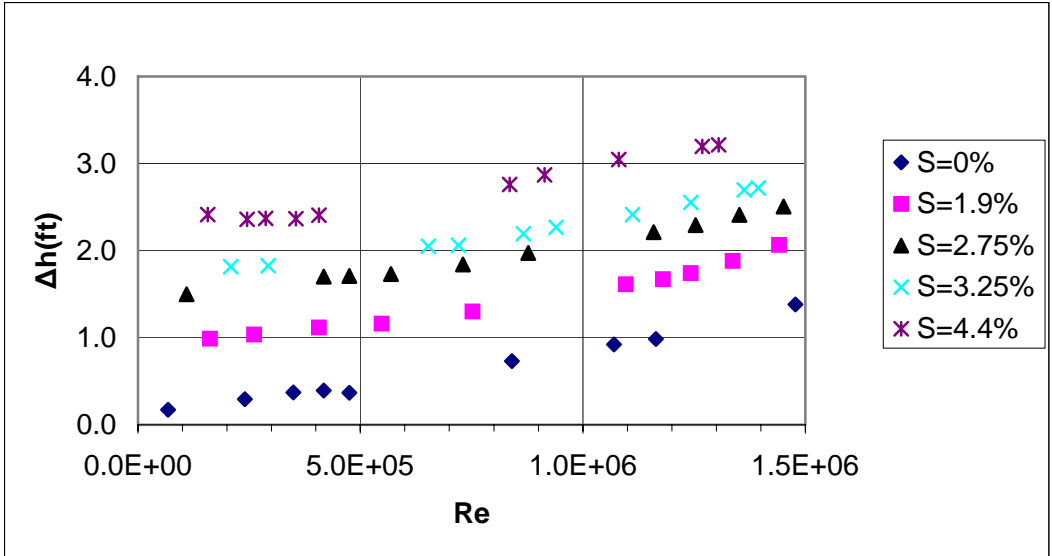


Fig. 4.52:  $\Delta h$  vs  $Re$  for all slopes

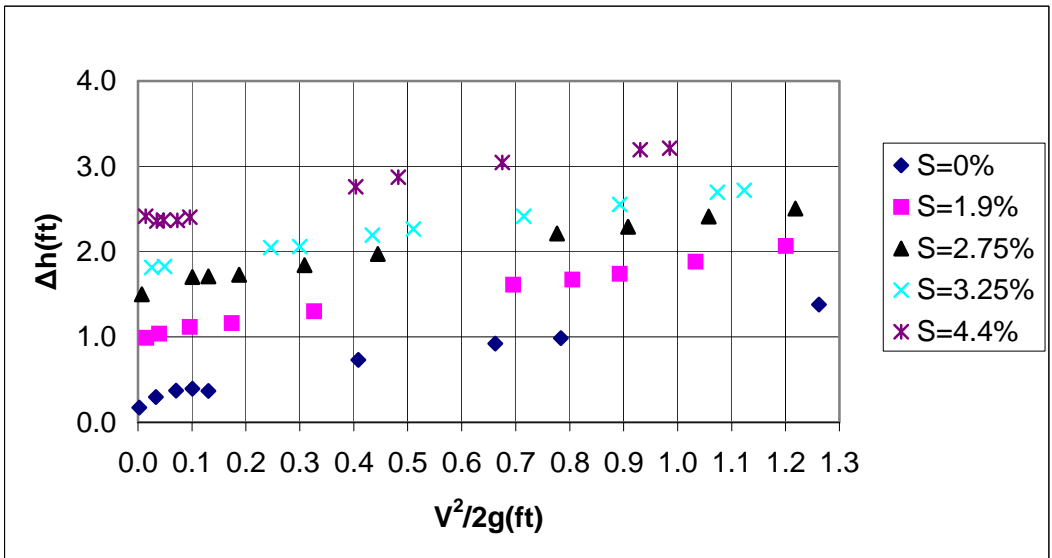


Fig. 4.53:  $\Delta h$  vs  $V^2/2g$  for all slopes

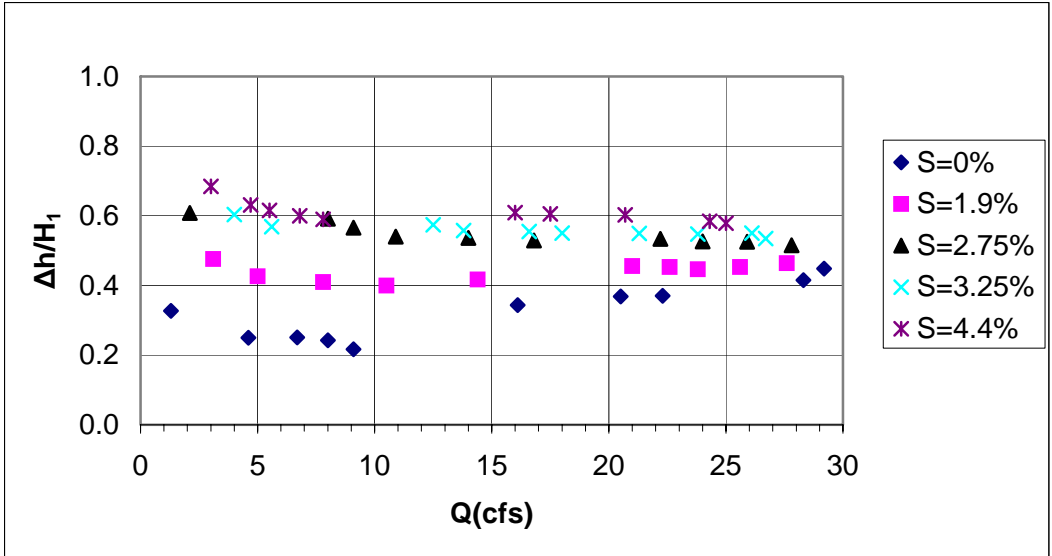


Fig. 4.54:  $\Delta h/H_1$  vs  $Q$  for all slopes

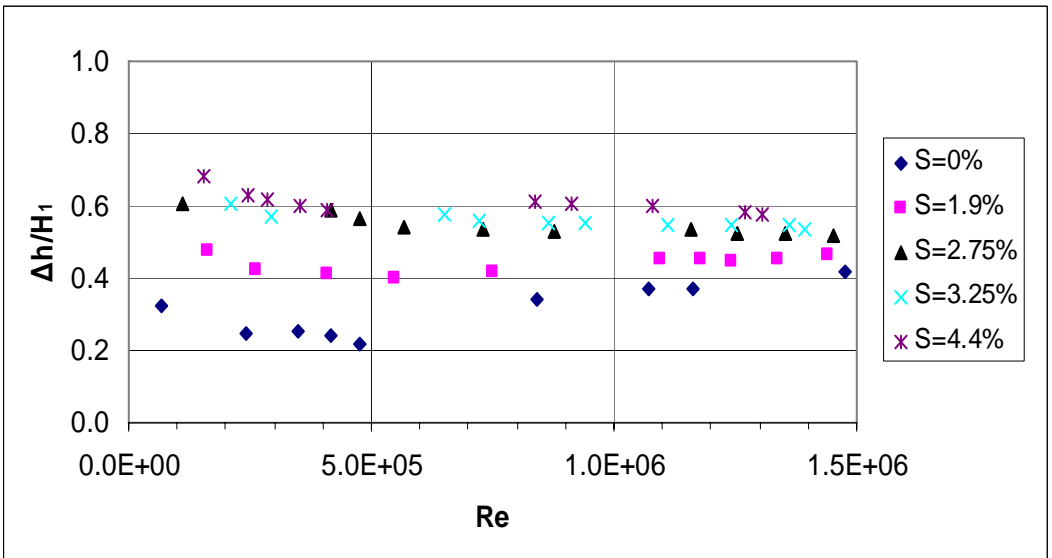


Fig. 4.55:  $\Delta h/H_1$  vs  $Re$  for all slopes

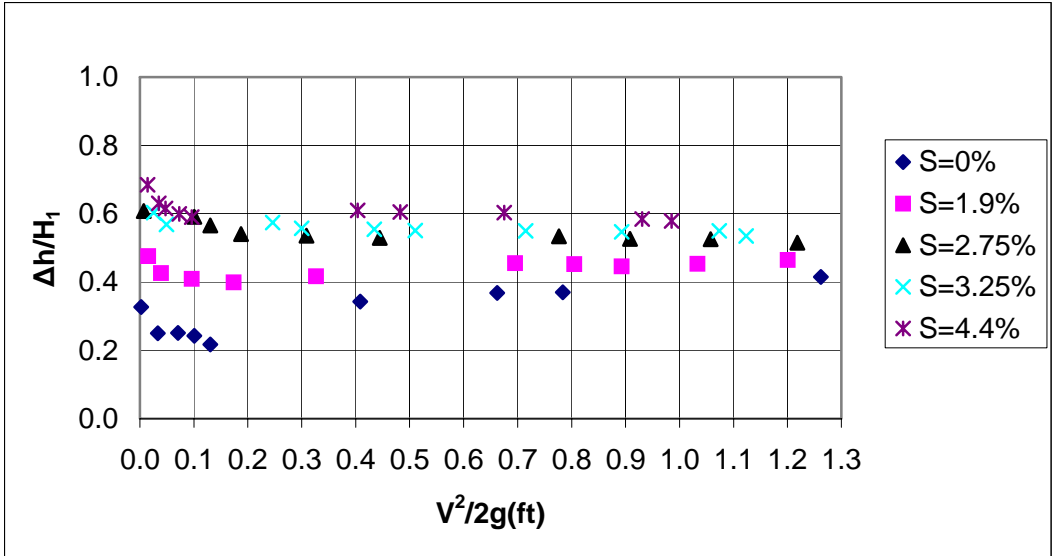


Fig. 4.56:  $\Delta h/H_1$  vs  $V^2/2g$  for all slopes

## 4.4 Observations

The tests reported in this section were recorded on digital video which can be viewed on the two CDs attached as Appendix 2.

From visual observations that can be seen from the recordings, and by measurement of weight of litter captured in 0.25 in square bag, it is concluded that the litter-capture efficacy of the linear GSRD device operating at relatively mild slope ( $S < 0.1\%$ ) appears to be of the order of 100%. This is quantified by the negligibly small volume of litter that escaped through the openings and was captured by the wire-mesh. The main constituent of the gross-solids mix that escaped from the device were tree leaves and popsicle sticks.

Tests conducted with a 1 hour triangular hydrograph did not produce results that were different qualitatively or quantitatively from those obtained with steady flow at peak discharge. Moreover, the patterns of trash compaction within the GSRD were identical irrespective of whether the flow rate was applied in the form of a hydrograph or simply as at its peak value.

Observations of the flow patterns at the free surface indicate extensive regions of strong reversed flow produced by high-speed flow emerging from the backward-facing louvers. This region of reversed flow extends an appreciable distance upstream of the end section of the device; its presence indicated strong departures from one-dimensional flow conditions.

Observations of the flow patterns near the outlet suggest appreciable head losses due to streamline convergence leading to the reduction of the effective area of flow. This result prompted later tests in which wing walls were installed in order to improve the overall hydraulic efficiency of the combination of vault and GSRD.

The performance of the Linear-Radial device totally fails when overflow occurs through the hatch located on the first section (which was unlouvered) at the entrance to the vault (see Figures 4.57 and 4.58). This overflow can result from inflow flow rates greater than 22 cfs when the gross-solids loading is greater than 50%. In operational terms, such a device, when deployed in the field, will be more likely to overflow towards the end of the rainy season as this is when accumulation of gross solids within the GSRD will be at its highest level.

The loss of storage capacity inside the Linear-Radial device due to the accumulation of gross solids can be seen in Figure 4.59. The observed overflow is partly due to blockage of the louvered openings by gross-solids items such as plastic sheeting and cardboard, as can be seen in Figure 4.60.



Fig. 4.57: Overflow for  $Q=29$  cfs and 90% loading.



Fig. 4.58: Close-up of overflow



Fig. 4.59: Patterns of accumulation of gross solids



Fig. 4.60: loss of conveyance through louvers due to accumulation of gross solids.

## 4.5 Data correlations

Correlations for the computed values of the head-loss coefficient are given below.

It is emphasized that these correlations are only applicable to the test conditions considered in this Report. The test results can not be extrapolated in the form of “universal” equations applicable to all conditions. Caution is necessary in the application of these equations to field conditions.

The head losses are fitted by linear regression as:

$$\Delta h = K \frac{V^2}{2g} + A' \quad \dots 7$$

where  $\Delta h$  and  $V^2/2g$  are in ft.  $K$  is the slope of the straight line.  $A'$  is the intercept. Equation (7) is the outcome of a best-fit to the data. The result is a straight line whose intercept is not zero. No attempt has been made to ‘force’ the line to pass through the origin even though, by doing so, the outcome would resemble the head-loss coefficient relation typically found in hydraulic design manuals. This point is discussed further in the Appendix.

The correlation coefficients  $K$  and  $A'$  are given in Tables 4.24 and 4.25. The numbers 7, 6, 5 in those Tables refer to the number of sections used. The designation ‘with’ and ‘without’ refers to the 45 degree wing walls.

It is important to note that (7) is only valid for  $Q > 2$  cfs.

	<b>K</b>	<b>A'</b>	<b>R<sup>2</sup></b>
7, with	0.9847	0.2034	0.9884
6, with	1.0051	0.2229	0.9825
5, with	0.9808	0.2597	0.9812
7, without	0.9871	0.2311	0.9806
6, without	0.9599	0.2341	0.9871
5, without	0.9445	0.2553	0.9853

Table 4.24:  $K$  and  $A'$  values for the  $S < 0.1\%$  tests

	<b>K</b>	<b>A'</b>	<b>R<sup>2</sup></b>
7, with	0.8442	1.0260	0.9930
6, with	0.9092	1.0331	0.9953
5, with	0.8555	1.0062	0.9964
7, without	0.7988	1.0099	0.9926
6, without	0.8287	1.0158	0.9959

5, without	0.8039	1.0123	0.9919
------------	--------	--------	--------

Table 4.25: K and A' values for the S=1.9% tests

The head losses are correlated with other variables as follows:

For the **S<0.1%** tests:

$$\Delta h = 0.0486 Q - 0.0196 \quad \dots 8$$

$$\text{with } R^2 = 0.9459$$

$$\Delta h = 9 \cdot 10^{-7} Re - 0.0196 \quad \dots 9$$

$$\text{with } R^2 = 0.9459$$

$$\frac{\Delta h}{H_1} = 10^{-7} Re + 0.1869 \quad \dots 10$$

$$\text{with } R^2 = 0.8019$$

$$\frac{\Delta h}{H_1} = 0.0077 Q + 0.1869 \quad \dots 11$$

$$\text{with } R^2 = 0.8019$$

$$\frac{\Delta h}{H_1} = 0.1556 \frac{V^2}{2g} + 0.2267 \quad \dots 12$$

$$\text{with } R^2 = 0.8458$$

For the **S=1.9%** tests:

$$\Delta h = 0.0409 Q + 0.8017 \quad \dots 13$$

$$\text{with } R^2 = 0.9596$$

$$\Delta h = 8 \cdot 10^{-7} Re + 0.8017 \quad \dots 14$$

$$\text{with } R^2 = 0.9596$$

$$\frac{\Delta h}{H_1} = 2 \cdot 10^{-8} \text{ Re} + 0.427 \quad \dots 15$$

with  $R^2 = 0.1067$

$$\frac{\Delta h}{H_1} = 0.0009 Q + 0.427 \quad \dots 16$$

with  $R^2 = 0.1067$

$$\frac{\Delta h}{H_1} = 0.0222 \frac{V^2}{2g} + 0.4293 \quad \dots 17$$

with  $R^2 = 0.1663$

It is important to note that the above correlations are only valid for  $Q > 2$  cfs.

Analysis of the test data for all slopes shows that the head losses can best fit with the following equation (with  $R^2 = 0.93$ ):

$$\Delta h = 0.043Q + 0.5S - 0.036 \quad \dots 18$$

where  $\Delta h$  in ft,  $Q$  in cfs,  $S$  in %, (i.e. 4.4% becomes 4.4 in this equation).

It is important to note that equation (18) is only valid for  $2 > Q$  cfs.

A plot of this regression equation is shown in Figure 4.51.

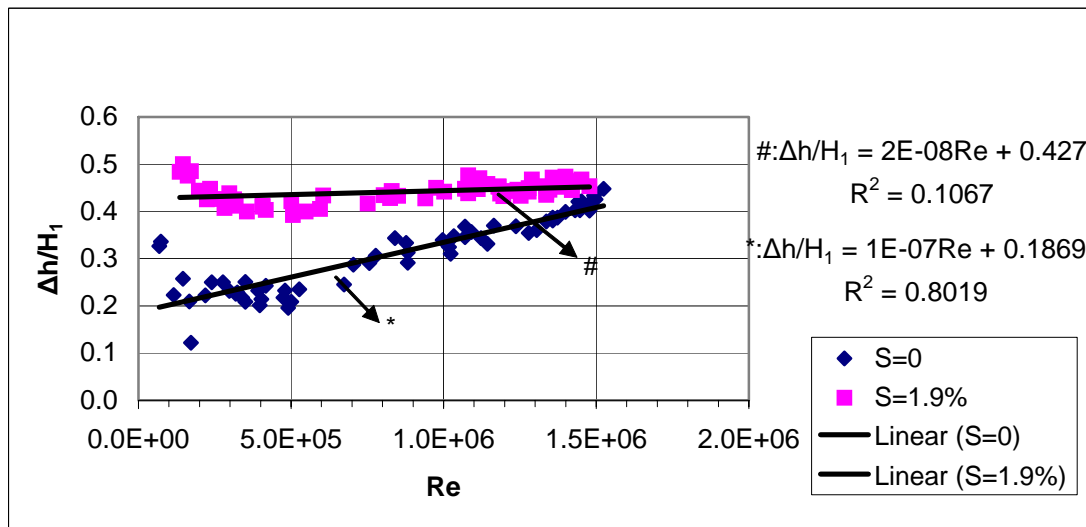


Fig. 4.61: Correlation of  $\Delta h/H_1$  with  $Re$  for  $S < 0.1\%$  and  $S = 1.9\%$

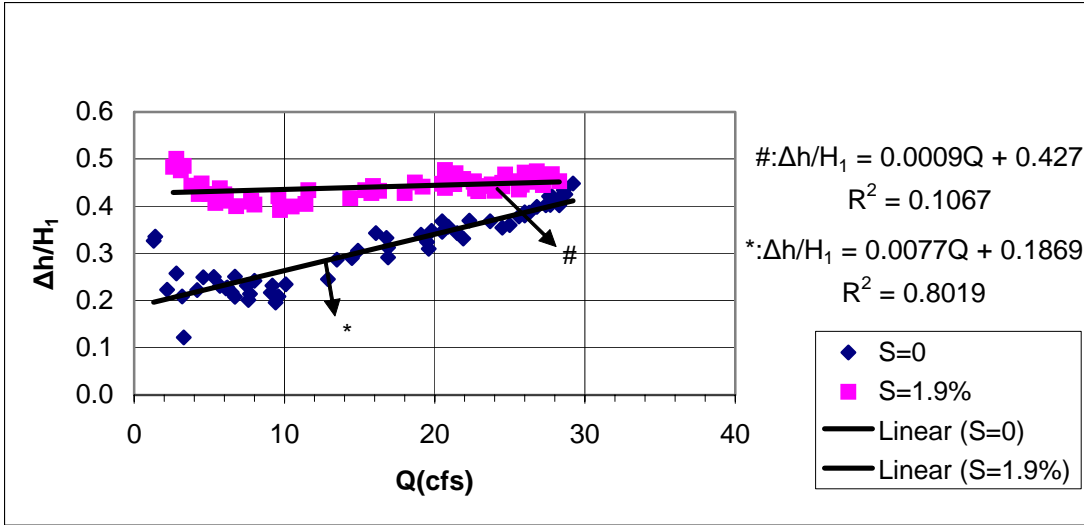


Fig. 4.62: Correlation of  $\Delta h/H_1$  with  $Q$  for  $S < 0.1\%$  and  $S = 1.9\%$

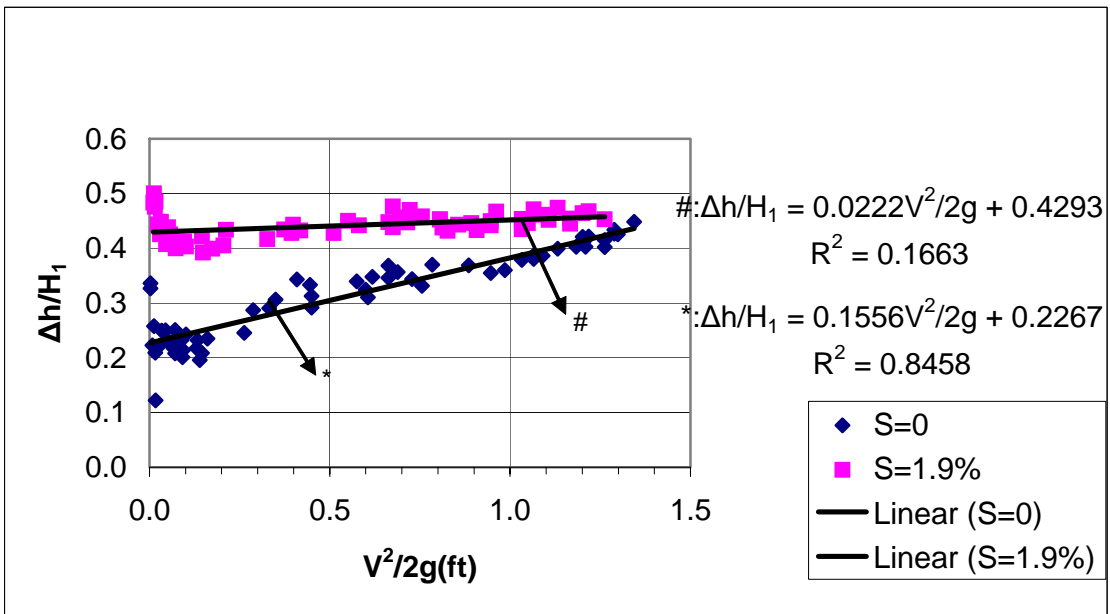


Fig. 4.63: Correlation of  $\Delta h/H_1$  with  $V^2/2g$  for  $S < 0.1\%$  and  $S = 1.9\%$

Q (cfs)	Re	V <sup>2</sup> /2g (ft)	H1 (ft)	Δh (ft)	Δh/H <sub>1</sub>	y <sub>1</sub> (ft)
29.2	1524486	1.344	3.758	1.683	0.448	2.416
28.3	1477498	1.262	3.328	1.380	0.415	2.067
22.3	1164248	0.784	2.667	0.986	0.370	1.785
20.5	1070273	0.662	2.503	0.921	0.368	1.681
16.1	840555	0.409	2.135	0.732	0.343	1.525
9.1	475097	0.131	1.697	0.368	0.217	1.494
8.0	417667	0.101	1.619	0.392	0.242	1.452
6.7	349796	0.071	1.485	0.372	0.251	1.348
4.6	240159	0.033	1.184	0.296	0.250	1.072
1.3	67871	0.003	0.532	0.174	0.326	0.410

Table 4.26: S<0.1%

Q (cfs)	Re	V <sup>2</sup> /2g (ft)	H1 (ft)	Δh (ft)	Δh/H <sub>1</sub>	y <sub>1</sub> (ft)
27.6	1440952	1.201	4.449	2.065	0.464	2.302
25.6	1336535	1.033	4.152	1.881	0.453	2.172
23.8	1242560	0.893	3.902	1.740	0.446	2.063
22.6	1179910	0.805	3.692	1.671	0.453	1.917
21.0	1096377	0.695	3.542	1.613	0.455	1.849
14.4	751801	0.327	3.120	1.300	0.417	1.813
10.5	548188	0.174	2.908	1.161	0.399	1.760
7.8	407226	0.096	2.731	1.118	0.410	1.661
5.0	261042	0.039	2.433	1.037	0.426	1.417
3.1	161846	0.015	2.081	0.990	0.476	1.083

Table 4.27: S=1.9%

Q (cfs)	Re	V <sup>2</sup> /2g (ft)	H1 (ft)	Δh (ft)	Δh/H <sub>1</sub>	y <sub>1</sub> (ft)
27.8	1451394	1.218	4.865	2.504	0.515	2.255
25.9	1352198	1.057	4.585	2.410	0.526	2.135
24.0	1253002	0.908	4.352	2.291	0.526	2.052
22.2	1159027	0.777	4.143	2.212	0.534	1.969
16.8	877101	0.445	3.726	1.972	0.529	1.859
14.0	730918	0.309	3.432	1.839	0.536	1.635
10.9	569072	0.187	3.202	1.728	0.540	1.531
9.1	475097	0.131	3.021	1.708	0.565	1.391
8.0	417667	0.101	2.879	1.702	0.591	1.255
2.1	109638	0.007	2.465	1.499	0.608	1.047

Table 4.28: S=2.75%

<b>Q (cfs)</b>	<b>Re</b>	<b>V<sup>2</sup>/2g (ft)</b>	<b>H1 (ft)</b>	<b>Δh (ft)</b>	<b>Δh/H<sub>1</sub></b>	<b>y<sub>1</sub> (ft)</b>
26.7	1393965	1.124	5.087	2.720	0.535	2.318
26.1	1362640	1.074	4.902	2.696	0.550	2.182
23.8	1242560	0.893	4.664	2.552	0.547	2.125
21.3	1112039	0.715	4.392	2.414	0.550	2.031
18.0	939751	0.511	4.116	2.266	0.550	1.953
16.6	866660	0.434	3.958	2.195	0.555	1.844
13.8	720476	0.300	3.698	2.060	0.557	1.677
12.5	652605	0.246	3.565	2.048	0.574	1.573
5.6	292367	0.049	3.209	1.824	0.568	1.484
4.0	208834	0.025	3.006	1.813	0.603	1.307

Table 4.29: S=3.25%

<b>Q (cfs)</b>	<b>Re</b>	<b>V<sup>2</sup>/2g (ft)</b>	<b>H1 (ft)</b>	<b>Δh (ft)</b>	<b>Δh/H<sub>1</sub></b>	<b>y<sub>1</sub> (ft)</b>
25.0	1305210	0.985	5.557	3.215	0.578	2.344
24.3	1268665	0.931	5.472	3.195	0.584	2.313
20.7	1080714	0.675	5.055	3.046	0.603	2.151
17.5	913647	0.483	4.743	2.870	0.605	2.031
16.0	835335	0.404	4.529	2.759	0.609	1.875
7.8	407226	0.096	4.077	2.405	0.590	1.734
6.8	355017	0.073	3.946	2.365	0.599	1.620
5.5	287146	0.048	3.850	2.368	0.615	1.552
4.7	245380	0.035	3.740	2.358	0.631	1.453
3.0	156625	0.014	3.527	2.414	0.684	1.266

Table 4.30: S=4.4%

## 4.6 Conclusions

Below is summary of the main conclusions on the tests on the Linear-Radial GSRD:

1. The gross-solids capture efficiency of this device is very high except when the device overflowed due to high flow rate and percentage loading. The volume of gross solids that escaped through the surface louvers and was captured in a downstream bag was negligibly small. The escaped material consisted mainly of tree leaves and other vegetation. The other main item of the gross solids mix that did leave the GSRD was the flat wooden (popsicle) sticks that floated inside the GSRD and were eventually ejected from it by force of the backward-directed flow leaving through the louvers.
2. The high efficiency of this device in litter capture is due in part to the backward-facing orientation of the surface louvers coupled with their small opening size (0.25 inches). This ensured that only slender items of gross solids that were also capable of floatation left the device. Items such as newspapers disintegrated and became attached to other items of the gross solids mix, or to the inside of the GSRD.
3. Items of cloths, cardboard and plastic sheets were forced to adhere to the GSRD's inner walls during a flow event but then largely fell away from it when dry. Cigarette filters remained lodged in the louvered sections but did not escape.
4. The capture efficiency of this device did not deteriorate noticeably with increase in longitudinal slope, up to the maximum value of 4.4% achievable in the test bed. The conditions of steeper slopes that could lead to failure of this device in the field could not be reproduced in the present tests.
5. The gross solids accumulated inside the device in the form of cone with base against the end door. This had the effect of causing blockage of the end-door louvers from the early stages of operation. As expected, the overall capacity deteriorated with higher percentage loading. Also, the conveyance through the louvers was reduced by the action of accumulation of wet gross solids items such as cardboard and paper.
6. The ability of this device to discharge high flow rates degraded with increased gross solids loading. For a 7-sections arrangement, for example, overflow was observed to occur for 90% gross solids loading at a flow rate of 22.5 cfs.

7. Flow through the outlet pipe was predominantly in 'inlet control'. This was evident from observation of the rapid reduction in water surface elevation in the outlet pipe. Increasing the longitudinal slope to the maximum value of 4.4% led to reduction in water surface elevation but the 'inlet control' conditions remained at exit from the vault.
8. The backward-facing orientation of the louvers generated a very strong reversed flow at the water's free surface inside the vault. The presence of this reversed flow increases the hydraulic losses associated with this device and introduces departures from one-dimensional flow assumptions.
9. Flow through the outlet pipe was predominantly in 'inlet control'. This was evident from observation of the rapid reduction in water surface elevation in the outlet pipe. Increasing the longitudinal slope to the maximum value of 4.4% led to reduction in water surface elevation but the 'inlet control' conditions remained at exit from the vault.
10. Installation of 45 degree wing walls on either side of the outlet pipe reduced the exit losses as was evidenced by visualization of water movement at the free surface.
11. Removal of gross solids from the Linear-Radial device is expected to pose significant operational problems in matters related to maintenance and litter removal. Access to the gross solids was via hatches that did not span the entire length of each section. Consequently, litter that accumulated in areas between these hatches, or compacted against the end plate, was difficult to access and remove. Repeated wetting and drying of cardboard and papers changed their constitution in such a way that they became lodged in the louvers thereby reducing their conveyance effectiveness.

## **Section 5: Results for parabolic screens (Type 1) GSRD**

### **5.1 Description of Type 1 device**

The particular inclined screens tested were manufactured and supplied by IPEC Industries (2889 Norland Avenue, Burnaby, BC Canada V5B 3A9 Tel: (604) 291-7150 Fax: (604) 291-7190).

The specifications quoted by the manufacturers were as follows:

1. Size: 72" by 40" (nominal)
2. Construction: 90 BF / 1/4 round
3. Material: 304 stainless steel
4. Slot: 3/16"
5. Trim: End caps and mounting plates
6. Accessories: Formed top crest with screen mounting saddle

The dimensions were as follows:

Screens:

Height 35 inches, height/run at 1:50, slot size 4.4 mm, length - on 2 legs, about 6.0 ft each leg.

Weir:

Weir at top of screen: about 4 inches in height and 8 inches in width.  
Distance between weir and top of 'vault' - 1.5 ft.

Interior litter box dimensions:

6 ft by 6 ft plus 'interior column' of 19 inches (between the two legs of the screens, related to the height:run ratio), giving 7.6 x 7.6 ft.

Distance from floor of litter storage area to top of outflow pipe (to represent a concrete floor in actual placement): 8 inches

Influent box dimensions:

Leg 1: 2 ft wide; Leg 2: 18 inches in width; 45 degree interior angles of the influent area.

Influent and litter boxes have a 2% slope in the direction of flow (i.e., for the influent box, towards the wall atop which the weir is placed; for the litter storage area).

Inflow pipe elevation:

28 inches below the top of weir.

Weep holes:

From influent trough through wall holding up the weir: 2 drain holes, one on each leg of the influent trough; diameter (5 ") sized to allow drainage from the influent trough area in 3 hours. A single drain hole from the litter storage area to the outflow pipe: estimate a 1/2 inch diameter, covered with a wire mesh (1/4" square).

A schematic of the layout is shown in Fig. 5.1a. The dimensions are shown on Fig. 5.1b.

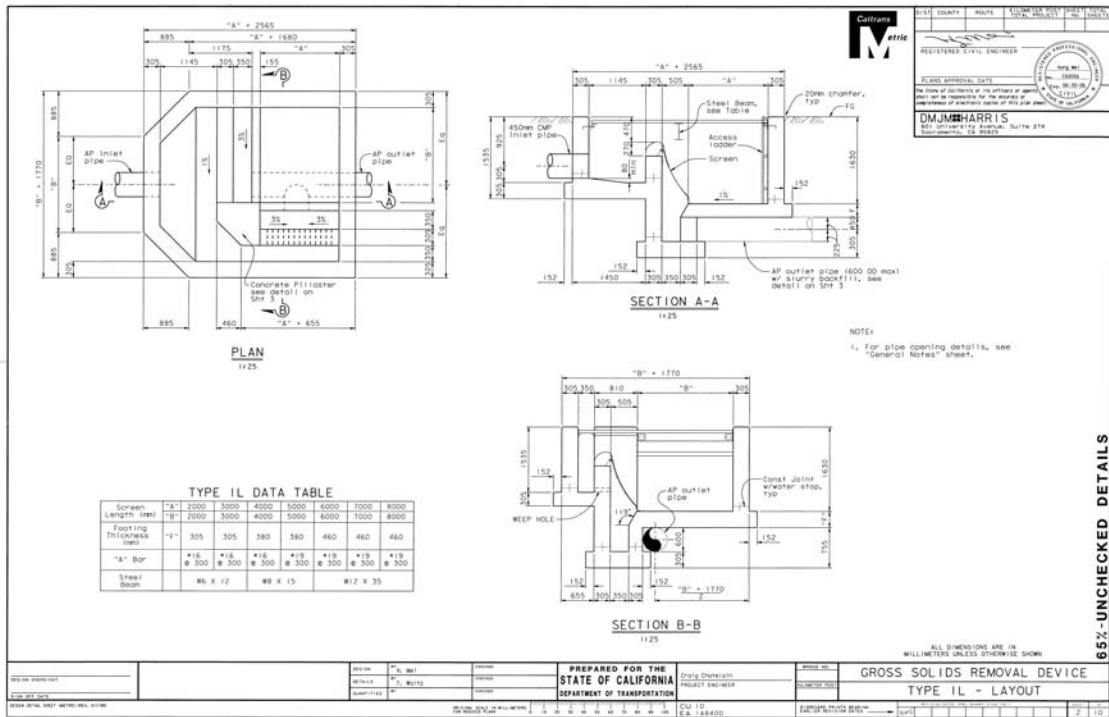
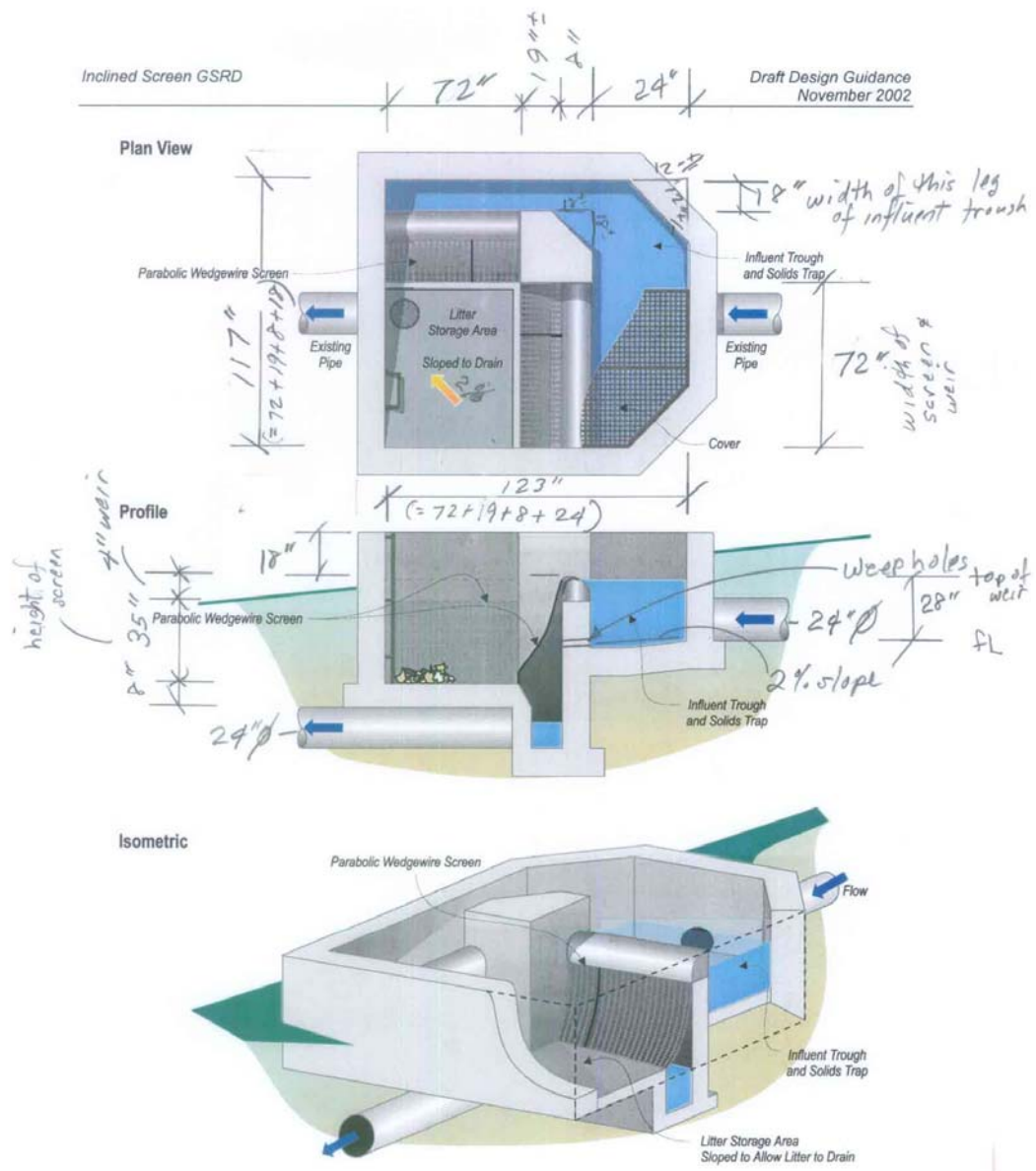


Fig. 5.1a: Layout of Type 1 parabolic screens tested.



Phase 1 **Figure 1-1**  
**Inclined Screen GSRD**

bb 6/21/04 Not to scale

Fig. 5.1b: Dimensions for Type1L GSRD.



Fig. 5.2: A close-up of the parabolic screen attached to a weir.



Fig. 5.3: Detail of the screen where it meets the sloped litter storage area.



Fig. 5.4: Weep holes used to drain the runoff which accumulates in the influent trough.



Fig. 5.5: View of the influent trough and solids trap showing the parabolic wedgewire screens in place below the curved weirs.

## 5.2 Scope and procedure of tests

All tests were conducted with the box containing the parabolic screens placed level with no significant longitudinal slope.

The slope of the inflow pipe was set to 4%.

The outflow pipe was sloped at approximately 1%.

The composition of the gross solids used in the tests was identical to that used for the Linear-Radial GSRD. A significant percentage of material used in the earlier tests was re-used, supplemented by new material mixed in the same proportions as before.

Testing was performed according to the schedule given in Table 5.1:

<b>Flow (% of Capacity/cfs)</b>	<b>Debris Volume (% of Capacity)</b>
10%/1.1 cfs	0
10%/1.1 cfs	10
10%/1.1 cfs	50
10%/1.1 cfs	90
50%/5.5 cfs	10
50%/5.5 cfs	50
50%/5.5 cfs	90
110%/11.1+/- cfs	10
110%/11.1+/- cfs	50
110%/11.1+/- cfs	90
110%/11.1+/- cfs	0

Table 5.1: Schedule of tests on the Type 1 parabolic screens GSRD.

In Table 5.1, 100% flow rate is the theoretical maximum flow rate defined for the Type 1 device. This was specified as 10.1 cfs. The maximum volume of gross solids tested was 33 cubic feet.

In all tests carried out, the flow rate was measured by means of the ultrasound flow meter used for the Linear-Radial GSRD.

The principal measurements taken were of the water depths at the influent trough for each flow rate, and of the water surface elevation in the litter storage area.

Also measured was the time taken for complete drainage of the influent trough area, a parameter indicative of the performance of the weep holes introduced for that purpose.

The procedure for the tests on the Type 1 device was as follows:

1. The flow rate is set to the required value by means of adjustment to opening of control valve on upstream storage tank. Once required value is obtained, the pump is closed.
2. The required volume of gross solids is added in the receiving tank upstream of the device.
3. Pump is restarted and the test is run for a period of one hour.
4. Water surface elevations at required locations are recorded.
5. Pump is closed and the time for complete drainage of influent trough is recorded.
6. Gross solids accumulated in influent trough and in storage area are cleared and dried for later re-use.

All tests were documented with a digital camcorder and are included on a CD in the Appendix.

### 5.3 Test results

Table 5.2 gives the measured water depth in the influent trough and in the litter storage tank as a function of flow rate and percentage litter loading.

The variation of these quantities with Q is shown in Figure 5.6.

Table 5.3 gives the measured water depth (in) at influent trough as a function of time (min). The results presented there are for the tests with a flow rate of 5.5 cfs and 50% loading and for flow rate of 11.1 cfs and 90% loading of litter.

A plot of water depth in influent trough (in inches) with time from pump stop is shown in Figure 5.7. From this plot it is clear that the time taken to drain this GSRD does not depend on the flow rate nor on the gross solids percentage loading.

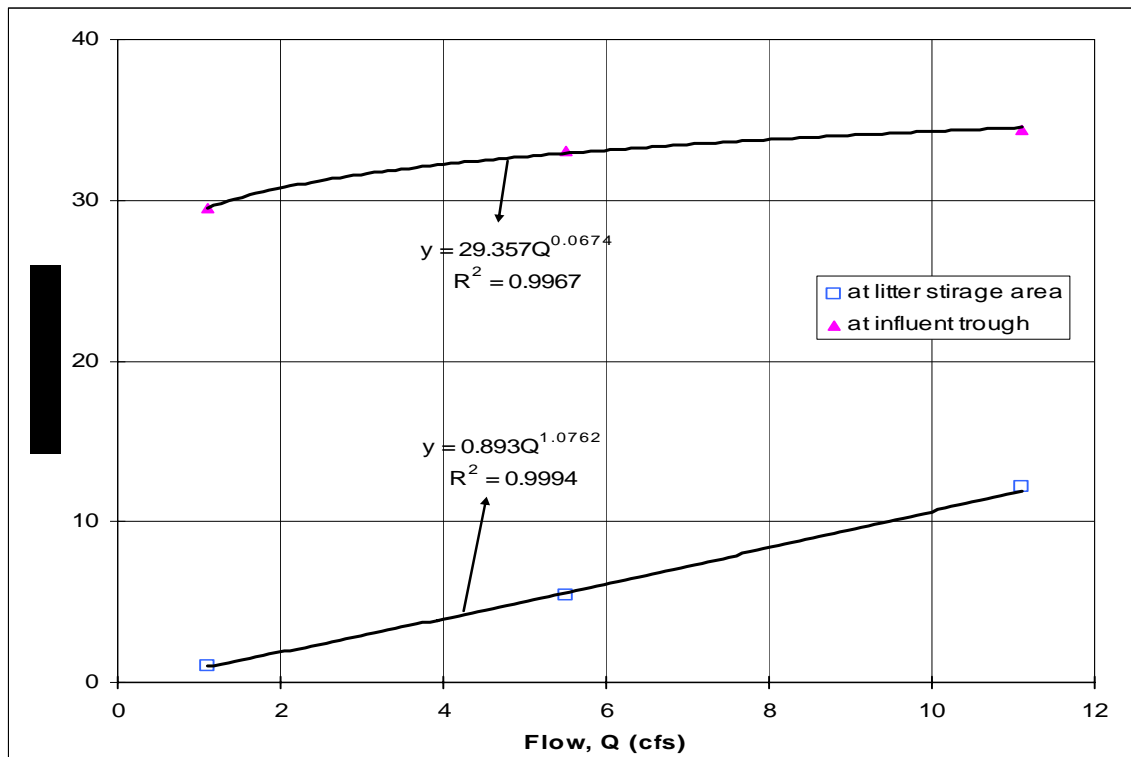


Fig. 5.6: Plot of water depth in influent trough (in inches) and in the litter storage area vs flow rate Q (in cfs).

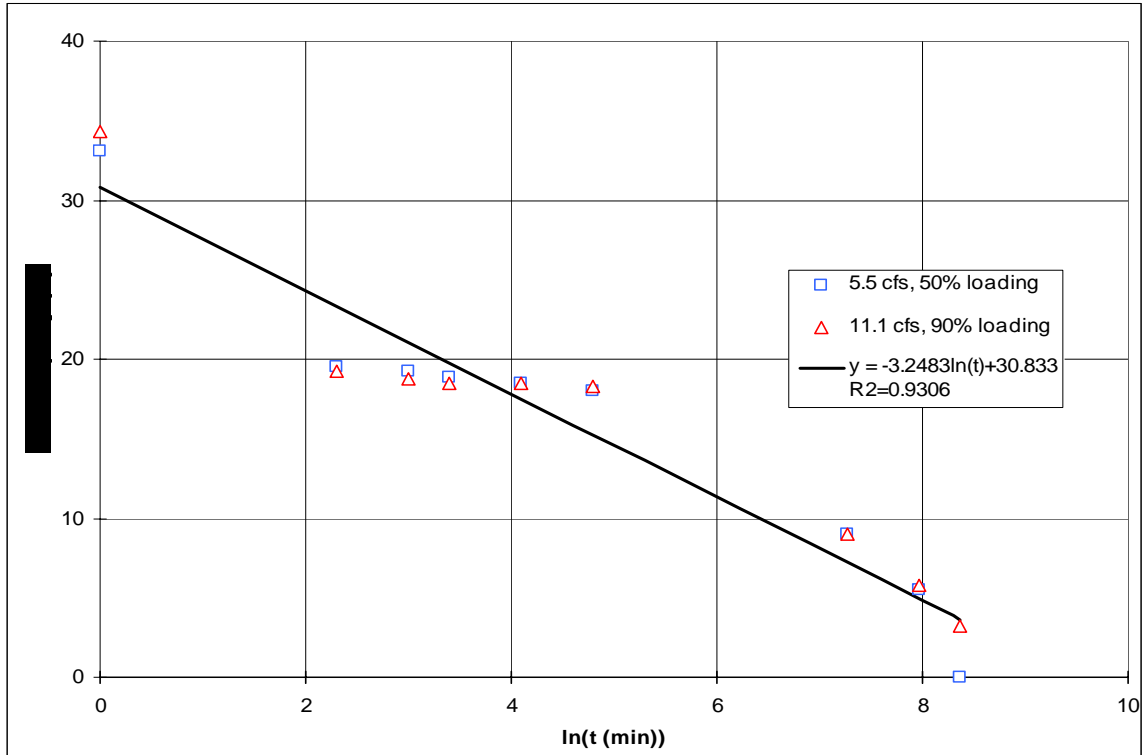


Fig. 5.7: Plot of water depth in influent trough (in inches) vs time from pump stop (plotted as natural log of time (in minutes)).

Test	Flow (cfs)	Litter volume (% of capacity)	Water depth during the test	
			at storage (in)	at influent trough (in)
1.1	1.1	0	1.0	29.5
2.1	1.1	10	1.0	29.5
3.1	1.1	50	1.0	29.5
4.1	1.1	90	1.0	29.5
5.1	5.5	10	5.4	33.1
6.1	5.5	50	5.4	33.1
7.1	5.5	90	5.4	33.1
8.1	11.1	10	12.2	34.4
9.1	11.1	50	12.2	34.4
10.1	11.1	90	12.2	34.4
11.1	11.1	0	12.2	34.4

Table 5.2: Measured water depths obtained for various flow rates and gross solids loading.

time (min)	water depth (in)	
	(A)	(B)
1	33.1	34.4
10	19.5	19.3
20	19.3	18.8
30	18.9	18.5
60	18.5	18.5
120	18.0	18.3
1440	9.0	9.1
2880	5.5	5.8
4320	0.0	3.3

Table 5.3: Measured water depth (in) at influent trough as a function of time (min). Column (A): results for test with 5.5 cfs and 50% loading of litter. Column (B): results for test with 11.1 cfs and 90% loading of litter. Time=1 min corresponds to time just before closing of pump.

## 5.4 Data correlations

The units in the correlations below are cfs for discharge, inches for water depth and minutes for time.

Note that all correlations are valid for  $Q > 1.1$  cfs.

Water depth at influent trough during the test:

$$y = 29.357Q^{0.0674}$$

with  $R^2=0.9967$

Water depth at litter storage area during the test:

$$y = 0.893Q^{1.0762}$$

with  $R^2=0.9994$

Water depth at influent trough after the test.  $t=0$  is 1 minute after pump is stopped:

$$y = -3.2483\ln(t) + 30.833$$

with  $R^2=0.9306$

## **5.5 Observations**

### **Q=1.1 cfs and 90% loading**

At this low flow rate, certain amounts of gross solids accumulated inside the inflow trough and did not clear when the pump was stopped. On completion of the test, this material settled within the inflow trough as can be seen from Figure 5.8. This material is expected to contribute to the blockage of the weep holes at the start of the following rainfall event.

The parabolic screens remained entirely free of debris after the conclusion of tests with this low flow rate. This can be seen in Figure 5.9. This is an entirely favorable feature of the design of this device and would suggest that the flow of water over the weirs remains attached to the screens thereby clearing them of debris that may have lodged in them.

### **Q=5.5 cfs and 10% loading**

Figure 5.10 presents a clear demonstration of the pattern of water flow over one of the weirs and a parabolic screen. The water remains largely attached to the screen thereby ensuring the self-cleaning of the screens and, in addition, facilitating the drainage of water out of the device without first accumulating in the litter storage tank.

Drainage through the weep holes is impeded by their blockage, as can be seen from Figure 5.11 which was taken 24 hours after completion of test.

### **Q=5.5 cfs and 50% loading**

The accumulation of litter in the inflow trough is clearly evident at the higher percentage loading, as can be seen from Figure 5.12. It is expected that litter remaining in the inlet trough will eventually cause blockage of the weep holes.

Figure 5.13 confirms that the screens remain essentially free of debris after testing at high flow rate and percentage loading.

### **Q=11.1 cfs, clean flow**

At the highest flow rate tested, the flow over the weir was deflected downwards and thus remained attached to the screen, as can be seen from Figures 5.14 and 5.15.

### **Q=11.1 cfs, 10% loading**

Figure 5.16 shows the patterns of water flow over the screen. The figure also suggests extensive water conveyance through the screen.

**Q=11.1 cfs, 50% loading**

Figures 5.17 and 5.18 show that at the higher flow rate, most gross solids introduced into the device are conveyed efficiently over the weirs without settling into the inflow troughs.

Some gross solids flowing into the inflow trough are caught in a recirculation zone that develops near the entrance, as can be seen in Figure 5.19. Some of this trapped load eventually settles into the inflow trough.

**Q=11.1 cfs, 90% loading**

Figure 5.20 shows that the gross solids introduced are swept off the screens to settle in the litter storage tank leaving the bulk of the screen area clear.



Fig. 5.8: Gross solids retained in inflow trough after completion of test.



Fig. 5.9: Screens remain clear of trash after flow rate of 1.1 cfs and 10% loading.



Fig. 5.10: Flow remains attached to the screens at  $Q=5.5$  cfs and 10% loading.



Fig. 5.11: Blockage of inflow trough 24 hours after completion of test.



Fig. 5.12: Inflow trough storage after completion of test with  $Q=5.5$  cfs and 50% loading.



Fig. 5.13: Clear screen is in evidence after test with  $Q=5.5$  cfs and 50% loading.



Fig. 5.14: Flow remaining attached to screen at  $Q=11.1$  cfs.



Fig. 5.15: Strong streamline curvature above weir for  $Q=11.1$  cfs.



Fig. 5.16: Conveyance through the screen at high flow rate.



Fig. 5.17: Gross solids conveyance over the screens at  $Q=11.1$  cfs and 50% loading.



Fig. 5.18: Efficient conveyance of gross solids over the screens at  $Q=11.1$  cfs and 50% loading.



Fig. 5.19: Gross solids trapped in recirculation zone ( $Q=11.1$  cfs, 50% loading).



Fig. 5.20: Clear screen with most of the gross solids settled in the litter storage tank.

## 5.6 Closure

1. Flow rate of 1.1 cfs did not produce enough force to move the gross solids completely. Most of the inserted material remained either in the litter insertion tank or in the influent trough. It is unlikely that this device will operate satisfactorily for low flow rates though the situation in the field may be different as the device there will be connected directly to the upstream pipe system where the flow velocities will be higher than those at exit from the insertion tank.
2. At the end of tests for the higher flow rates of 5.5 cfs and 11.1 cfs, most of the gross solids accumulated in the litter storage area, as intended. Significant quantities, however, also accumulated in the far end of the influent trough.
3. The parabolic wedge wire screens appear to be fairly efficient in conveying litter-free water to the outflow pipe. There was no significant escape of litter through the screens' openings.
4. Drainage of the influent trough through the weeping holes did not proceed satisfactorily. The wire mesh screens used to guard these holes quickly became blocked with items of litter such as leaves and disintegrated paper and cardboard. This was especially the case for the wire screens at the far end of the trough.
5. Drainage from the litter storage area proceeded very rapidly once the pump was stopped. In contrast, drainage of the influent troughs occurred over two days or more.
6. The head losses in this device are largely due to the enormous difference in elevation between the inflow section and outlet from the litter storage area; a quantity which far exceeds the combined minor and frictional losses.

## **Section 6: Results for straight screens (Type 2) GSRD**

### **6.1 Description of Type 2 device**

The dimensions are as per plan sheets supplied by the manufacturer (IPEC Industries, 2889 Norland Avenue, Burnaby, BC, Canada V5B 3A9 ,Tel: (604) 291-7150 Fax: (604) 291-7190) whose specification were as follows:

1. The type tested were the "Sidehill Screen Panels" with mounting brackets, hinges and support bars. These panels were constructed as per Sheet 28, Gross Solids Removal Device, Type 2 – Inclined Screen
2. Size: 1 m x 2.0 m
3. Construction: 90F /  $\frac{1}{4}$  rod @ 2 $\frac{1}{2}$ " c/c
4. Material: 304 stainless steel
5. Slot: 3/16" (4.7 mm)
6. Trim: 76 mm x 5 mm flat bar, 38 mm x 38 mm x 5 mm angle, 100 mm x 100 mm x 110 mm mounting anchors and pins, 72 mm x 75 mm x 9.5 mm base pads

Figures 6.1(a) and 6.1(b) provide details of the panels used.

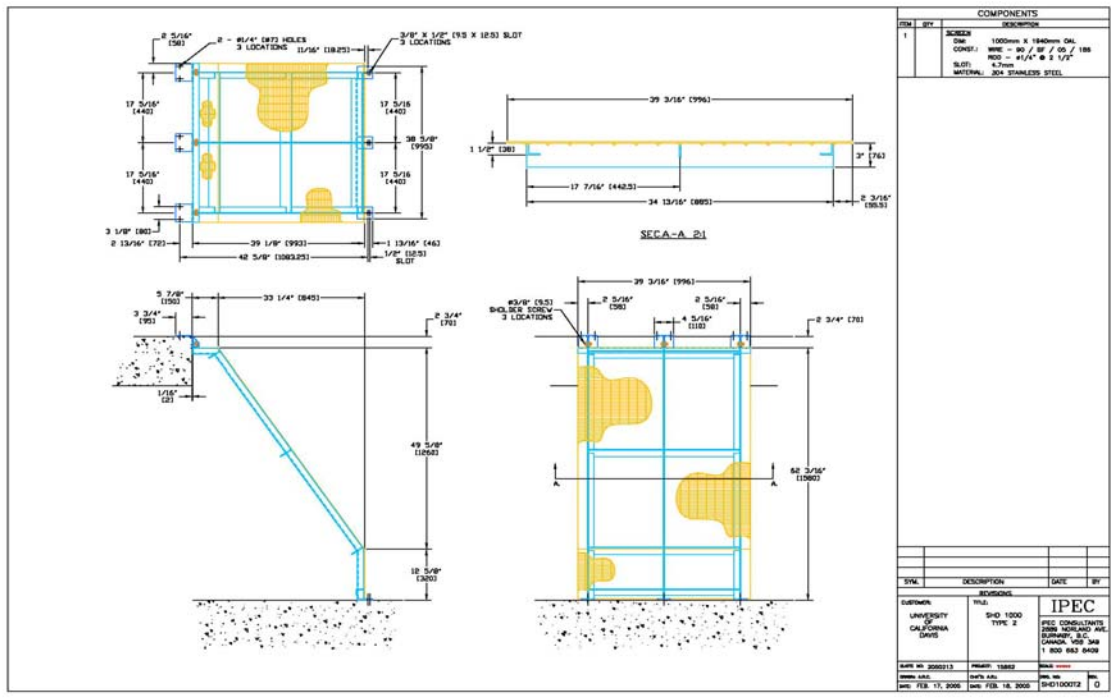


Fig. 6.1a: details of Type 2 panels.

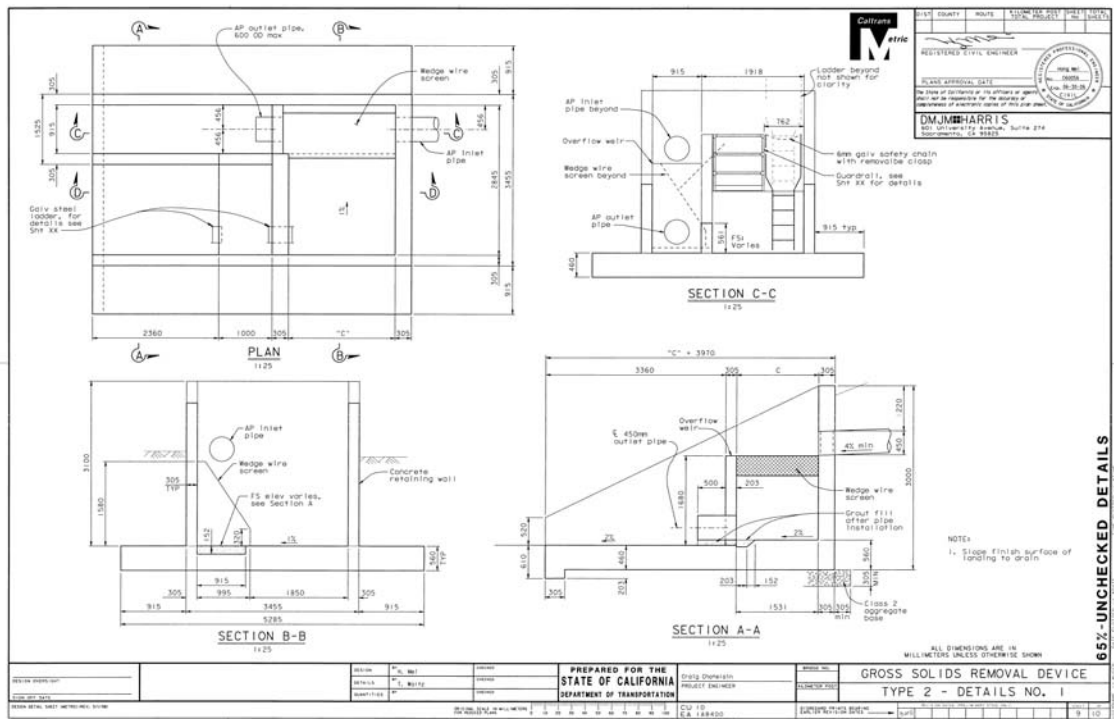


Fig. 6.1b: Construction plan for Type 2 panel.

## 6.2 Scope and procedure

All tests were conducted with the box containing the straight screens placed level with no significant longitudinal slope.

The slope of the inflow pipe was set to 4%.

The outflow pipe was sloped at approximately 1%.

The composition of the gross solids used in the tests was identical to that used for all the previous tests.

Testing was performed according to the schedule given in Table 6.1:

<b>Flow (cfs)</b>	<b>Debris volume (% of capacity)</b>
0.94	0
1.85	0
2.7	0
3.5	0
4.35	0
5.0	0
6.13	0
7.06	0
8.24	0
9.0	0
1.1	10
1.1	50
1.1	90
5.5	10
5.5	50

Table 6.1: Tests performed on straight inclined screens (Type 2)

The tests performed were in accordance with the following procedure:

1. Pump is opened and the gate valve adjusted till the required flow rate was attained.
2. Pump is closed and litter is added in the gross solids insertion tank upstream of the Type 2 device.

3. Pump is opened and the test is run for approximately 20 minutes. This time was sufficient for the hydraulic parameters of the system to reach equilibrium state. Specifically, the water depths attained steady-state levels and all the gross solids that were introduced were transported into the storage area.
4. The water depths at outlet from the trash insertion tank ( $y_i$ ), at the outlet pipe from the device ( $y_e$ ) and inside the litter storage area are measured.  $y_i$  and  $y_e$  are measured from the pipes' invert.
5. Prior to the commencement of each test, all gross solids accumulated within the storage tank were removed, and the screens cleared of debris lodged within it.
6. Movement of litter and water was recorded by a digital camcorder and camera.

## 6.3 Data collection and analysis

### 6.3.1 Head Water

The Head Water at inlet  $y_1$  refers to the water depth in the trash insertion tank relative to the invert of the outlet pipe of the tank.

The Head Water at outlet  $y_2$  refers to the water depth at outlet pipe from the device relative to the invert of the outlet the pipe.

These measurements are reported in Figure 6.2. The maximum water depth in the litter storage area was 53" which occurred for  $Q=9$  cfs.

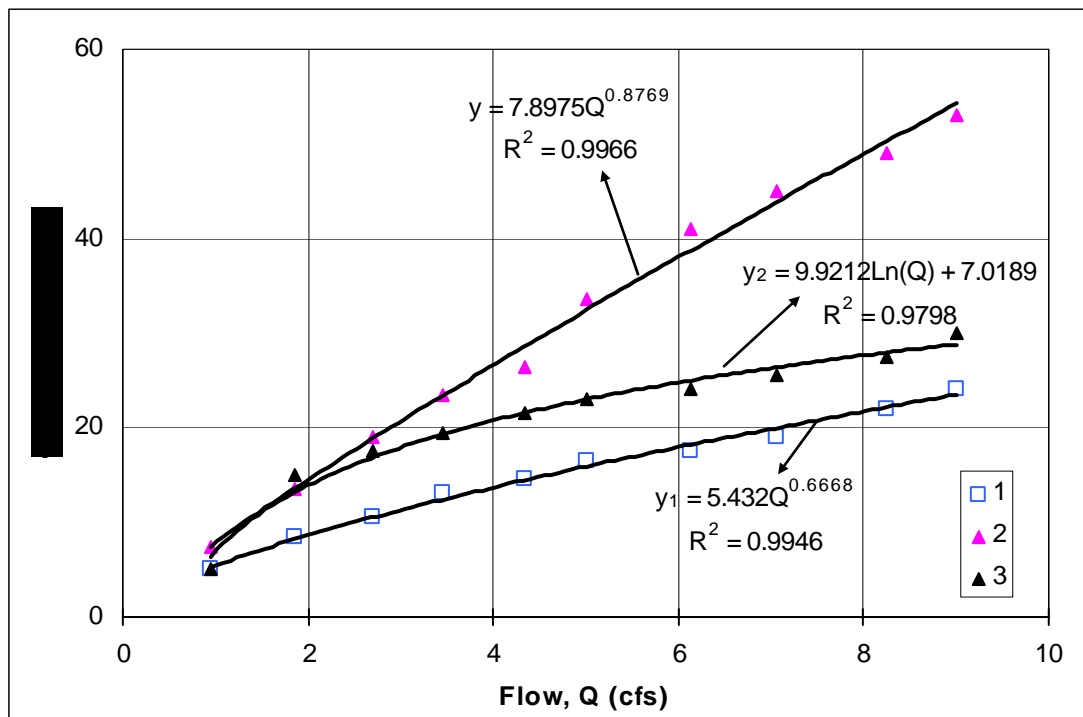


Fig. 6.2: Water depth vs discharge for inclined straight screen. Curves plotted are: 1: water depth at outlet of trash insertion tank ( $y_1$ ), 2: water depth inside the litter storage area ( $y$ ), and 3: water depth at outlet pipe from the device ( $y_2$ ).

## 6.3.2 Head loss

The total energy head at the inlet tank is:

$$H_1 = y_1 + \frac{V_1^2}{2g} + z_1 \quad \dots 1$$

where  $y_1$  is the water surface elevation referenced to the outlet pipe invert,  $\frac{V_1^2}{2g}$  is the velocity head, and  $z_1$  is elevation head. Here,  $V_1 = \frac{Q}{A_1}$  where  $A_1$  is area of water just inside the pipe.

Computed values of  $H_1$  are given in figures 6.3 and 6.4.

The head loss is defined in the usual way, i.e. the difference between the EGL at inlet and exit from the device:

$$y_1 + \frac{V_1^2}{2g} + z_1 = y_2 + \frac{V_2^2}{2g} + z_2 + \Delta h \quad \dots 2$$

The variations of this parameter with the velocity head and with the head water are shown in figures 6.5 and 6.6, respectively.

The velocity  $V$  in the x axis of figure 6.5 is obtained from  $V=Q/A$  where  $A$  is the cross-sectional area of a circular pipe of diameter 18”.

The measured data are given in Table 6.2.

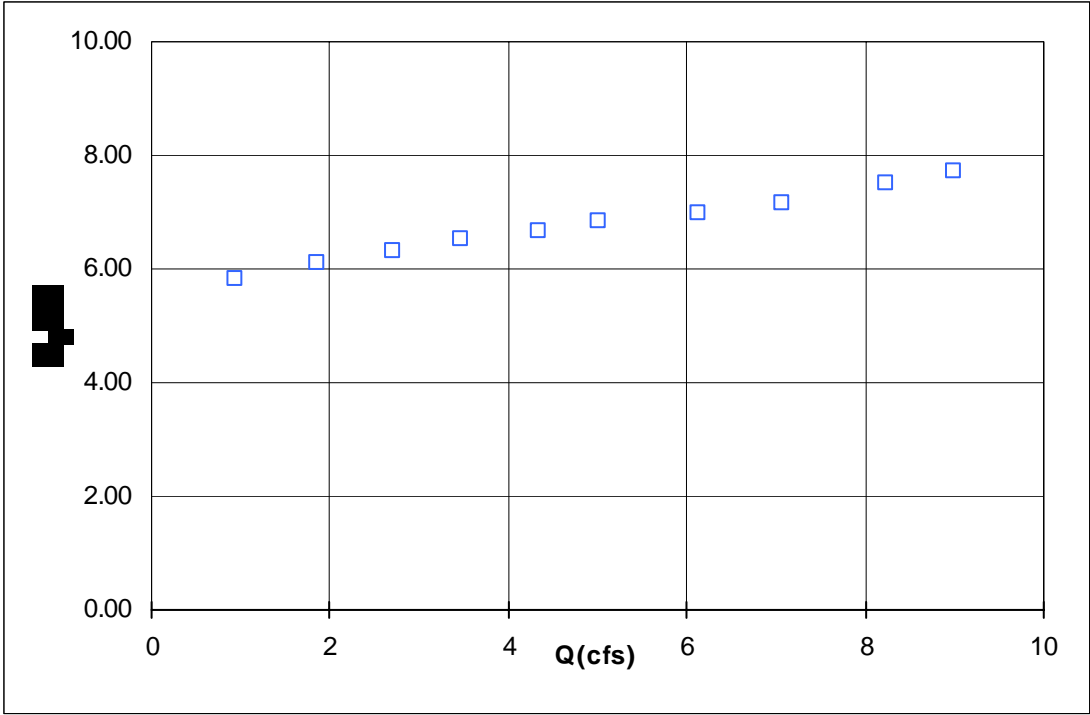


Fig. 6.3:  $H_1$  vs  $Q$  for Type 2 inclined screen.

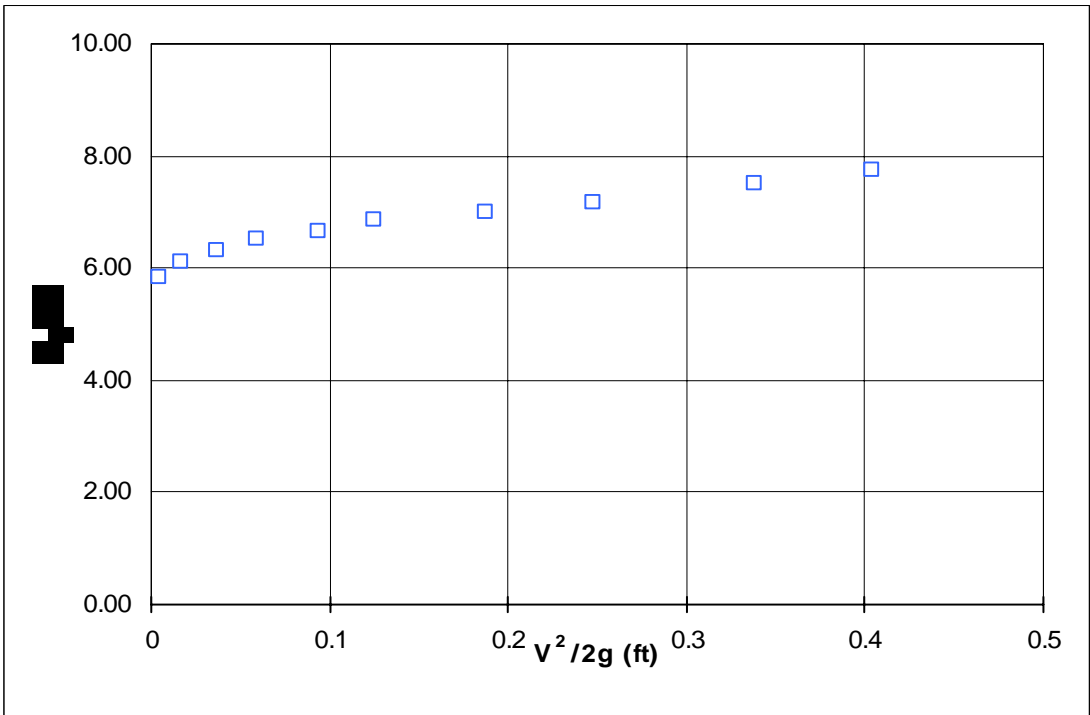


Fig. 6.4:  $H_1$  vs  $V^2/2g$  for Type 2 inclined screen.

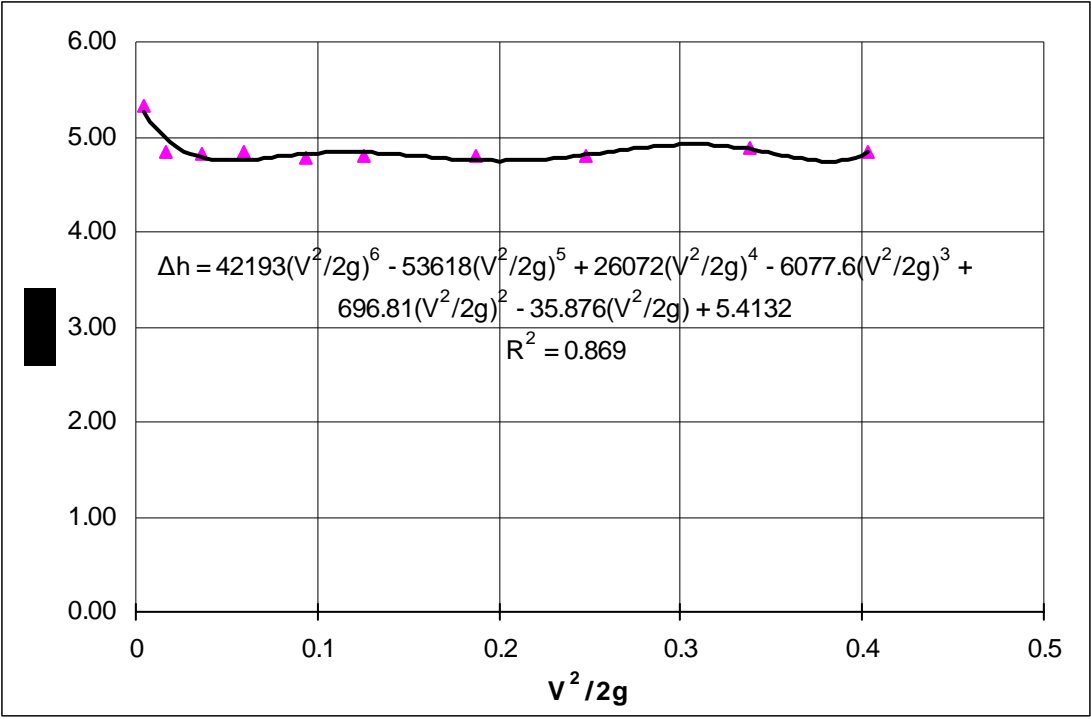


Fig. 6.5:  $\Delta h$  vs  $V^2/2g$  for Type 2 inclined screen.

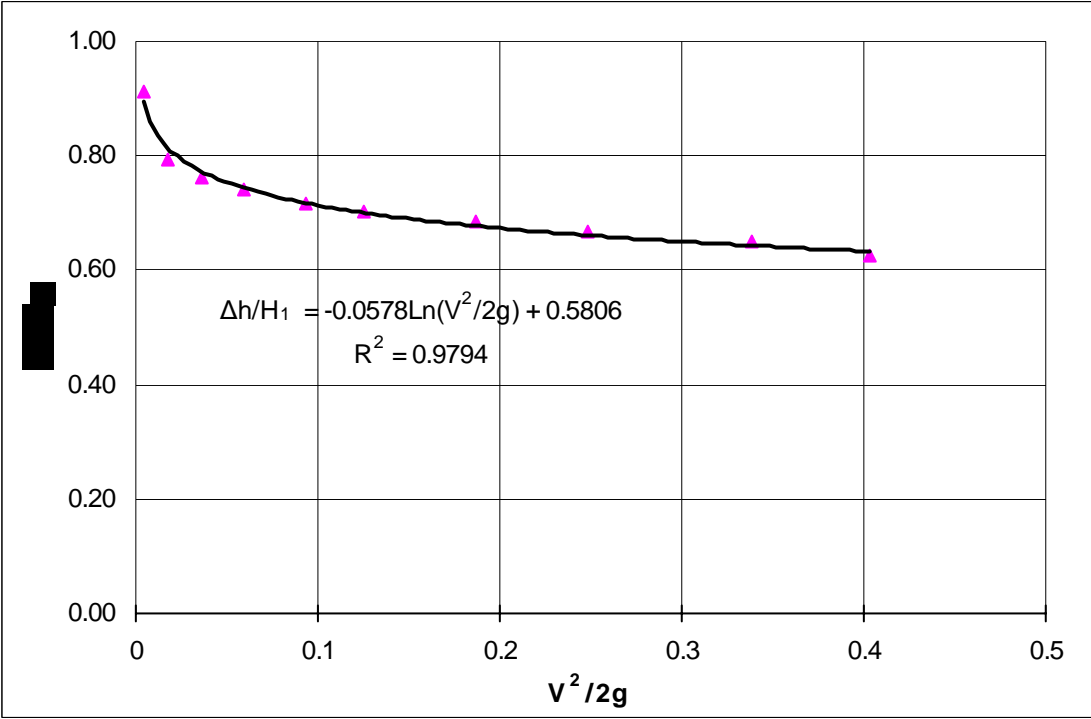


Fig. 6.6:  $\Delta h/H_1$  vs  $V^2/2g$  for Type 2 inclined screen.

Q(cfs)	$V^2/2g$ (ft)	$y_i$ (ft)	$H_i$ (ft)	$y_e$ (ft)	$H_e$ (ft)	$\Delta h$ (ft)	$\Delta h/H_i$
0.94	0.00	0.42	5.84	0.42	0.50	5.33	0.91
1.85	0.02	0.71	6.12	1.25	1.27	4.85	0.79
2.70	0.04	0.88	6.31	1.46	1.50	4.81	0.76
3.46	0.06	1.08	6.52	1.63	1.68	4.83	0.74
4.34	0.09	1.21	6.67	1.79	1.89	4.78	0.72
5.01	0.13	1.38	6.84	1.92	2.04	4.80	0.70
6.13	0.19	1.46	6.98	2.00	2.19	4.79	0.69
7.06	0.25	1.58	7.16	2.13	2.37	4.79	0.67
8.24	0.34	1.83	7.50	2.29	2.63	4.88	0.65
9.00	0.40	2.00	7.74	2.50	2.90	4.83	0.62

Table 6.2: Clean water tests energy loss calculations for Type 2 inclined screen.

### 6.3.3 Data correlations

The correlations below are for data from clean water tests.

The units are inches for  $y$ , ft for  $\frac{V^2}{2g}$ ,  $\Delta h$ ,  $H_i$  and cfs for  $Q$ .

Note that all correlations are only valid for  $Q > 0.94$  cfs.

It should be noted that the head loss in this device is dominated largely by the difference in elevation between the inflow and the outflow from the litter storage device. When correlated with the dynamic head, this will yield values of  $K$ , the head-loss coefficient, which are far greater than values typically encountered in flows in conduits.

The values of  $y_i$  can form the control values for the start of water-profile calculations using the Standard-Step Method or a similar procedure.

The best fit for the water depth at outlet pipe of the trash insertion tank is:

$$y_i = 5.432Q^{0.6668}$$

with  $R^2=0.9946$

...3

For the water depth at the outlet pipe from the device, the best fit is:

$$y_e = 9.9212 \ln(Q) + 7.0189 \quad \dots 4$$

with  $R^2=0.9798$

For the water depth in the litter storage area, the best fit is:

$$y = 7.8975 Q^{0.8769} \quad \dots 5$$

with  $R^2=0.9966$

The total head loss (from outlet pipe of trash insertion tank to the outlet pipe from the device), is correlated as:

$$\Delta h = 42193 \left(\frac{V^2}{2g}\right)^6 - 53618 \left(\frac{V^2}{2g}\right)^5 + 26072 \left(\frac{V^2}{2g}\right)^4 - 6077.6 \left(\frac{V^2}{2g}\right)^3 + 696.81 \left(\frac{V^2}{2g}\right)^2 - 35.876 \left(\frac{V^2}{2g}\right) + 5.4132 \quad \dots 6$$

with  $R^2=0.869$

The ratio of head loss to total head at inlet is:

$$\frac{\Delta h}{H_i} = -0.0578 \ln\left(\frac{V^2}{2g}\right) + 0.5806 \quad \dots 7$$

with  $R^2=0.9794$

## 6.4 Observations

### 6.4.1 Clean water runs

The ability to discharge influent flow without overflowing is obviously an important requirement for the field deployment of this device.

The following sequence of photographs shows the patterns of flows at exit from the inflow pipe and within the device that occur with increased flow rate.

#### **Q=0.94 cfs**

Figure 6.7 shows the water level in inflow pipe and pattern of water spread on influent shelf. Note the strongly non-uniform distribution of water over the screens, with larger flow rates occurring at the downstream end of the influent shelf.

Figure 6.8 shows a surface profile representative on “inlet control” flow with significant reduction in water surface elevation occurring inside the inflow pipe.

Figure 6.9 confirms the strongly non-uniform water distribution over the screens. Note the strong flow deflected directly into the gross solids storage area.

#### **Q=1.85 cfs**

Figure 6.10 shows the “inlet control” condition existing for the inflow pipe for this flow rate.

Figure 6.11 shows that the non-uniform distribution over the inflow shelf is emphasized with increasing flow rate. Water that does not leave the storage area directly through the top sections of the screen represents a loss of conveyance efficiency across the entire device.

Figure 6.12 presents another view of the patterns of water flow over the screen.

Figure 6.13 shows the patterns of water flow through the device and into the outflow pipe.

### **Q=2.7 cfs**

Figure 6.14 shows that the flow in the inflow pipe is still under 'inlet control' condition. Note the increase in water surface elevation towards the end of the inflow shelf arising from stagnation flow conditions there.

Figure 6.15 shows that the non-uniform flow distribution over the screens, evident at lower flow rates, is even more pronounced at the higher flow rate.

### **Q=3.5 cfs**

Figure 6.16 shows the conditions existing over the screen for Q=3.5 cfs. There is now increased coverage over the parts of the screen closest to the inflow pipe but the patterns of uneven distribution are still very apparent.

Figure 6.17 shows the elevated water surface level near the splash plate, and the subsequent increase in flow rate over the back part of the screen.

### **Q=4.35 cfs**

Figure 6.18 shows that very little of the inflow remains attached to the screen. The increased flow rate causes the water to leave the top of the inflow shelf and to accumulate in the gross-solids storage area before eventually being forced out from the lower parts of the screen. Note the significant flow from the downstream end of the shelf, most of which flows directly into the storage area.

Figure 6.19 shows the build up of water at the end of the inflow shelf, leading to reduction in efficiency of water extraction from the device.

### **Q=5.0 cfs**

Figures 6.20 and 6.21 show views of the screen flow and the water surface elevation near the splash plate for Q=5.0 cfs.

### **Q=6.13 cfs**

Figure 6.22 shows that the inflow conditions are still under 'inlet control'.

Figure 6.23 provides a view of water rise in the gross solids storage tank arising from the loss of efficiency of the screens. Little water remains attached to the screens especially towards the downstream end.

Figure 6.24 shows the conditions at the outflow area.

### **Q=7.06 cfs**

Figure 6.25 shows the inflow conditions for  $Q=7.06$  cfs. Note the pronounced departure of the exit flow from the surface of the screens.

The associated rise in water level in both the gross-solids storage area and in the exit trough is shown in Figures 6.26 and 6.27.

### **Q=8.24 cfs**

Figure 6.28 shows the 'inlet control' conditions at this higher flow rate and loss of screens conveyance efficiency from the top parts of the screens where the flow is fully detached. The accumulated flow next to the splash plate also contributes to the overall loss of conveyance.

### **Q=9.0 cfs**

Figure 6.29 shows the inflow conditions for  $Q=9.0$  cfs. Note the very large build-up of water ahead of the splash plate, and the beginning of device failure by passage of flow directly over this plate. Note also the increase in water surface elevation in the gross solids storage tank.

Figure 6.30 provides another view of conditions in the litter storage tank.

Figure 6.31 shows the conditions in the outflow tank and the total submergence of the inlet to the outflow pipe. Note the passage of water in the form of a sheet over the splash tank and directly into the exit tank.

Figures 6.32 and 6.33 provide further views that demonstrate the failure of conveyance by overflow from the inflow shelf.

## 6.4.2 Tests with gross solids



Fig. 6.7: Inflow conditions for  $Q=0.94$  cfs.



Fig. 6.8: View inside inflow pipe for  $Q=0.94$  cfs.



Fig. 6.9: Deflected flow into gross-solids storage area.



Fig. 6.10: Flow inside inflow pipe for  $Q=1.85$  cfs.



Fig. 6.11: Non-uniform distribution for  $Q=1.85$  cfs.



Fig. 6.12: Water distribution over screen for  $Q=1.85$  cfs.



Fig. 6.13: Outflow at  $Q=1.85$  cfs.



Fig. 6.14: Conditions inside inflow pipe at  $Q=2.7$  cfs.



Fig. 6.15: Conditions over screen at  $Q=2.7$  cfs.



Fig. 6.16: Flow over screen at  $Q=3.5$  cfs

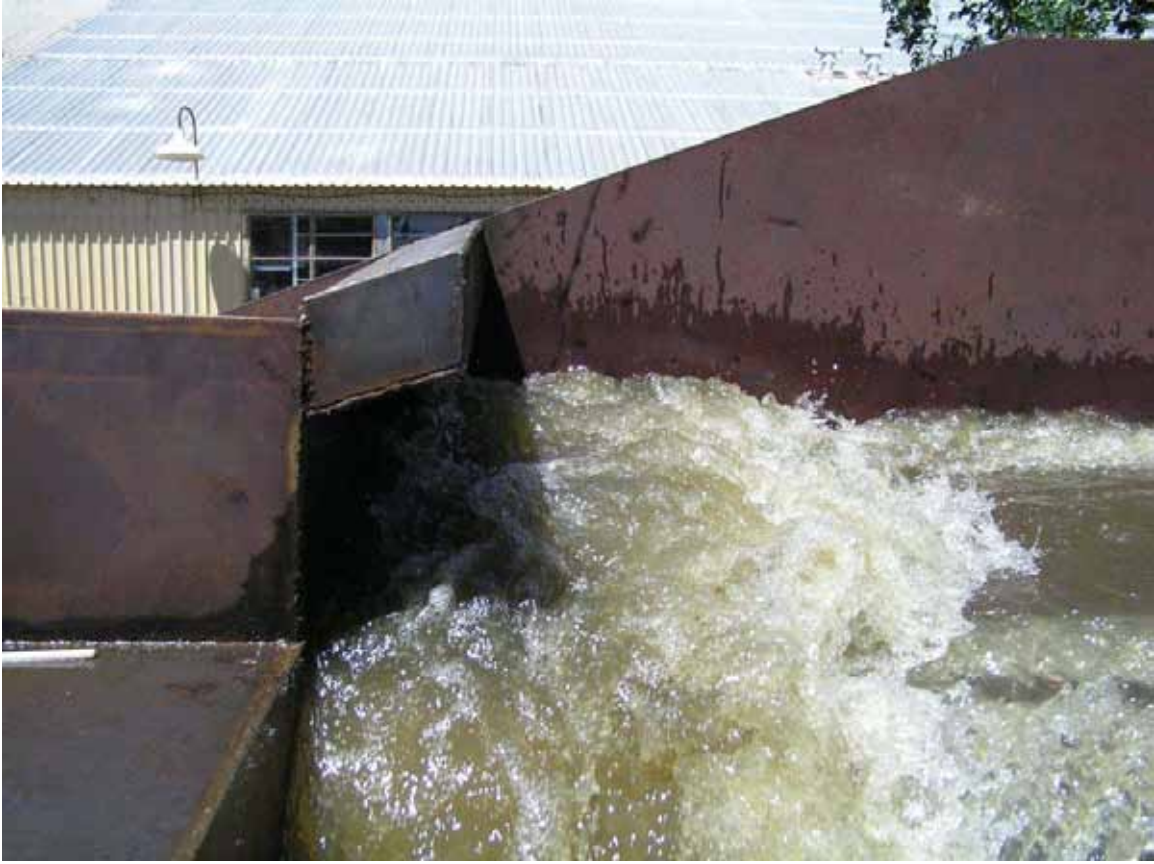


Fig. 6.17: Increase in water surface level produced by splash plate.



Fig. 6.18: Flow over screens for  $Q=4.35$  cfs.



Fig. 6.19: View of water accumulation towards end of inflow shelf for  $Q=4.35$  cfs.



Fig. 6.20: Flow over screens for  $Q=5.0$



Fig. 6.21: Water surface elevation at splash shelf for  $Q=5.0$  cfs.



Fig. 6.22: Inlet conditions for  $Q=6.13$  cfs.



Fig. 6.23: Flow over shelf showing significant loss of screen conveyance efficiency.



Fig. 6.24: Conditions at outflow for  $Q=6.13$  cfs.



Fig. 6.25: Inflow conditions for  $Q=7.06$  cfs.



Fig. 6.26: Water level rise in gross solids storage tank for  $Q=7.06$  cfs.



Fig. 6.27: Conditions at outlet tank for  $Q=7.06$  cfs.



Fig. 6.28: Inflow conditions for  $Q=8.24$  cfs.



Fig. 6.29: Inlet conditions for  $Q=9.0$  cfs.



Fig. 6.30: Conditions in gross solids storage device for  $Q=9.0$  cfs.



Fig. 6.31: Conditions in exit tank and the spill over of flow from the inflow shelf.



Fig. 6.32: Water overflow from gross solids storage device for  $Q=9.0$  cfs.



Fig. 6.33: Overflow over splash plate for  $Q=9.0$  cfs.

**$Q=1.1$  cfs, 10% litter loading**

Figure 6.34 shows a gross solids loading of 10% being through the inflow pipe before spreading over the inflow shelf and, eventually, running over the screens to settle in the gross solids storage tank.

Figure 6.35 shows that the low momentum of the transporting flow does not completely clear the gross solids from the screens, portions of which become entangled in the screen openings.

**$Q=1.1$  cfs, 50% litter loading**

A similar behavior is observed for the 50% loading at the same flow rate, seen in Figure 6.36.

Figure 6.37 shows the build up of litter in regions where the inflow over the screens is very small; the bulk of the flow being directed towards the splash plate and exiting from further downstream.

Evidence of increased clogging of the screens with cigarette filters, paper, cardboard and fabrics is evident from Figure 6.38.

Figure 6.39 is a view of the flow inside the outflow tank which shows that the litter capturing efficiency of the screens is high.

### **Q=1.1 cfs, 90% litter loading**

Figure 6.40 shows excessive accumulation of litter on the inflow shelf due to increased litter loading and low flow momentum.

Figures 6.41 and 6.42 show the worsening of the clogging problem observed with lower percentage loading.

### **Q=5.5 cfs, 10% litter loading**

Figure 6.43 shows the transport of gross solids through the inflow pipe, and its passage over the shelf and over the screens. Note the non-uniform flow and litter distribution over the screens.

Figure 6.44 demonstrate the early failure of this device in allowing certain types of gross solids to be swept over the weir and deposited directly into the outflow tank.

### **Q=5.5 cfs, 50% litter loading**

Figures 6.45 and 6.46 illustrate the failure of this device. The gross solids are transported by overflow from the litter storage device and into the outflow tank.

Overflow to outside of this device is evident from Figure 6.47.

Figures 6.48-6.51 present clear views of the causes for the failure of this device at high flow rates and percentage loading. The screens have become completely clogged preventing adequate conveyance of water to the outflow tank. The clogging is due to the absence of direct contact between high velocity flow and the screens: such contact may have had a beneficial effect of cleansing the screens and preventing overflow. In the absence of this contact, gross solids accumulated in the storage tank floated with the rising levels of water there and migrated towards the screens carried by flow passing through the screens before

these became clogged. Once the gross solids came into contact with the screens, the through flow dropped to very small level and the solids were compacted onto the screens by the force of the essentially stagnant water in the storage tank. Once this process is initiated, it continues till failure of the device due to the absence of a mechanism for clearing the accumulated litter.



Fig. 6.34: Litter transport with  $Q=1.1$  cfs (10% loading).



Fig. 6.35: Gross solids not being cleared entirely at low flow rates ( $Q=1.1$  cfs, 10% loading).



Fig. 6.36: 50% loading at  $Q=1.1$  cfs.



Fig. 6.37: Build-up of gross solids over portions of the screens ( $Q=1.1$  cfs, 50% loading).



Fig. 6.38: Clogging of screens for  $Q=1.1$  cfs and 50% loading.



Fig. 6.39: View of clear water in outflow tank ( $Q=1.1$  cfs, 50% loading).



Fig. 6.40: Inflow patterns for  $Q=1.1$  cfs and 90% loading.



Fig. 6.41: Screen clogging with  $Q=1.1$  cfs and 90% loading.



Fig. 6.42: A view of screen operation for  $Q=1.1$  cfs and 90% loading.



Fig. 6.43: Inflow patterns with  $Q=5.5$  cfs and 10% loading.



Fig. 6.44: Gross solids being carried over the splash plate and deposited in outflow tank.



Fig. 6.45: Overflow for  $Q=5.5$  cfs and 50% loading.



Fig. 6.46: Overflow for  $Q=5.5$  cfs and 50% loading.



Fig. 6.47: Overflow for  $Q=5.5$  cfs and 50% loading.



Fig. 6.48: Aftermath of  $Q=5.5$  cfs and 50% loading.



Fig. 6.49: Aftermath of  $Q=5.5$  cfs and 50% loading.



Fig. 6.50: Aftermath of  $Q=5.5$  cfs and 50% loading.



Fig. 6.51: Aftermath of  $Q=5.5$  cfs and 50% loading.

## 6.5 Conclusions

Below is a summary of the main conclusions of this phase of tests:

1. The flow over the inflow shelf was strongly influenced by the close proximity of the splash plate opposite to the inlet. Consequently, the flow of water over the screens exhibited strong non-uniform distribution with large amounts of water flow leaving from the downstream end. This non-uniform distribution becomes more prominent with increase in flow rate.
2. Only a small percentage of the flow into the litter storage tank remains attached to the screens. At high flow rates, the inflow leaves the trailing edge of the shelf in the form of a sheet which arcs over the screens. This leads to significant loss of conveyance efficiency through the screens.
3. The non-attachment of the flow to the screens also leads to loss of self-cleaning benefits and allows build-up of litter on the screens. This is evident even at small flow rates where items of litter including cigarette filters and paper are seen to remain lodged in the screens.
4. Initial failure of this device occurs at 5.5 cfs and 10% litter loading, the mechanism of failure being splashing of litter-laden water over the splash plate and into the outflow tank.
5. Drastic failure of this device occurs at 5.5 cfs and 50% litter loading. The mechanism for this failure is the near-complete blockage of the screens leading to significant overflow of litter-laden water over the outside walls of this device.
6. The performance of this device can be greatly improved by introducing design changes to force a larger portion of the flow to remain attached to the screen.

## **Section 7: Summary and recommendations**

The report details the results of tests carried out to quantify the hydraulic performance and gross-solids capture efficiency of the three Gross Solids Removal Devices (GSRDs) developed by Caltrans: the Linear-radial GSRD, the parabolic screen GSRD (also known as the Type 1 device) and the straight screen GSRD (also known as the Type 2 device).

All the tests were carried out on full-scale models of these GSRDs which were provided by their respective manufacturers to Caltrans specifications. Testing on full-scale models removes the uncertainty associated with scale effects.

Moreover, the tests were conducted with flow rates and litter loading percentages that correspond to the values encountered in Caltrans drainage facilities.

The results of these tests are provided in the forms of figures, tables and correlations of parameters measured, together with qualitative assessment of each device performance based on observations.

For the Linear-radial device, the results are incorporated into a design methodology based on HEC-22 procedure.

Detailed conclusions regarding the performance of each device were reported at the end of the relevant section. Below is a summary of the main findings and recommendations based on the observed test results.

### **Linear-Radial GSRD**

1. The litter capture efficiency of this device generally meets the requirement that litter items with dimensions larger than 0.25 inches are retained within the device.
2. The addition of wing walls at the downstream end of the vault streamlines the flow through the outlet pipe and improves the overall hydraulic efficiency of this device.
3. Loss of flow conveyance through the louvers occurred at high litter loading and was caused by cigarette filters becoming lodged in the openings, and sheets of plastic covering a significant number of them. This was especially noticeable at the downstream end of the device. The louvers of the end door became ineffective first.
4. Failure by overflow from the overflow hatch occurred at 90% loading and at flow rate of 22.5 cfs.
5. Litter compaction and limited accessibility through the litter removal doors will likely be a problem in the field operation and maintenance of this device.

### **Type 1 parabolic screen GSRD**

6. At low flow rates, there is a tendency for some litter to settle in the influent trough and not flow over the weir into the litter storage tank. In field operations, the continued wetting and drying of litter trapped in the inflow trough will cause its disintegration. This will likely exacerbate the problem of blockage of the weep holes and further degrade the drainage of the inflow troughs.
7. At high flow rates, a larger proportion of litter is carried over the weirs and into the litter storage tank. Some litter is nevertheless retained in the inflow trough. Design changes may be needed to reduce litter retention within the trough.
8. The combination of weirs and parabolic screens appears to be most efficient in causing the flow to remain attached to the screens over a large portion of their length. This makes for a very successful design in that it ensures that the essential features of this device are essentially self-cleaning.
9. Drainage of the litter storage tank appears to be satisfactory.

### **Type 2 screen GSRD**

10. The distribution of flow over the screens is very strongly non-uniform due to the rise in water level at the splash plate. This non-uniform flow distribution is detrimental to the overall efficiency of this device.
11. At moderate flow rates and small litter loading, the device experiences partial failure by the splashing of litter-laden flow over the splash plate. A design modification can remove this problem.
12. At a flow rate of 5.5 cfs and 50% litter loading, the device fails by allowing significant amounts of litter-laden water to over-top its outer walls.
13. The failure is due to the non-adherence of the water flow to the screens, thereby not providing the self-cleaning feature obtained in the Type 1 device. Design changes would be required to force the inflow water to remain attached to the screens over a longer run along their length.

## References

1. Caltrans. *Litter Management Pilot Study*, Final Report prepared for the California Department of Transportation, Sacramento, California, CTSW-RT-00-013, 2000.
2. Kayhanian, M., Kummerfeldt, S., Lee-Hyung, K., Gardiner, N. and Tsay, K. Litter Pollutograph and Loadograph. Proceedings of 9th International Conference on Urban Drainage, September, Portland, Oregon, 2002.
3. Endicott, J. D., Berger, B. J. and Stone, S. J. Design and Performance of Non-Proprietary Devices for Highway Runoff Litter Removal, Proceedings of 9th International Conference on Urban Drainage, September, Portland, Oregon, 2002.
4. Kim, H. L., Kayhanian, M. and Stenstrom, M.K. Event Mean Concentration and Mass Loading of Litter in Highway Outfalls during Rainstorms. *Journal of Total Science for Environment*, In Press, 2003.
5. Caltrans. Phase I-Gross Solids Removal Devices (GSRD) Pilot Study, 2000-2002 Final Report. Caltrans Document No. CTSW-RT-03-072.31.22, 2003.
6. Kayhanian, M., Johnston, J., Yamaguchi, H. and Borroum, S. Caltrans Storm Water Management Program. *Stormwater*, Vol. 2, No. 2, pp. 52-67, 2002.

## APPENDIX 1

### Guidelines on Design of Storm Drains with Linear-Radial GSRD

#### 1. Description of GSRD

The Gross Solids Removal Device (GSRD) is designed to remove gross solids from water collected in storm drains. A Linear-Radial GSRD comprises of a stainless steel well casing with 5 mm (0.25 inch) louvers that is contained in a concrete vault (see Picture 1 for the actual device tested at UC Davis Hydraulics Laboratory). Flow enters the inside of the well casing and passes radially through the louvers. Litter and solids are trapped inside the casing. Doors or hatches are provided at the end and on the top of the well casing to allow access for periodic cleaning of the trapped gross solids. An overflow or bypass is provided to allow drain water to pass when the well screen is fully loaded with gross solids.



Picture 1: Linear-Radial Gross Solid Removal Device (GSRD) tested at UC Davis Hydraulics Laboratory (date is erroneous).

The GSRD is sized to accommodate gross pollutants for a one-year maintenance period, and should be sized on litter and debris accumulation data for a particular location. In the absence of data, 0.7 m<sup>3</sup>/ha/year can be used as default.

## 2. Hydraulic Considerations

The equations presented in this report were developed on the basis of data obtained from tests conducted for the specific conditions listed in the Report. These conditions broadly correspond to those found in practice however, the relations developed are NOT “universal” – their validity for actual design purposes will depend on the precise conditions that prevail in practice. We can not put forward a design methodology which would be universally valid as we are unable to extrapolate our test results to cover the entire range of values over which the design parameters may vary. What follows is therefore an example of the use of the test data for design applications and not a universally valid procedure.

In principle, the inclusion of the Linear-Radial GSRD structure in the storm drains system will disrupt the flow, resulting in a loss of energy across the structure.

The measurements reported in the Report show that when the head loss is correlated with the dynamic head to obtain a “best fit” relation, a straight line is obtained but that the intercept of this line (i.e. the value of head loss when V=0) is finite (this is the A’ term in the equations of Section 4). In hydraulics practice, it is more usual to place greater emphasis on the maximum head loss values as these are the values used for design purposes. Consequently, the measured data are correlated not via a “best fit” but by a straight line which passes through the point of origin (i.e. with A’=0). The slope of this line is “K”, the head-loss coefficient, i.e.:

$$\Delta h = K (V^2/2g) \quad (1)$$

Where:       $\Delta h$  is the total energy loss across the device (ft)  
              K is the loss coefficient  
              V is the velocity (ft/s)  
              g is the gravitational constant (ft/s<sup>2</sup>)

A plot of the head-loss coefficient K against the slope is shown in Figure 1:

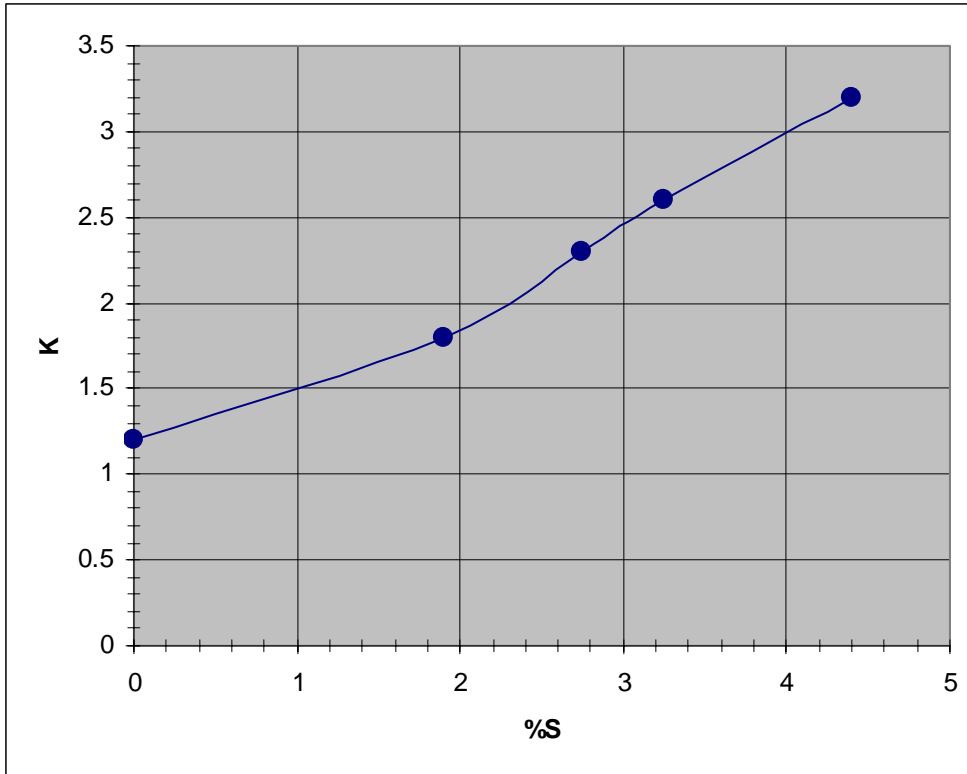


Figure 1: Plot of Head-loss coefficient vs. slope (percent).

For the entire Linear-Radial GSRD, the loss coefficient can be expressed as

$$K = K_{\text{entrance}} + K_{\text{device}} + K_{\text{exit}} \quad (2)$$

Where:  $K_{\text{entrance}}$  is the entrance loss coefficient  
 $K_{\text{device}}$  is the loss coefficient of flow through the device  
 $K_{\text{exit}}$  is the exit loss coefficient

In the model tests, the entrance and device loss coefficients were combined. The measurements given in Figure 4.27 and in Tables 4.12, 4.13, 4.14 and 4.15 and summarized in Fig. 1 suggest that, for the  $S < 0.1\%$  flow, the average value of  $K$  is 1.2. This means:

$$K_{\text{entrance}} + K_{\text{device}} = 1.2 \quad (3)$$

In the model tests, the entrance losses were caused by the contraction of flow from the water holding tank upstream into the inlet pipe of the GSRD. In field conditions, water will typically flow directly from the storm drain into the GSRD, and hence there will be no energy loss at the entrance (i.e.  $K_{\text{entrance}} = 0$ ).

For the conditions that existed in the laboratory test,  $K_{\text{entrance}}$  is likely to be 0.5 as the pipe entrance is sharp-edged with no rounding. Therefore:

$$K_{\text{device}} = 1.2 - 0.5 = 0.7 \quad (4)$$

Further, in the test model,  $K_{\text{device}}$  was measured to just upstream of the outlet pipe from the vault. Hence it is necessary to add a  $K_{\text{exit}}$  term to take account of the exit losses from the vault and into the outflow pipe.

In the laboratory tests,  $K_{\text{exit}}$  is likely to be about 0.3 with the addition of 45° wing walls.

Hence overall, the loss coefficient for the GSRD is taken as:

$$K = K_{\text{device}} + K_{\text{exit}} = 0.7 + 0.3 = 1.0 \quad (5)$$

### 3. Example of design of storm drain outlet with Linear-Radial GSRD

Given: The storm drain profile illustrated in Figure 2.

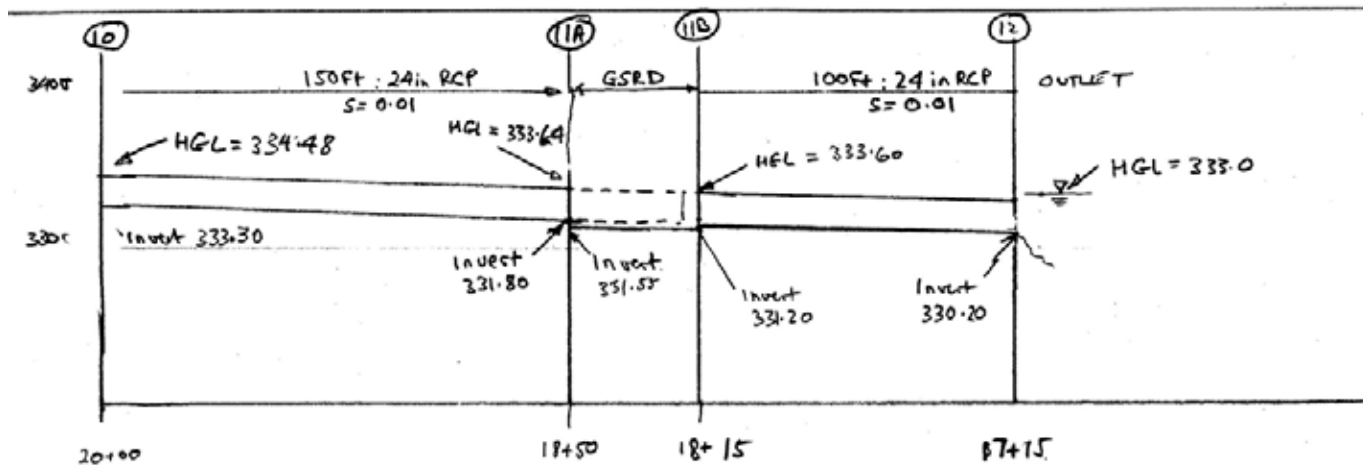


Figure 2. GSRD and Pipeline Profiles.

Task:

1. Determine appropriate pipe sizes and inverts, and the dimensions of the gross solids removal device.
2. Evaluate the HGL for the system configuration determined in part (1).

Note: Equations and Charts referenced are in HEC-22 Urban Drainage Design Manual, (US Department of Transportation, August 2001).

## **Part I: Preliminary Design of Storm Drain Outlet with GSRD (English Units)**

Step 1 Figure 2 illustrates the profile of the proposed system including the location of the Linear-Radial Gross Solids Removal Device (GSRD) and the associated storm drains.

All structures have been numbered for reference.

Step 2 Starting from the upstream end, determine:

1. The physical parameters for the inlet pipe to the GSRD,
2. The layout of the GSRD and,
3. The outlet pipe.

Summary tabulations of the computational process are provided in Figures 3 and 4.

The column by column computations for each section follow:

## Section 10 to Section 11A

(see Figures 2 and 3)

Col. 1 from section 10		Upstream storm drain
Col. 2 to section 11A		Upstream end of GSRD
Col. 3 Run length	L= 2000-1850 ft L= 150 ft	From Figure 2
Col 4 & Col 5 Drainage area (incremental and total)	$A_t = 4.17$ acres	Total drainage area upstream of Section 10
Col. 6 Runoff coefficient	$C = 1.0$	Typical value for highway tributary areas
Col 7 and 8 Inlet CA (incremental and total)	$CA = (1.)*(4.17)$ $CA = 4.17$ ac	Col 4 times Col 5
Col 9 and 10 Time of concentration	Not used	
Col 11 Rainfall intensity	$I = 3.238$ in/hr	Typical intensity for GSRD sites in Southern California
Col 12 Runoff	$Q = (CA) (I) /K_u$ $Q = (4.17) (3.238)/(1.0)$ $Q = 13.50$ ft <sup>3</sup> /s	Equation 3-1: Rational formula with conversion factor ( $K_u$ ) =1.0
Col 21 Slope	$S = 0.01$	Desired pipe slope
Col 13 Pipe diameter	$D = ((Q_n)/(K_Q S_o^{0.5}))^{0.375}$ $D =$ $((13.50)*(0.013)/((0.46)*(0.01)^{0.5}))^{0.375}$ $D = 1.65$ ft $D = 2$ ft	Equation 7-1 or chart 25 With $n = 0.013$ for concrete $K_Q = 0.46$  Use nearest larger size: $D=2.0$
Col 14 Full capacity	$Q_f = (K_Q/n)*(D^{2.67})*(S_o^{0.5})$ $Q_f = (0.46)/0.013* (2.0^{2.67})*(0.01^{0.5})$ $Q_f = 22.52$ cfs	Equation 7-1 or chart 25
Col 15 velocity Full	$V_f = (K_v/n) D^{0.67} S_o^{0.5}$ $V_f = (0.59)/(0.013) (2.0)^{0.67} (0.01)^{0.5}$ $V_f = 7.22$ ft/s	Equation 7-1 or chart 25
Col 16 velocity design	$Q/Q_f = 13.50/22.50 = 0.6$ $V/V_f = 1.05$ $V = (1.05)*(7.22)$ $V = 7.581$ ft/s	Chart 26
Col 17	$T_s = L/V = 100/7.58 = 0.21$ min Use $T_s = 1$ min	
Col 20 Crown drop	=0	Upstream most invert
Col 18 U/S invert	=333.30	Check for Minimum cover = 3ft
Col 19 D/S invert	= (U/S invert – (Length *slope))	

	$=(333.30)-(150*0.01)$ $=331.80$	
--	-------------------------------------	--

## Section 11A to Section 11B

(see Figure 4)

Col. 1 Drainage area	$A_t = 4.17$ acres	From design of storm drains
Col. 2 Volume of litter $V_L$	$V_L = 10.8$ ft <sup>3</sup> /acre/year	Use Default value of 10.8 ft <sup>3</sup> /acre/year in absence of local data
Col. 3 Volume of linear radial device (well screen) $V_D$	$V_D = 2 * V_L * A_t$ $V_D = 2 * 10.8 * 4.17$ $V_D = 90.07$ ft <sup>3</sup>	Assumes maximum storage volume is 50% of the total volume of the screen
Col. 4 Diameter of device	$D = 2.0$ ft	Use same diameter as storm drain
Col 5 Length of device (L)	$L_D = V_D / A_D$ $L_D = 90.07 / ((3.14 * 2.0^3) / 4)$ $L_D = 28.66$	Volume of device divided by cross sectional area of device
Col 6. Number of sections	$N_s = L_D / 6$ $N_s = 5$	Louvered pipe available in 6ft sections. Need to round number up to nearest whole section.
<b>Length of vault</b>		
Col 7 Length of inflow pipe	$L_{inflow} = D$ $L_{inflow} = 2.0$	Length of inflow pipe equal to diameter of screen to allow for overflow of length 0.75 D and width 0.5D
Col 8 Length of screens	Revised $L_D = N_s * 6$ ft Revised $L_D = 5 * 6$ ft Revised $L_D = 30$ ft	Number of screens times length of one screen
Col 9 Allowance for end door opening	$L_{end} = 1.5 * D$ $L_{end} = 1.5 * 2.0$ $L_{end} = 3.0$	Required to allow opening of end cap.
Col 10 Total internal length of vault	$L_{total} = L_{inflow} + \text{Revised } L_D + L_{end} =$ $L_{total} = 2.0 + 30.0 + 3.0$ $L_{total} = 35$ ft	Sum length components
<b>Width of Vault</b>		
Col 11 Width of Linear radial device (screens)	$W_{device} = 2.0$ ft	From Column 4
Col 12 allowance for flow and access around device	$W_{allow} = 2 * D$ ft $W_{allow} = 2 * 2.0$ ft $W_{allow} = 4.0$ ft	Allow equivalent to one diameter of the device (D) on each of the device
Col 13 total internal width of vault	$W_{vault} = W_{device} + W_{allow} =$ $W_{vault} = 2.0 + 4.0$ ft $W_{vault} = 6.0$ ft	Sum width components
Col 14 Bed slope	$S = 0.01$	Provide minimum bed slope to ensure all water can drain from vault

Col 15 U/S invert	= 331.80 – 0.25 = 331.55	From Figure 3 Col 19 less 0.25 ft to provide 1 in minimum clearance between linear radial device and floor
Col 16 D/S invert	= 331.80- (L <sub>total</sub> ) * (S) =331.55- (35.0)*(0.01) =331.20 ft	Col 15 –(Col 10)*(Col 14)

Check there is sufficient ground available for the footprint of the GSRD and adequate cover the inlet and outlet pipes.

### Section 11B to Section 12

(see Figures 2 and 3)

Col. 1 from section 11B		Downstream end of GSRD
Col. 2 to section 12		Outlet
Col. 3 Run length	L= 2000-1900 ft L= 100 ft	From Proforma 2
Col 4 and 5 Drainage area Incremental and total	A <sub>t</sub> = 4.17 acres	Total drainage area upstream of Section 10- no additional inflow
Col. 6 Runoff coefficient	N/a	Typical value for highway tributary areas
Col 7 and 8. Inlet CA Incremental and total	N/a	Col 4 times Col 5
Col 9 and 10 Time of concentration	Not used	
Col 11 Rainfall intensity	I = 3.238 in/hr	Typical intensity for GSRD sites in Southern California
Col 12 Runoff	Q = 13.50	No additional inflows
Col 18 Slope	S = 0.01	Desired pipe slope
Col 13 Pipe diameter	$D = ((Q_n)/(K_Q S_o^{0.5}))^{0.375}$ D = $((13.50)*(0.013)/((0.46)*(0.01)^{0.5}))^{0.375}$ D = 1.65 ft D = 2.0ft	Equation 7-1 or chart 25 With n= 0.013 for concrete K <sub>Q</sub> = 0.46  Use D = 2.0 ft-same as storm drain upstream
Col 14 Full capacity	$Q_f = (K_Q/n)*(D^{2.67})*(S_o^{0.5})$ $Q_f = (0.46)/0.013*(2.0^{2.67})*(0.01^{0.5})$ Q <sub>f</sub> = 22.52 cfs	Equation 7-1 or chart 25
Col 15 velocity Full	$V_f = (K_v/n) D^{0.67} S_o^{0.5}$ $V_f = (0.59)/(0.013) (2.0)^{0.67} (0.01)^{0.5}$ V <sub>f</sub> = 7.22 ft/s	Equation 7-1 or chart 25
Col 16 velocity design	Q/Q <sub>f</sub> =13.50/22.52 = 0.60 V/V <sub>f</sub> = 1.05 V = (1.10)*(7.22) = 7.58 ft/s	

Col 17	Not used	
Col 18 U/S invert	=331.20 ft	From Figure 4. Check for Minimum cover = 3ft
Col 19 D/S invert	= (U/S invert – (Length *slope)) =(331.20)-(100*0.01) =330.20	

## Part II: Energy grade Line Evaluation Computations- English Units

(Note: Equations and Charts referenced are in HEC-22 Urban Drainage Design Manual (US Department of Transportation, August 2001)

The flowing computational procedure follows the steps outlined in Section 7.5 (HEC 22). Starting at structure 12, computations proceed in the upstream direction.

Summary tabulations of the computational process are provided in Figure 5 and Figure 6.

The column by column computations for each section of the storm drains and the GSRD follow:

Step 1	Col 1	Outlet	
	Col 14	HGL = 333.00	Downstream pool elevation
	Col 10	EGL= 333.00	Assume no velocity in the pool
<b><u>Section 12</u></b>			
Step 2	Col 1A, 1B	Section ID = 12	Outlet
	Col 15A	Invert = 330.20 ft	Outfall invert
		TOC = 330.20 + 2.0 TOC = 332.20 ft	Top of storm drain at outfall
Step 3		HGL <sub>i</sub> = TW = 333.0	From Step 1
	Col 13A	EGL <sub>i</sub> = HGL + V <sup>2</sup> /2g EGL <sub>i</sub> = 333.0 + (13.50/(3.14*(2.0/2))) <sup>2</sup> /(2*32.2) EGL <sub>i</sub> = 333.0 + 0.29 EGL <sub>i</sub> = 333.29	Use Case 1 since TW is above the top of the conduit  EGL <sub>i</sub> at Str 12

<b>Section 11A-11B</b>			
Step 4	Col 1A, 1B	Section. ID 11A	Next section
	Col 2A	D = 2.0 ft	Pipe diameter
	Col 3A	Q = 13.50 cfs	Conduit discharge (Design value)
	Col 4A	L = 100 ft	Outlet conduit length
Step 5	Col 5A	V = Q/A V = (13.50)/(3.14*(2.0/2) <sup>2</sup> V = 4.3 ft/s	Velocity in conduit
	Col 7A	=V <sup>2</sup> /2g =(4.3) <sup>2</sup> /(2*32.2) =0.3 ft	Velocity head in conduit
Step 6	Col 8	Sf = ((Q*n)/(K <sub>o</sub> D <sup>2.67</sup> )) <sup>2</sup> Sf = ((13.50)*(0.013)/(0.46)*(2.0) <sup>2.67</sup> ) <sup>2</sup> Sf = 0.00359 ft/ft	Friction slope
Step 7	Col 2B	Hf = Sf*L Hf = (0.00359)*(100) Hf = 0.359	Col 8A * Col 4A
	Col 7B and Col 9A	Total = Hf+hb+Hc+He+Hj Total = 0.359	hb, Hc, He, Hj = 0
Step 8	Col 10A	EGL <sub>o</sub> = EGL <sub>i</sub> + pipe loss EGL <sub>o</sub> = 333.29+0.359 EGL <sub>o</sub> = 333.6	
		HGL = 333.6-0.3 HGL=333.3 TOC = 331.20+2.0 TOC = 333.20	Check for full flow  Close: Assumption valid
Step 9	Col 8B	Daho = EGL <sub>i</sub> – velocity head –pipe invert 333.60-0.3-331.20 Daho = 2.1 ft	
Step 10	Col 9B	K <sub>device</sub> =1.0	
Step 17	Col 12A	K <sub>device</sub> * (V <sup>2</sup> /2g)=(1.0) * (0.3) = 0.3 ft	Head loss
Step 18	Col 13A	=EGL <sub>o</sub> +head loss +Sf =333.60+0.3+(35*0.001) =333.94 ft	
Step 19	Col 14A	HGL <sub>i</sub> = EGL <sub>i</sub> –(V <sup>2</sup> /2g) = 333.94-0.3 = 333.64 ft	
Step 20	Col 15A	U/s TOC = invert +dia = 331.80+2.0 =333.80 ft	
Step 21	Col 16A	=(333.80+1.0) – 331.55 = 3.25 ft	Depth of vault-providing 1 ft freeboard

<b>Section 10</b>			
Step 4	Col 1A, 1B	Section. ID 11A	Next section
	Col 2A	D = 2.0 ft	Pipe diameter
	Col 3A	Q = 13.50	Conduit discharge (Design value)
	Col 4A	L = 150 ft	Outlet conduit length
Step 5	Col 5A	V = Q/A V = (13.50)/(3.14*(2.0/2) <sup>2</sup> V = 4.3 ft/s	Velocity in conduit
	Col 7A	=V <sup>2</sup> /2g =(4.3) <sup>2</sup> /(2*32.2) =0.3 ft	Velocity head in conduit
Step 6	Col 8	Sf = ((Q*n)/(K <sub>Q</sub> D <sup>2.67</sup> )) <sup>2</sup> Sf = ((13.50)*(0.013)/(0.46)*(2.0) <sup>2.67</sup> ) <sup>2</sup> Sf = 0.00359 ft/ft	Friction slope
Step 7	Col 2B	Hf = Sf*L Hf = (0.00359)*(150) Hf = 0.54	Col 8A * Col 4A
	Col 7B and Col 9A	Total = Hf+hb+Hc+He+Hj Total = 0.54	hb, Hc, He, Hj = 0
Step 8	Col 10A	EGLo = EGLi + pipe loss EGLo = 333.94+0.54 EGLo = 334.48	
		HGL = 334.48-0.3 HGL = 334.18 TOC = 331.20+2.0 TOC = 333.20	Check for full flow  Close: Assumption valid

**Figure 3: PRELIMINARY STORM DRAIN COMPUTATION SHEET**

Str ID		Length	Drainage area		Runoff Coeff. "C"	Area * C		Time of Concentration		Rain Intensity	Runoff "Q"	Pipe diameter	Q full
From	To		Inc	total		inc	total	inlet	system				
		(ft)	(acre)	(acre)		(acres)	(acres)	(min)	(min)	(in/hr)	(cfs)	(ft)	(cfs)
(1)	(2)	(3)	(4)	(5)	(6)	(7)	(8)	(9)	(10)	(11)	(12)	(13)	(14)
10	11A	150	4.17	4.17	1.0	4.17	4.17	n/a	n/a	3.24	13.50	2.0	22.5
11A	11B	35	n/a	n/a	n/a	n/a	n/a	n/a	n/a	3.24	13.50	2.0	n/a
11b	12	100	n/a	n/a	n/a	n/a	n/a	n/a	n/a	3.24	13.50	2.0	22.5
12													

**Figure 4: COMPUTATION SHEET FOR GSRD**

Drainage Area	Volume of litter	Volume of Linear radial device (well screen)	Diameter of linear radial device	Length of Linear radial device	Number of sections	Length of vault				width of screen
						length of inflow pipe	length of screens	allowance for end door opening	Total length of vault	
(acres)	(ft <sup>3</sup> /acre/year)	(ft <sup>3</sup> )	(ft)	(ft)		(ft)	(ft)	(ft)	(ft)	(ft)
(1)	(2)	(3)	(4)	(5)	(6)	(7)	(8)	(9)	(10)	(11)
4.17	10.8	90.07	2.0	28.66	5	2	30	3	35	

**Figure 5: ENERGY GRADE LINE COMPUTATION SHEET-TABLE A**

Str ID	Diam.	Flow	Length	Velocity	d	dc	$v^2/2g$	Sf	Total Pipe loss (table B)	EGLoutlet	K Table B	$K(V^2/2g)$
	(ft)	(ft <sup>3</sup> /s)	(ft)	(ft/s)	(ft)		(ft)	(ft/ft)	(ft)	(ft)		(ft)
(1)	(2)	(3)	(4)	(5)	(6a)	(6b)	(7)	(8)	(9)	(10)	(11)	(12)
Outlet										333.00		
12												
11A-11B	2.0	13.5	100.0	4.3	Full	n/a	0.3	0.00359	0.36	333.65	1.0	
10	2	13.5	150	4.3	full	n/a	0.3	0.00359	0.54	334.48		GSR
Note: n/a indicates not available or not used												

**Figure 6: ENERGY GRADE LINE COMPUTATION SHEET- TABLE B**

Str ID	Hf	hbend	Hcontr	Hexp	Hjunct	Total	d(aho)	Kc	CD	Cd	CQ	Cp	Cb	K
(1)	(2)	(3)	(4)	(5)	(6)	(7)	(8)	(9)	(10)	(11)	(12)	(13)	(14)	(15)
Outlet														
12	0.359					0.359								
11b-11A								1.00						1.00
								Kdevice						
10	0.585					0.585								

## **APPENDIX 2**

### **CDs for Linear-Radial GSRD footage**

This Appendix consists of 2 CDs containing digital video footage of tests carried out on the Linear-Radial GSRD.

CD 1 is labeled "Linear-Radial 0-55 min".

CD 2 is labeled "Linear-Radial 55+".

**Copyright of all images contained on these CDs remains with the University of California, Davis.**

## **APPENDIX 3**

### **CDs for screens GSRDs footage**

This Appendix 3 consists of 2 CDs containing digital video footage of tests conducted on the parabolic (Type 1) and the straight (Type 2) screen GSRDs (Phases II and III).

CD 1 is labeled "Phase II parabolic screen".

CD 2 is labeled "Phase II parabolic screen and straight screen".

**Copyright of all images contained on these CDs remains with the University of California, Davis.**